THE UNIVERSITY OF MANITOBA

ON THE THERMAL BUCKLING OF THIN WALL TUBES

By

Glenn John Merrett

A Thesis
Submitted to the Faculty of Graduate Studies
In Partial Fulfillment of the Requirements for the Degree of
Master of Science

Winnipeg, Manitoba
1977

ON THE THERMAL BUCKLING OF THIN WALL TUBES

BY

GLENN JOHN MERRETT

A dissertation submitted to the Faculty of Graduate Studies of the University of Manitoba in partial fulfillment of the requirements of the degree of

MASTER OF SCIENCE

ABSTRACT

The investigation in this thesis concerns the thermal buckling of cylinders heated uniformly around the circumference and symmetrically with respect to the axial half-length.

Aluminum cylinders, machined to a thin wall, were threaded into a rigid frame and heated by means of a radiation type internal heater until buckling occurred. The temperature profile of the tube was recorded by thermocouples and this profile was used to simulate the test by using a successive approximation technique on an IBM 370/168 digital computer.

Axial load versus the centerline temperature plots were obtained for all specimens. The centerline radial displacement was also plotted as a function of the centerline temperature for several specimens. These results were compared to the successive approximation solutions and to the results of other investigators. Agreement with other works is noted, and any discrepancies are explained. Suggestions are also made as to areas with a need for further study to clarify the problem.

ACKNOWLEDGEMENT

The author would like to extend his sincere appreciation to his advisor Dr. T. R. Hsu for his advice and guidance in the preparation of this thesis. The assistance of Dr. S. Cheng is also acknowledged. Special thanks are given to Mr. F. Kapitoler for his help in the experimental work, to Ms. C. Kohut for her fine work in the typing of this manuscript and to Mr. Y. J. Kim for his capable drafting. Financial support was provided by the National Research Council of Canada and University of Manitoba Research Board.

Finally, the author would like to thank his family for their continued support and encouragement during his studies.

TABLE OF CONTENTS

Page

Abstract . . . . i.

Acknowledgement . . . . ii.

Table of Contents . . . . iii.

List of Tables . . . . v.

List of Figures . . . . vi.

List of Symbols . . . . viii.

CHAPTER I INTRODUCTION . . . . 1.

1.1 Statement of the Problem . . . . 1.

1.2 Scope of Thesis . . . . 1.

CHAPTER II LITERATURE REVIEW . . . . 3.

CHAPTER III THEORY . . . . 6.

3.1 The Differential Equations of Buckling . . . . 6.

3.1.1 The Equilibrium Method . . . . 6.

3.1.2 Variational Methods . . . . 19.

3.2 Theoretical Methods of Solution . . . . 20.

3.2.1 The Direct Substitution Method . . . . 20.

3.2.2 The Rayleigh-Ritz Method . . . . 21.

3.2.3 The Galerkin Method . . . . 22.

3.3 Numerical Methods of Solution . . . . 27.

3.3.1 Successive Approximation . . . . 27.

3.3.2 Finite Difference & Finite Elements . . . . . 28.

Page

CHAPTER IV EXPERIMENTAL WORK . . . . 38.

4.1 Experimental Apparatus . . . . 38.

4.2 Test Specimens . . . . 39.

4.3 Experimental Procedure . . . . 40.

4.4 Results . . . . 42.

CHAPTER V DISCUSSION OF RESULTS . . . . 44.

5.1 Buckling Phenomenon . . . . 44.

5.2 Load Vs. Temperature Curves . . . . 46.

5.3 Displacement Measurement . . . . 52.

CHAPTER VI SUMMARY OF RESULTS . . . . 53.

References . . . . 55.

Appendices . . . . 58.

A. Variational Methods For Equilibrium Equations . . . . 58.

B. Equations Of The Successive Approximation Method . . . . . 68.

C. Computer Program Listing . . . . 76.

LIST OF TABLES

TABLE I. Test Results

TABLE II. Displacement Results.

TABLE III. Comparison of Experimental and Theoretical Results.

TABLE IV. Dimensionless Coefficients.

LIST OF FIGURES

1. Coordinate Systems.
2. Finite Element - Finite Difference Models.
3. Overall Test Set-up.
4. Test Set-up Details.
5. Test Set-up Schematic.
6. Temperature Control Unit.
7. Details of Load Measurement Apparatus.
8. Fotonic Sensor.
9. Dimensions of Test Specimen.
10. Photograph of Test Specimen.
11. Load Cell Output Vs. Central Thermocouple Output.
12. Typical Thermocouple Output.
13. Fotonic Sensor Output Vs. Central Thermocouple Output.
14. Axial Load Vs. Mid-Span Temperature. Test No. 6.
15. Axial Load Vs. Mid-Span Temperature. Test No. 8.
16. Axial Load Vs. Mid-Span Temperature. Test No. 10.
17. Axial Load Vs. Mid-Span Temperature. Test No. 12.
18. Axial Load Vs. Mid-Span Temperature. Test No. 13.
19. Axial Load Vs. Mid-Span Temperature. Test No. 14.
20. Axial Load Vs. Mid-Span Temperature. Test No. 15.
21. Axial Load Vs. Mid-Span Temperature. Test No. 16.
22. Axial Load Vs. Mid-Span Temperature. Test No. 19.
23. Axial Load Vs. Mid-Span Temperature. Test No. 21.
24. Mid-Span Radial Deflection. Test No. 12.
25. Mid-Span Radial Deflection. Test No. 14.

26. Mid-Span Radial Deflection. Test No. 15.

27. Mid-Span Radial Deflection. Test No. 19.

28. Buckling Pattern. Test No. 8.

29. Buckling Pattern. Test No. 14.

30. Buckling Pattern. Test No. 18.

31. Buckling Pattern. Test No. 21.

32. Secondary Buckling. Test No. 18.

33. Temperature Distribution. Test No. 11.

34. Temperature Distribution. Test No. 16.

35. Temperature Distribution. Test No. 20.

36. Temperature Distribution. Test No. 21.

37. Theoretical Load Vs. Mid-Span Temperature Plot for Test No. 19.

38. Percentage Theoretical Loads Vs. Radius to Thickness Ratio.

39. Percentage Theoretical Temperatures Vs. Radius to Thickness Ratio.

40. Dimensionless Test Results.

41. Percentage Theoretical Deflections Vs. Radius to Thickness Ratio.

LIST OF SYMBOLS

Symbols

r	-	radius of curvature
L	-	length of cylinder
R	-	radius of cylinder
d	-	thickness of cylinder
D	-	flexural modulus of rigidity $D=Ed^3/12(1-\mu^2)$
E	-	modulus of elasticity
μ	-	Poisson's ratio
T	-	temperature rise above the unstrained state
u,v,w	-	displacement components in the median surface in the x,y,z, directions
P	-	normal primary surface force present prior to buckling
S	-	shear force present prior to buckling
ψ	-	Airy Stress function
N	-	total middle surface force
M	-	shell bending moment
Q	-	transverse shear force
ε	-	normal strain
σ	-	normal stress
γ	-	shear strain
τ	-	shear stress
U	-	elastic strain energy
V	-	potential energy of the external loads
ϕ	-	displacement function
α	-	coefficient of thermal expansion
λ	-	eigenvalue parameter
κ	-	curvature of shell
β	-	rotation of shell
q	-	general displacement term
z	-	dimensionless coefficient for geometry
k	-	dimensionless coefficient for loading
n	-	number of circumferential waves in buckling pattern
$\gamma_1 \cdots \gamma_8$	-	interpolation coefficients

Subscripts

o	-	in-plane component
x,y,z	-	denotes component in the axial, circumferential,radial direction
b	-	refers to bending component
B	-	refers to value at buckling
t	-	theoretical value
i	-	summation index
n	-	number of terms in the summation
m	-	maximum value
∇	-	indicates the change of the variable
ms	-	middle surface variable
E	-	experimental value
ψ	-	meridional direction
θ	-	circumferential direction

Superscripts

n	-	element node number
e	-	experimental value
t	-	theoretical value
1,2	-	refers to the type of stress coefficient
T	-	transpose of a matrix

CHAPTER I

INTRODUCTION

1.1 Statement of the Problem

Recent advances in the aerospace industry have imposed a great need for structures which have a very high strength to weight ratio. Lighter structures are also in demand for some of the key core components in nuclear reactors for low neutron absorption and better heat transfer capability. Shell type structures continue to be a main structural component in these industries.

In addition to an accurate stress analysis, the stability of shells as a function of the radius to thickness ratio is also an important design consideration. This stability problem may arise from a mechanical loading, or from a thermal loading from the harsh environment many of these shells must endure.

The use of long thin-walled tubes or pipes is common in engineering practise. Many of these tubes (or pipes) have to be held rigidly at the ends. These tubes are vulnerable to buckling due to the excess compressive longitudinal and circumferential stresses caused by the rising environmental temperature.

1.2 Scope of Thesis

This thesis deals with the analysis and subsequent experimental verification of the thermal buckling of thin-walled tubes rigidly held at both ends to a bulky attachment which acts as a heat sink, which in turn causes a non-uniform temperature profile along the tube length with the peak at the half-length.

The primary objectives of this thesis can be outlined as follows:

(1) To investigate the stability of thin-walled tubes that have higher length-to-radius and lower radius-to-thickness ratios than those tested by previous researchers.

(2) To compare the results derived from previous works to determine if the conclusions reached by other authors can be extended to the present work.

(3) To investigate if any conclusions drawn from the present work can be used to establish certain design criteria for thermally loaded shells.

(4) To recommend further studies necessary for a more complete understanding of the problem.

Chapter II reviews the related literature published on the thermal buckling of shells. Chapter III of this thesis reviews the basic equations of cylindrical shell stability problems and discusses some of the techiques available to solve these equations. Chapter IV describes the testing setup used in this work, and Chapter V discusses the results of that testing. The results are compared to other researcher's data and to a numerical solution of the problem. Chapter VI ends the thesis with the conclusions drawn from this work.

CHAPTER II

Literature Review

The equations for the stability of cylindrical shells have been made available for many years. An infinite series solution involving trigonometric functions was assumed by Lorenz in 1911 [1]* for solving the problem of a cylinder under uniform axial compression. Similar methods of solution were used by Southwell in 1913 [2] and von Mises in 1914 [3] for cylinders under uniform lateral pressure, and by Flügge in 1932 [4] for combined loading and bending.

In 1933 Donnell [5] proposed the use of a simpler form of stability equations in his solution for the buckling of cylinders subject to torsion. For simply supported cylinders,a solution was obtained by the use of an infinite trigonometric series.However,the problem of a cylinder with clamped ends could not be solved in this manner because of the divergence of the series solution. Singer [6] later showed that this result was due to the fact that Donnell's equation was an equilibrium equation and could not be used with the Galerkin method. Batdorf [7] proposed a modified equilibrium equation which could be used with the Galerkin method and proceeded to solve the problem of clamped shells under axial [8], shear [9], and combined axial and shear [10] loadings.

The first treatment of the thermal stability problem of

*Number in brackets denote the reference number cited in this thesis.

shells was undertaken by Hoff [11] in his analysis of cylindrical shells subjected to hoop stresses varying in the axial direction. The three main types of thermal conditions that could cause a shell to buckle are: 1) a temperature gradient through the shell thickness, 2) a circumferential temperature gradient, and 3) an axial temperature gradient. The first condition was shown to be very unlikely to cause buckling [12]. The second condition has been investigated by several authors. Hoff, Chao & Madsen [13] and Hill [14] investigated the problem of buckling due to heating along a thin axial strip, while Ross, Mayers & Jaworski [15] extended their methods to include wide axial bonds, and Frum and Baruch [16] examined the buckling effect of heating along two opposite axial generators. It was found that buckling can easily be induced as a result of circumferential temperature gradients, even if the latter are fairly small.

The third temperature condition was first examined by Hoff [11] who concluded that simply supported cylinders were not likely to fail under uniform heating conditions. This work was extended by Anderson [17] to include both simply supported and clamped cylinders under combinations of axial pressure and uniform heating, using the Galerkin method along with Batdorf's modified equilibrium equation. Zuk [18] also presented a solution for the uniformly heated clamped shell using Donnell's equation with the Galerkin method; however,this method was found to be in error,as discussed previously. An experimental investigation of the clamped cylinder subject to uniform heating was presented by Ross, Hoff & Horton [19]. This problem has also been extended to investigate the non-linear aspects of the stability suggested by Hoff [20] and Ross [21] using a column-spring analogy. These papers were an extension of the work done by Tsein [22], who used this analogy to obtain a better understanding of some of the parameters involved in shell buckling.

In recent years much of the work in instability problems has been concerned with numerical techniques in order that solutions may be obtained for more complicated structures and loadings. The two principal methods that have been used widely are the finite difference method and the finite element method.

The finite element method was first introduced to analyse shell buckling by assuming the shell to be made of a series of truncated cones [23]. This method was later abandoned due to computational difficulties, and the principal approach recently has been to use curved shell elements and to approximate the displacement components by polynomials. This method is used in references [24], [25].

The finite difference technique has been used by many investigators to approximate shell buckling problems. The principal effort in recent years has been the development of computer programs based on the finite difference approximation to the variational problem. Some examples are given in references [26] [27]. An excellent comparison of the finite element and finite difference method is given by Bushnell [28].

CHAPTER III

THEORETICAL BACKGROUND

3.1 The Differential Equations of Buckling

The differential equations of a continuous system may be obtained either by considering the equilibrium of a deformed element, or by utilizing the principle of stationary potential energy and the calculus of variations.

For fairly simple systems the former method is usually the easiest and the most direct. For more complicated systems the latter method may be a more direct procedure for obtaining the solutions.

The consideration of equilibrium of a deformed element is explained in detail in the next section, for both small and large deflection theories. The stationary potential energy method is then explained as presented in detail in Appendix A.

3.1.1 Equilibrium Method

The differential equation which is most widely used in cylindrical buckling problems is the Donnell equation for small deflections. This can be derived as follows:

Using the notation given in figure 1; the equilibrium equations of in-plane forces in the x, and y directions are:

$$\frac{\partial N_x}{\partial x} + \frac{\partial N_{xy}}{\partial y} = 0 \tag{1}$$

$$\frac{\partial N_y}{\partial y} + \frac{\partial N_{yx}}{\partial x} = 0 \tag{2}$$

where N_x, N_y = the in-plane forces in the x and y directions

N_{yx}, N_{xy} = the in-plane shear forces

For the z direction, taking the equilibrium:

$$- N_x \frac{\partial w}{\partial x} dy + \left(N_x + \frac{\partial N_x}{\partial x} dx\right)\left(\frac{\partial w}{\partial x} + \frac{\partial}{\partial x}\left(\frac{\partial w}{\partial x}\right) dx\right) dy - N_y \frac{\partial w}{\partial y} dx$$

$$+ \left(N_y + \frac{\partial N_y}{\partial y} dy\right)\left(\frac{\partial w}{\partial y} + \frac{\partial}{\partial y}\left(\frac{\partial w}{\partial y}\right) dy + \frac{dy}{R}\right) dx - N_{xy} \frac{\partial w}{\partial y} dy$$

$$+ \left(N_{xy} + \frac{\partial N_{xy}}{\partial x} dx\right)\left(\frac{\partial w}{\partial y} + \frac{\partial}{\partial x}\left(\frac{\partial w}{\partial y}\right) dx\right) dy - N_{yx} \frac{\partial w}{\partial x} dy$$

$$+ \left(N_{yx} + \frac{\partial N_{yx}}{\partial y} dy\right)\left(\frac{\partial w}{\partial x} + \frac{\partial}{\partial y}\left(\frac{\partial w}{\partial x}\right) dy\right) dx$$

where R = the radius of the cylinder

w = the radial displacement

After simplifying, neglecting terms of higher order, and using equations (1) and (2) the z components of the in-plane forces are:

$$N_x \frac{\partial^2 w}{\partial x^2} + 2N_{xy} \frac{\partial^2 w}{\partial x \partial y} + N_y\left(\frac{\partial^2 w}{\partial y^2} + \frac{1}{R}\right) dx\ dy \qquad (3)$$

The shear forces must be added to this for the equilibrium of the z direction. These forces are:

$$\left(\frac{\partial Q_x}{\partial x} + \frac{\partial Q_y}{\partial y}\right) dx\ dy \tag{4}$$

where Q_x and Q_y = the normal shear forces

taking moments about the x axis yields

$$\left(\frac{\partial M_y}{\partial y} - \frac{\partial M_{xy}}{\partial x} - \frac{1}{2}\frac{\partial Q_x}{\partial x}\ dx - Q_y - \frac{\partial Q_y}{\partial y}\ dy\right) dxdy = 0$$

where M_x, M_y, M_{xy} = the shell bending moments

After simplifying one gets

$$\frac{\partial M_y}{\partial y} - \frac{\partial M_{xy}}{\partial x} - Q_y = 0 \tag{5}$$

Similarily for the x direction

$$\frac{\partial M_x}{\partial x} - \frac{\partial M_{yx}}{\partial y} - Q_x = 0 \tag{6}$$

Inserting Q_x and Q_y from equations (5) and (6) into equation (4) the total equilibrium in the z direction becomes:

$$\frac{\partial^2 M_x}{\partial x^2} - 2\frac{\partial^2 M_{xy}}{\partial x \partial y} + \frac{\partial^2 M_y}{\partial y^2} + N_x \frac{\partial^2 w}{\partial x^2} + 2N_{xy} \frac{\partial^2 w}{\partial x \partial y}$$

$$+ N_y\left(\frac{1}{R} + \frac{\partial^2 w}{\partial y^2}\right) = 0 \tag{7}$$

The moment curvature relationships for the cylinder will be derived from:

$$M_x = \int_{d/2}^{d/2} \sigma_x z dz \tag{8}$$

$$M_y = \int_{d/2}^{d/2} \sigma_y z dz \tag{9}$$

$$M_{xy} = \int_{d/2}^{d/2} \tau_{xy} z dz \tag{10}$$

The shell displacements u, v are separated into middle surface strains (resulting only from the in-plane forces N) and bending strains (resulting only from the moments M)

$$\left.\begin{aligned} u &= u_o + u_b \\ v &= v_o + v_b \\ \varepsilon_x &= \varepsilon_{xo} + \varepsilon_{xb} \\ \varepsilon_y &= \varepsilon_{yo} + \varepsilon_{yb} \\ \gamma_{xy} &= \gamma_{xyo} + \gamma_{xyb} \end{aligned}\right\} \quad (11)$$

The bending strains in the above expressions can be expressed in terms of displacements as following:

$$\left.\begin{aligned} \varepsilon_{xb} &= \frac{\partial u_b}{\partial x} \\ \varepsilon_{yb} &= \frac{\partial v_b}{\partial y} \\ \gamma_{xyb} &= \frac{\partial u_b}{\partial y} + \frac{\partial v_b}{\partial x} \end{aligned}\right\} \quad (12)$$

Since during bending plane sections are assumed to remain plane we have:

$$\left.\begin{aligned} u_b &= - z \frac{\partial w}{\partial x} \\ v_b &= - z \frac{\partial w}{\partial y} \end{aligned}\right\} \quad (13)$$

so the equations for total strain become

$$\varepsilon_x = - z \frac{\partial^2 w}{\partial x^2}$$

$$\left.\begin{aligned} \varepsilon_y &= -z\frac{\partial^2 w}{\partial y^2} \\ \gamma_{xy} &= -2z\frac{\partial^2 w}{\partial x \partial y} \end{aligned}\right\} \quad (14)$$

Now, using the well-known stress-strain equations for plane stress this becomes

$$\left.\begin{aligned} \sigma_{xb} &= -\frac{Ez}{1-\mu^2}\left(\frac{\partial^2 w}{\partial x^2} + \mu\frac{\partial^2 w}{\partial y^2}\right) \\ \sigma_{yb} &= -\frac{Ez}{1-\mu^2}\left(\frac{\partial^2 w}{\partial y^2} + \mu\frac{\partial^2 w}{\partial x^2}\right) \\ \tau_{xyb} &= -\frac{Ez}{1+\mu}\left(\frac{\partial^2 w}{\partial x \partial y}\right) \end{aligned}\right\} \quad (15)$$

Substituting this into equations (8), (9), and (10) gives:

$$M_x = -D\left(\frac{\partial^2 w}{\partial x^2} + \mu\frac{\partial^2 w}{\partial y^2}\right) \quad (16)$$

$$M_y = -D\left(\frac{\partial^2 w}{\partial y^2} + \mu\frac{\partial^2 w}{\partial x^2}\right) \quad (17)$$

$$M_{xy} = D(1-\mu)\left(\frac{\partial^2 w}{\partial x \partial y}\right) \quad (18)$$

where $D = Ed^3/12(1-\mu^2)$

The middle surface strains for the element are:

$$\varepsilon_{xo} = \frac{\partial u_o}{\partial x} + \frac{1}{2}\left(\frac{\partial w}{\partial x}\right)^2 \tag{19}$$

$$\varepsilon_{yo} = \frac{\partial v_o}{\partial y} + \frac{1}{2}\left(\frac{\partial w}{\partial y}\right)^2 - \frac{w}{R} \tag{20}$$

$$\gamma_{xyo} = \frac{\partial u_o}{\partial y} + \frac{\partial v_o}{\partial x} + \frac{\partial w}{\partial x}\frac{\partial w}{\partial y} \tag{21}$$

For small deflections these can be simplified to:

$$\varepsilon_{xo} = \frac{\partial u_o}{\partial x} \tag{22}$$

$$\varepsilon_{yo} = \frac{\partial v_o}{\partial y} - \frac{w}{R} \tag{23}$$

$$\gamma_{xyo} = \frac{\partial u_o}{\partial y} + \frac{\partial v_o}{\partial x} \tag{24}$$

Using the stress-strain relationships equations (15) the following middle surface force-deflection equations are obtained:

$$N_x^1 = \sigma x_o d = \frac{Ed}{1-\mu^2}\left[\frac{\partial u_o}{\partial x} +\mu \frac{\partial v_o}{\partial y} -\mu \frac{w}{R}\right] \tag{25}$$

$$N_y^1 = \sigma y_o d = \frac{Ed}{1-\mu^2}\left[\frac{\partial v_o}{\partial y} +\mu \frac{\partial u_o}{\partial x} - \frac{w}{R}\right] \tag{26}$$

$$N_{xy}^1 = \tau xy_o d = \frac{Ed(1-\mu)}{2(1-\mu^2)}\left[\frac{\partial u_o}{\partial y} + \frac{\partial v_o}{\partial x}\right] \tag{27}$$

These forces are due to loads present due to buckling. Setting the pre-buckling forces equal to:

$$N_x = P_x$$

$$N_y = P_y$$

$$N_{xy} = S_{xy}$$

and now introducing the secondary buckling forces, equations (25) to (27), the total forces are:

$$N_x = \frac{Ed}{1-\mu^2}\left(\frac{\partial u_o}{\partial x} + \mu \frac{\partial v_o}{\partial y} - \mu \frac{w}{R}\right) + P_x \tag{28}$$

$$N_y = \frac{Ed}{1-\mu^2}\left(\frac{\partial v_o}{\partial y} + \mu \frac{\partial u_o}{\partial x} - \frac{w}{R}\right) + P_y \tag{29}$$

$$N_{xy} = \frac{Ed(1-\mu)}{2(1-\mu^2)}\left(\frac{\partial u_o}{\partial y} + \frac{\partial v_o}{\partial x}\right) + S_{xy} \tag{30}$$

Inserting the appropriate moment-deflection relationships in equations (16) to (18) and middle surface force-deflection equations (28) to (30) into the three equilibrium equations in (1), (2) and (7) the equations of equilibrium for a cylindrical shell using small deflection theory become:

$$\frac{\partial^2 u_o}{\partial x^2} + \frac{(1-\mu)}{2}\frac{\partial^2 u_o}{\partial y^2} + \frac{(1+\mu)}{2}\frac{\partial^2 v_o}{\partial x \partial y} - \frac{\mu}{R}\frac{\partial w}{\partial x} = 0 \tag{31}$$

$$\frac{\partial^2 v_o}{\partial y^2} + \frac{1-\mu}{2}\frac{\partial^2 v_o}{\partial x^2} + \frac{(1+\mu)}{2}\frac{\partial^2 u_o}{\partial x \partial y} - \frac{1}{R}\frac{\partial w}{\partial y} = 0 \tag{32}$$

$$- D\left(\frac{\partial^4 w}{\partial x^4} + 2\frac{\partial^4 w}{\partial x^2 \partial y^2} + \frac{\partial^4 w}{\partial y^4}\right) + \left(N_x^1 + P_x\right)\frac{\partial^2 w}{\partial x^2} + \left(N_y^1 + P_y\right)\left(\frac{1}{R} + \frac{\partial^2 w}{\partial y^2}\right)$$

$$+ 2(N^1{}_{xy} + S_{xy})\frac{\partial^2 w}{\partial x \partial y} = 0 \tag{33}$$

The initial curvature and primary middle surface forces in equation (33) are much larger than the curvatures due to bending, and the secondary middle surface forces. This makes it possible to re-arrange equation (33) to the form:

$$- D\left(\frac{\partial^4 w}{\partial x^4} + 2\frac{\partial^4 w}{\partial x^2 \partial y^2} + \frac{\partial^4 w}{\partial y^4}\right) + P_x \frac{\partial^2 w}{\partial x^2} + P_y \frac{\partial^2 w}{\partial y^2} + \frac{P_y}{R}$$

$$+ \frac{1}{R}\frac{Ed}{1-\mu^2}\left(\frac{\partial v_o}{\partial y} - \frac{w}{R} + \mu\frac{\partial u_o}{\partial x}\right) + 2 S_{xy}\frac{\partial^2 w}{\partial x \partial y} = 0 \tag{34}$$

Because all the secondary middle surface forces are not negligible in linear shell theory the three equilibrium equations (31), (32) and (34) are coupled and must be solved simultaneously. It is often more convenient to combine the three equations to obtain a single equation in w. If equation (32) is operated on by $\partial^2/\partial x \partial y$, and equation (31) by $\partial^2/\partial x^2$, and $\partial^2/\partial y^2$, one obtains three equations which may be reduced to:

$$\nabla^4 u = \frac{\mu}{R}\frac{\partial^3 w}{\partial x^3} - \frac{1}{R}\frac{\partial^3 w}{\partial y^2 \partial x} \tag{35}$$

where $$\nabla^4 = \frac{\partial^4}{\partial x^4} + 2\frac{\partial^4}{\partial x^2 \partial y^2} + \frac{\partial^4}{\partial y^4}$$

Similarily if equation (31) is operated on by $\partial^2/\partial x\, \partial y$, and equation (32) by $\partial^2/\partial x^2$ and $\partial^2/\partial y^2$ one obtains three equations which may be reduced to the form:

$$\nabla^4 v = \frac{\mu+2}{R}\frac{\partial^3 w}{\partial x^2 \partial y} + \frac{1}{R}\frac{\partial^3 w}{\partial y^3} \tag{36}$$

Equation (34) is now operated on by ∇^4, yielding:

$$- D\nabla^8 w + \nabla^4\left(P_x \frac{\partial^2 w}{\partial x^2} + P_y \frac{\partial^2 w}{\partial y^2} + 2\, S_{xy} \frac{\partial^2 w}{\partial x \partial y}\right) +$$

$$\frac{1}{R}\frac{Ed}{(1-\mu^2)}\left(\nabla^4 \frac{\partial v}{\partial y} + \mu\, \nabla^4 \frac{\partial u}{\partial x} - \frac{1}{R}\nabla^4 w\right) = 0 \tag{37}$$

Operating on equation (35) by $\partial/\partial x$, and equation (36) by $\partial/\partial y$, and substituting the results in equation (37) one obtains:

$$D\nabla^8 w - \nabla^4\left(P_x \frac{\partial^2 w}{\partial x^2} + P_y \frac{\partial^2 w}{\partial y^2} + 2\, S_{xy} \frac{\partial^2 w}{\partial x \partial y}\right) + \frac{Ed}{R^2}\frac{\partial^4 w}{\partial x^4} = 0 \tag{38}$$

This equation is known as the Donnell small deflection equation for shell buckling. As was shown by Batdorf [7] the use of equation (38) implies certain boundary conditions on the solution. These are, for simply supported edges:

$$w = \frac{\partial^2 w}{\partial x^2} = v = \frac{\partial^2 \psi}{\partial^2 y} = 0 \quad (x = \text{constant}) \tag{39}$$

$$w = \frac{\partial^2 w}{\partial y^2} = u = \frac{\partial^2 \psi}{\partial x^2} = 0 \quad (y = \text{constant}) \tag{40}$$

For clamped edges the Donnell small deflection equation (38) should not be used. This will be discussed in more depth in section 3.2.3. The more realistic solution to the buckling problems and all post buckling analysis should involve the large deflection theory. The equilibrium equations (1), (2) and (7) remain valid since no assumptions were made to limit these to small displacements. These are repeated here:

$$\frac{\partial N_x}{\partial x} + \frac{\partial N_{xy}}{\partial y} = 0 \tag{1}$$

$$\frac{\partial N_x}{\partial y} + \frac{\partial N_{xy}}{\partial x} = 0 \tag{2}$$

$$\frac{\partial^2 M_x}{\partial x^2} - 2\frac{\partial^2 M_{xy}}{\partial x \partial y} + \frac{\partial^2 M_y}{\partial y^2} + N_x \frac{\partial^2 w}{\partial x^2} + 2N_{xy}\frac{\partial^2 w}{\partial x \partial y}$$

$$+ N_y\left(\frac{1}{R} + \frac{\partial^2 w}{\partial y^2}\right) = 0 \tag{7}$$

Transverse deflections are not small with respect to the surface thickness, but they are still small compared to the shell dimensions so the moment deflection equations (16), (17) and (18) are still valid. Equation (7) may then be written as:

$$- D\left(\frac{\partial^4 w}{\partial x^4} + 2\frac{\partial^4 w}{\partial x^2 \partial y^2} + \frac{\partial^4 w}{\partial y^4}\right) + N_x \frac{\partial^2 w}{\partial x^2} + 2N_{xy} \frac{\partial^2 w}{\partial x \partial y}$$

$$+ N_y\left(\frac{1}{R} + \frac{\partial^2 w}{\partial y^2}\right) = 0 \tag{41}$$

The strain-displacement equations can no longer be simplified, so equations (19) to (21) must be used in their entirety. Including constant thermal strain in the middle surface strain equations:

$$\varepsilon_{xo} = \frac{1}{Ed}(N_x - \mu N_y) + \alpha T \tag{42}$$

$$\varepsilon_{yo} = \frac{1}{Ed}(N_y - \mu N_x) + \alpha T \tag{43}$$

$$\gamma_{xyo} = \frac{2}{Ed}(1 + \mu)N_{xy} \tag{44}$$

Now, to obtain the compatibility equation, equation (19) is differentiated twice with respect to y, and also differential equation (20) twice with respect to x and, as for equation (21), successively with respect to x and y to obtain:

$$\frac{\partial^2 \varepsilon_{xo}}{\partial y^2} + \frac{\partial^2 \varepsilon_{yo}}{\partial x^2} - \frac{\partial^2 \gamma_{xyo}}{\partial x \partial y} = \left(\frac{\partial^2 w}{\partial x \partial y}\right)^2 - \frac{\partial^2 w}{\partial x^2}\frac{\partial^2 w}{\partial y^2} - \frac{1}{R}\frac{\partial^2 w}{\partial x^2} \tag{45}$$

Introducing the stress function ψ defined by:

$$N_x = d\frac{\partial^2\psi}{\partial y^2} \qquad N_y = d\frac{\partial^2\psi}{\partial x^2} \qquad N_{xy} = -d\frac{\partial^2\psi}{\partial x\partial y} \tag{46}$$

The strain equations (42), (43) and (44) become:

$$\varepsilon_{xo} = \frac{1}{E}\left(\frac{\partial^2\psi}{\partial y^2} - \mu\frac{\partial^2\psi}{\partial x^2}\right) + \alpha T \tag{47}$$

$$\varepsilon_{yo} = \frac{1}{E}\left(\frac{\partial^2\psi}{\partial x^2} - \mu\frac{\partial^2\psi}{\partial y^2}\right) + \alpha T \tag{48}$$

$$\gamma_{xyo} = \frac{-2(1+\mu)}{E}\frac{\partial^2\psi}{\partial x\partial y} \tag{49}$$

Using the relationships in equations (46) to (49) the equilibrium equation (41) and compatibility equation (45) may be written as:

$$\frac{\partial^4 w}{\partial w^4} + 2\frac{\partial^4 w}{\partial x^2\partial y^2} + \frac{\partial^4 w}{\partial y^4} - \frac{d}{D}\left[\frac{\partial^2\psi}{\partial y^2}\frac{\partial^2 w}{\partial x^2} - 2\frac{\partial^2\psi}{\partial x\partial y}\frac{\partial^2 w}{\partial x\partial y} + \frac{\partial^2\psi}{\partial x^2}\left(\frac{1}{R} + \frac{\partial^2 w}{\partial y^2}\right)\right] = 0 \tag{50}$$

$$\frac{\partial^4\psi}{\partial x^4} + \frac{2\partial^2\psi}{\partial x^2\partial y^2} + \frac{\partial^4\psi}{\partial y^4} = E\left[\left(\frac{\partial^2\psi}{\partial x\partial y}\right)^2 - \frac{\partial^2 w}{\partial x^2}\frac{\partial^2 w}{\partial y^2} - \frac{1}{R}\frac{\partial^2 w}{\partial x^2}\right] - E\alpha\nabla^2 T \tag{51}$$

These two equations are the differential equations for shell buckling on large deflection theory often referred to as the Karman-Donnell equations. They are, in general, very difficult to solve and much effort has gone into developing their solutions for different buckling problems.

Note that the constant temperature increase term is not present in the equilibrium equation directly. It is introduced through the equations of the stress function.

3.1.2 Variational Methods

The differential equations derived from the energy concept are based on the stationary potential energy theorem which states: An elastic structure is in equilibrium if no change takes place in the total potential energy of the system when its displacement is changed by a small arbitrary amount.

This can be expressed mathematically as:

$$\delta(U + V) = 0 \tag{52}$$

where U = the elastic strain energy

V = the potential energy of external loads

The strain energy of a thin elastic cylinder is given as [29]:

$$= \frac{1}{2}\iint \frac{Ed}{(1-\mu^2)}\left\{(\varepsilon_{xo} + \varepsilon_{yo})^2 + 2(1-\mu)\left(\frac{1}{4}\gamma_{xyo}^2 - \varepsilon_{xo}\,\varepsilon_{yo}\right)\right\} +$$

$$D\left\{\left(\frac{\partial w}{\partial x} + \frac{\partial w}{\partial y}\right)^2 = 2\,(1-\mu)\left(\frac{\partial^2 w}{\partial x \partial y} - \frac{\partial w}{\partial x}\frac{\partial w}{\partial y}\right)\right\} \tag{53}$$

A variational operation is taken on u, v, and w using equation (53), and the three equations of equilibrium can be derived. This technique was used by Sunakawa [30] in a more general case where the loading included axially symmetric temperature increase with a temperature gradient through the wall thickness, and external pressure. The equations derived reduce identically to equations (50), and (51) of this paper for the case with no temperature gradient through the wall and no external applied pressure. It should be noted that Sunakawa's equation for equilibrium has two extra terms due to his using an extra term in his strain-displacement functions.

This technique is described in more detail in Appendix A.

3.2 Theoretical Methods of Solution

The differential equations for stability problems are generally in very complex forms and exact solutions are impractical for most important cases. For this reason there has been a great deal of effort put into finding approximate solutions. These methods must be reasonably simple to use, yet they must be capable of yielding results with good accuracy.

3.2.1 The Direct Substitution Method

For a few simple buckling problems such as a simply-supported, axially loaded cylinder, the Donnell equation for small deflections can be solved by the use of an assumed displacement field which is generally in a series consisting of trigonometric functions.

This method is effective for simple cases, but for more complicated loads or clamped boundary conditions,these assumed displacement fields cannot be used. For these cases,where the exact form of the solution is not known,the following methods are considered to be better as they allow the solution to be known to a certain fixed accuracy according to the requirement.

3.2.2 The Rayleigh-Ritz Method

The rigorous application of the stationary potential energy theorem to more complicated structures has two main disadvantages. First, the variational calculus involved is much too complex to be used for routine problem solving, and secondly only the governing differential equations are obtained, and not their solution. To avoid these problems an approximate technique known as the Rayleigh-Ritz technique is used to reduce the problem from an infinite to a finite number of degrees of freedom. This is done by assuming an appropriate shape for the deflection of the system.

The deflection can be expressed in the form:

$$w\,(x,y,z) = a_1\ f_1\,(x,y,z) + a_2\ f_2\,(x,y,z) + \dots\ \dots$$

$$a_n\ f_n\,(x,y,z) \tag{54}$$

where a_n = arbitrary constants

f_n = assumed deflection shape function

The deflection functions should satisfy the geometric boundary conditions but not necessarily the natural ones. The theorem of Stationary Potential Energy can then be stated:

$$\delta(u + v) = \frac{\partial(u+v)}{\partial a_1}\delta a_1 + \frac{\partial(u+v)}{\partial a_2}\delta a_2 + \dots\ \dots$$

$$\frac{\partial(u+v)}{\partial a_n}\delta a_n = 0 \tag{55}$$

This is true providing the total potential energy can be expressed as a function of $w(x,y,z)$ only. Because δ_1, δ_2, ... δ_n are arbitrary equation (55) becomes:

$$\frac{\partial(u+v)}{\partial a_1} = 0, \quad \frac{\partial(u+v)}{\partial a_2} = 0, \ldots \frac{\partial(u+v)}{\partial a_n} = 0 \qquad (56)$$

Thus, using the above method a system of n homogeneous equations with n unknowns is set up. By setting the determinant of all the coefficients equal to zero a characteristic equation is set up with the smallest resulting eigenvalue becoming the critical load of the system.

This method, although very useful for many problems, is not used often to solve the problem of shell buckling involving finite deflections since the expression for strain energy given in equation (A-8) is very complicated and tedious to obtain.

3.2.3 The Galerkin Method

The Galerkin method is, again, an approximate method of analysis which reduces the deflection function from an infinite to a finite number of degrees of freedom. The main distinction between the Rayleigh-Ritz method and the Galerkin method is that the former begins with an expression for total potential energy, while the latter begins with an equation of equilibrium.

The engineering formulation of the Galerkin method is derived using the principle of virtual displacements, with the equation of equilibrium expressed as a generalized force. The

Galerkin integrals have the dimensions of work and the method is equivalent to the Rayleigh-Ritz method. In the mathematical formulation of the method [31] the Galerkin integrals are obtained by imposing an orthogonality condition on the error function obtained by substituting the assumed shape function into the differential equation. This formulation is not connected to the variational problem and is not, in general, equivalent to the Rayleigh-Ritz method.

In order for the Galerkin method to be equivalent to the Rayleigh-Ritz method and thus yield an upper bound solution to the buckling problem there are two conditions which must be satisfied. The method must be applied to the equilibrium equation of the problem that resulted from the variation of the total potential energy, and this must be in the form of a generalized force or moment.

The Galerkin method is applied as follows:

When the variational method is used to minimize the total potential energy of the system the following form of equation is obtained:

$$\iiint Q(w)\ dw\ dxdydz + B.C. = 0 \tag{57}$$

where Q = the differential operator of the equilibrium equation

B.C. = the natural boundary conditions

w = the dependent displacement variable

An approximate displacement function is assumed which satisfies the geometric and natural boundary conditions. This can usually be accomplished by assuming a power series and evaluating as many arbitrary constants as possible from the boundary conditions.

$$\Theta = \sum_{i=1}^{n} a_i \; g_i(x,y,z)$$

where Θ = the total approximate displacement function

n = the number of terms

a_i = the arbitrary constant

$g_i(x,y,z)$ = the approximate displacement functions

Since these all satisfy the boundary conditions equation 57 becomes:

$$\iiint Q(\theta) \; \delta\Theta \; dxdydz = 0 \qquad (58)$$

Since $\quad d\theta = \frac{\partial\theta}{\partial a_1} \delta a_1 + \frac{\partial\theta}{\partial a_2} \delta a_2 \ldots.$

$$= \sum_{i=1}^{n} g_i(x,y,z) \; \delta a_i$$

So equation (58) becomes:

$$\iiint Q(\theta) \sum_{i=1}^{n} g_i(x,y,z) \; \delta a_i \; dxdydz = 0$$

Since the n functions g_i used are assumed to be independent of each other each, and every term must equal zero. Finally, since the choice of a_i is arbitrary

$$\iiint Q(\theta)\ g_i(x,y,z)\ dxdydz = 0 \qquad (59)$$

In order to use this method to solve a differential equation the equation must have only one independent variable and is not coupled such as the equilibrium equations for buckling. For this reason the Donnell equation cannot be used with this method as it is not the equilibrium equation derived from the variation of total potential energy and it leads to a divergent trigonometric series. The equation for radial equilibrium (equation 34) should be used except that this equation has a term coupling it to the equilibrium requirement in the x, and y direction. Batdorf [7] has modified this coupling term to make theequation adaptable to the Galerkin technique.

By introducing a stress function ψ, equation (33) can be rewritten as:

$$-D\nabla^4 w + \left(Px\ \frac{\partial^2 w}{\partial x^2} + Py\ \frac{\partial^2 w}{\partial y^2} + 2\ Sxy\ \frac{\partial^2 w}{\partial x \partial y}\right) + \frac{1}{R}\left(Py + \frac{\partial^2 \psi}{\partial x^2}\right) = 0 \qquad (60)$$

The compatibility equation for small deflection theory is:

$$\nabla^4 \psi + \frac{E}{R}\,\frac{\partial^2 w}{\partial x^2} = 0 \qquad (61)$$

Solving equation (61) for $\frac{\partial^2\psi}{\partial x^2}$ and substituting it into equation (60) yields:

$$-D\nabla^4 w + \frac{Ed}{R^2}\nabla^{-4}\frac{\partial^2 w}{\partial x^2} + \left(P_x \frac{\partial^2 w}{\partial x^2} + P_y \frac{\partial^2 w}{\partial y^2} + 2S_{xy}\frac{\partial^2 w}{\partial x \partial y}\right) + \frac{P_y}{R} = 0 \tag{62}$$

This equation is still in a form that, if solved by means of the Galerkin method,is still an upper bound solution to the problem for buckling. Indeed,this has been done for several types of buckling problems.

For a cylinder Batdorf [7] has proposed the following approximate deflection functions:

$$w = \sin\frac{\pi y}{\lambda}\sum_{m=1}^{\infty} a_m \sin\frac{m\pi x}{L}$$

for simply supported ends, and (63)

$$w = \sin\frac{\pi y}{\lambda}\sum_{m=1}^{\infty} \cos\left\{(m-1)\frac{\pi x}{L}\right\} - \cos\left\{(m+1)\frac{\pi x}{L}\right\}$$

for clamped ends.

Anderson [17] used the above equations to solve the buckling of a cylinder under combinations of axial pressure and heating. The thermal stresses (circumferential only) were expanded into a Fourier series which was substituted into equation (62) and solved for a Fourier series circumferential stress component.

It is not possible to solve the large deflection buckling equation (50) by this method as each equation of equilibrium is coupled to the other equations and cannot be easily uncoupled as is the case with the small deflection equation.

3.3 Numerical Methods of Solution

3.3.1 Successive Approximation

It is very difficult to obtain a solution for the non-linear large deflection buckling equations (50) and (51). Sunakawa [30] has used the method of successive approximations to obtain their solution. In this method the equilibrium equation (50) is integrated satisfying the boundary conditions on radial displacements and slopes, allowing the deformation mode to be expressed through the unknown axial stress. The compatability equation (51) is then solved subject to the in-plane boundary conditions, and substituting the deformation expression obtained from the equilibrium equation.

The result from this is a transcendental equation relating the axial stress to the temperature rise. This cannot be solved explicitly and so an iterative technique such as the Wegstein or Newton-Raphson method must be used. Once the axial stress is known for a particular temperature rise the solution to the equilibrium equation may be used to obtain the deformation mode.

The equations used in this method are extremely long and cumbersome and the derivation is given in Appendix B.

In his solution Sunakawa assumed the temperature distribution to be uniform around the circumference of the cylinder and symmetric with respect to the cylinder half length in the axial direction, in the form of:

$$T = \Sigma_i T_i \cos\left(\frac{i\pi n}{2L}\right) \quad (i = 0, 2, 4, \ldots\ldots \text{ even})$$

The symmetric temperature profile made this method a useful way of analysing the case presented in this thesis. In addition, the programming required for this technique is much simpler than what would be required for a finite element, or finite difference program to solve this problem. A listing of this program and some typical output is given in Appendix C.

3.3.2 Finite Difference and Finite Element Methods

The finite difference and finite element methods are techniques for discretizing the continuous system and replacing the partial differential equations governing the continuum by a series of algebraic equations. These equations may then be solved by a digital computer.

For simple cases the equilibrium equation can be solved by applying the finite difference method directly. A set of simultaneous, homogenous algebraic equations is obtained with the characteristic value on the diagonal. Setting the determinant of these equations equal to zero yields the characteristic equation, and the eigenvalues for the problem. This may be done for the Donnell small deflection buckling equation (38) but the expression for the ∇^8 term is very tedious.

A more general and common technique is to use a variational approach for employing the finite element or finite difference methods.

The second variation of total potential energy for a shell of resolution along arc-length A-B is given as [29] is:

$$\frac{1}{2}\,\delta^2 U = \frac{1}{2}\int_A^B \left(\{\varepsilon\}^T [c]\,\{\varepsilon\} + \lambda\,\{\beta\}^T [No]\,\{\beta\}\right) r\,ds \qquad (64)$$

where $\{\varepsilon\} = [\varepsilon_\psi,\ \varepsilon_\theta,\ \gamma_{\psi\theta},\ \kappa_{\psi\psi},\ \kappa_{\theta\theta},\ 2\kappa_{\psi\theta}]^T$

is the strain vector,

$$\{\beta\} = [\beta_\psi,\ \beta_\theta,\ \beta_z]^T$$

is the rotation vector,

$$[N_o] = \begin{bmatrix} N_{10} & 0 & 0 \\ 0 & N_{20} & 0 \\ 0 & 0 & (N_{10}+N_{20}) \end{bmatrix}$$

is the prestress matrix, and matrix [c] is a matrix of coefficients relating stress and moment resultants to strains and changes in curvature, with the nonzero coefficients:

$$c_{11} = c_{22}\ \frac{Ed}{1-\mu^2} \qquad c_{12} = c_{21} = -\mu c_{11}$$

$$c_{33} = \frac{(1-\mu)\ Ed}{2} \qquad c_{44} = c_{55} = D$$

$$c_{66} = 2(1-\mu)D \qquad c_{45} = c_{54} = \mu D$$

The assumptions implied in equation (64) are:

(1) That the prestress matrix $[N_o]$ is known and linearly dependent on the eigenvalue parameter λ (i.e. the prebuckling rotations are negligible).

(2) That the material is linearly elastic so that the stress matrix is simply related to the strain matrix by the relationship

$$\{S\} = [c]\ \{\varepsilon\}$$

The strain vector used here is in a different form from those given in section 3.1. This is due to the fact that the relationships used in this section are valid for any shell of revolution while those of section 3.1 are derived for a cylindrical shell. For this section the reader is referred to the more general coordinate system of Fig. (1B).

It should also be noted that the strain displacement relationships given in equations (65) assume an axisymmetric loading so that the incremental displacements vary harmonically with the circumferential shell coordinate θ.

$$
\left.
\begin{aligned}
\varepsilon_{\psi} &= \frac{\partial u}{\partial s} + \frac{w}{r\psi} \\
\varepsilon_{\theta} &= -n\frac{v}{R} + \frac{u}{R}\frac{\partial R}{\partial s} + \frac{w}{r_{\theta}} \\
\gamma_{\psi\theta} &= \frac{\partial v}{\partial s} - \frac{v}{R}\frac{\partial R}{\partial s} + n\frac{u}{R} \\
\kappa_{\psi\psi} &= \frac{\partial \beta_{\psi}}{\partial s} \\
\kappa_{\theta\theta} &= -\frac{n}{R}\beta_{\theta} + \frac{\beta_{\psi}}{R}\frac{\partial R}{\partial s} \\
\kappa_{\psi\theta} &= \frac{-n\beta_{\psi}}{R} + \frac{\beta_{\theta}}{R}\frac{\partial R}{\partial s} + \frac{1}{r_{\theta}}\frac{\partial v}{\partial s} \\
\beta_{\psi} &= \frac{\partial w}{\partial s} - \frac{u}{r_{\psi}} \\
\beta_{\theta} &= \frac{nw}{R} - \frac{v}{r_{\theta}} \\
\beta_{z} &= \frac{1}{2}\quad \frac{nu}{R} - \frac{\partial v}{\partial s} - \frac{v}{R}\frac{\partial R}{\partial s}
\end{aligned}
\right\} \quad (65)
$$

With this identical basis the finite difference and finite element methods can be formulated. The differences between the two methods lie mainly in the selection of the generalized displacement components. In the finite element method these components are selected to be located at the nodal points of the elements, whereas in the finite difference method the displacement components u_i, v_i,

w_i do not necessarily occur at a given node. With the finite difference method the rotation β_ψ is not a nodal point unknown and the displacement polynomial for w is not necessarily restricted to the domain of the element.

Two common interpolation functions used in shell analysis are, for finite element analysis:

$$\left.\begin{array}{l} u = \gamma_1 + \gamma_2 s \\ \\ v = \gamma_3 + \gamma_4 s \\ \\ w = \gamma_5 + \gamma_6 s + \gamma_7 s^2 + \gamma_8 s^3 \\ \\ \text{and finite difference analysis} \\ \\ u = \gamma_1 + \gamma_2 s \\ \\ u = \gamma_3 + \gamma_4 s \\ \\ w = \gamma_5 + \gamma_6 s + \gamma_7 s^2 \end{array}\right\} \quad (66)$$

The elements used with these displacement functions are shown in Fig. 2 .

It should be noted that for finite difference analysis the interpolation functions are related, simply, to the usual difference formuli by the relationships;

$$\left.\begin{aligned} \frac{\partial u}{\partial s} &= \frac{u_{i+1} - u_{i-1}}{2\ell} = \gamma_2 \quad \frac{\partial v}{\partial s} = \frac{v_{i+1} - v_{i-1}}{2\ell} = \gamma_4 \\ \frac{\partial^2 w}{\partial s^2} &= \frac{1}{\ell^2} (w_{i+1} - 2w_i + w_{i-1}) = 2\,\gamma_7 \end{aligned}\right\} \quad (67)$$

In order to obtain the stationary value of the second variation of total potential energy (equation (64)) it must be expressed in terms of the nodal point variables {q}.

Using the interpolation functions the nodal variables can be expressed as:

$$\{q\} = [A]\,\{\gamma\} \qquad (68)$$

where {q} is the generalized displacement vector,

[A] is a matrix defined by the interpolation functions chosen (as in equation (66)),

$\{\gamma\}$ is the vector of the interpolation coefficients chosen.

The exact form of the vectors and matrix of equation (68) will depend on the nature of the interpolation functions chosen. For example, using the finite element model in Fig. 2, these become:

$$\{q\} = \left\{u_i,\ u_{i+1},\ v_i,\ v_{i+1},\ w_i,\ w_{i+1},\ \frac{\partial w}{\partial s}_i,\ \frac{\partial w}{\partial s}_{i+1}\right\}$$

$$[A] = \begin{bmatrix} 1 & 0 & 0 & 0 & 0 & 0 & 0 & 0 \\ 1 & \ell & 0 & 0 & 0 & 0 & 0 & 0 \\ 0 & 0 & 1 & 0 & 0 & 0 & 0 & 0 \\ 0 & 0 & 1 & \ell & 0 & 0 & 0 & 0 \\ 0 & 0 & 0 & 0 & 1 & 0 & 0 & 0 \\ 0 & 0 & 0 & 0 & 1 & \ell & \ell^2 & \ell^3 \\ 0 & 0 & 0 & 0 & 0 & 1 & 0 & 0 \\ 0 & 0 & 0 & 0 & 0 & 1 & 2\ell & 3\ell^2 \end{bmatrix}$$

$$\{\gamma\} = \{\ell_1, \ell_2, \ell_3, \ell_4, \ell_5, \ell_6, \ell_7, \ell_8\}$$

Since the derivatives of the generalized displacements are easily obtained in terms of the ℓ coefficients, equations (65) can be expressed as:

$$\{\varepsilon\} = [F]\ \{\gamma\}$$

$$\{\beta\} = [G]\ \{\gamma\}$$

where the matrices [F] and [G] give the relationship between the strain (and rotation) vector to the interpolation functions. These will vary according to the interpolation function used. Inverting equation 68 becomes:

$$\{\gamma\} = [A]^{-1}\ \{q\} \equiv [B]\ \{q\}$$

Substituting this gives the element strains as a function of the nodal, or generalized displacement vector.

$$\left.\begin{aligned} \{\varepsilon\} &= [F]\ [B]\ \{q\} \\ \{\beta\} &= [G]\ [B]\ \{q\} \end{aligned}\right\} \quad (69)$$

In the finite difference solution the above formulations, although valid, are seldom used. The finite difference formulations of equations (67) express the displacement derivatives directly in terms of the nodal displacements (i.e. the generalized displacements). Thus by substituting these relationships into equations (65) the element strains can be expressed as a function of the generalized displacement vector.

The variation of potential energy equation has now become:

$$\frac{1}{2}\,\delta^2 U = \frac{1}{2}\,\{q\}^T \int_0^{\ell} [B]^T\ [F]^T\ [C]\ [F]\ [B]\ ds\ +$$

$$\lambda \int_0^{\ell} [B]^T\ [G]^T\ [N_0]\ [G]\ [B]\ ds\ \{q\} \qquad (70)$$

or,

$$\delta^2 U = \{q\}^T\ \ [K^e]\ + \lambda\ [n^e]\ \{q\} \qquad (71)$$

where $$[K^e] = \int_0^{\ell} ([B]^T\ [F]\ [C]\ [F]\ [B])\ ds$$

$$[n^e] = \int_0^{\ell} ([B]^T\ [G]^T\ [No]\ [G]\ [B])\ ds$$

Thus using an appropriate integration technique,the element stiffness and geometric matrices may be determined. These are then assembled into global stiffness and geometric matrices by using:

$$q^{n+1}_{2i-1} = q^{n}_{2i}$$

where the subscript indicates the component number in the element displacement vector and the superscript indicates the element number. By applying the appropriate boundary conditions the critical value of the eigenvalue λ is found to satisfy:

$$[K]\ \{q\} + \lambda[G]\ \{q\} = 0 \tag{72}$$

This is the general eigenvalue equation and there are many standard techniques available for solving it.

As mentioned previously the expression for the element stiffness and geometric matrices involves an integration over the element. In the finite difference solution the integrand in equation (71) is evaluated at only one point in the element and the total energy obtained by multiplying this value by the element length ℓ. The element centroid properties that are necessary to obtain the stiffness and geometric matrices could be provided as the input to the computation.

For the finite element method the integration of equation (71) is usually obtained by a Gaussian quadrature numerical integration. The relevant nodal information must be provided to the program with an appropriate interpolation subroutine used to obtain the necessary values at the Gaussian integration points. The Gaussian integration may be a very time consuming and expensive computer operation.

For the solution to a buckling problem the prestress matrix $[N_0]$ must be known. This can be determined analytically or from a linear finite element analysis for a unit load (or temperature). With specified the unit prestressing values known,the eigenvalue problem can then be solved for the critical load (or temperature).

CHAPTER IV

Experimental Work

4.1 Experimental Apparatus.

The test setup is shown in the photograph Fig. 3. Schematics of the setup and its accessories are shown in Figs. 4 and 5.

The tubular specimen was heated by radiation from an internal stainless steel resistance heater powered by a 20 K.W. D-C Sorensen power supply. This unit was controlled by a Paramec process controller (Fig. 6) which compared the feedback signal from a thermocouple on the specimen to a desired temperature ramp defined by a Data Trak programmer. All temperatures were measured continuously by chromel-alumel thermocouples cemented to the outside surface of the tube. The thermocouple readings were input to an Acromag millivolt transmitter which converted the millivolt values into current to drive a Kyowa model RMV - 540 A twelve-pen recorder. These temperatures were also checked by a hand held Atkins Technical temperature probe.

The axial load of the cylinder was transmitted through a carefully controlling floating grip shown in detail in Fig. 7. This allowed the load to apply on an Interface model 1310 - AF, 10000 pound load cell, while preventing unwanted displacements. The output from the loadcell was monitored by a Vishay model P-350A strain indicator whose output was in turn,fed to a Hewlett Packard 7046A, x-y recorder as the y input. The x input for this recorder was the mid-span tube temperature read by a Chromel-Alumel thermocouple. In this way a load-temperature graph could be obtained for each test.

The mid-span radial displacement of the tube was measured for a number of specimens. An optical-fibre displacement probe known as the model KD-45A Fotonic Sensor manufactured by the Mechanical Technology Inc. as shown in Fig. 8, was used to measure this displacement without contacting the buckling specimen. The output from this sensor was fed to a Hewlett-Packard model 7035 B x-y recorder as the y-input channel. Again the midspan cylinder temperature was used as the x input channel so that a plot of displacement verses temperature was obtained for each test.

The natural convection of the heat present around the tube specimen tended to shift the heat upward along the cylinder, so it was necessary to employ a bleed-through system of gas inside the tube to regain a symmetrical temperature profile about the mid-span of the specimen. A slow air flow down the cylinder between its inner wall and the heater was introduced by using a needle valve attached to a compressed air supply. This allowed the flow to be varied as needed. The air flow was too small to cause extra internal pressure on the tube.

4.2 Test Specimens

The test specimens used in this investigation were made of aluminum alloy tubing 6061-T6. This was turned on a lathe to the dimensions given in Fig. 9. The thin wall thickness of the tubes were obtained by using a mandrel during a delicate machining process. The range of wall thickness thus obtained varied from .009 to .015 inch. Tube thickness was measured at 9 points in even spaces and the average value was used as the nominal specimen thickness.

No attempt was made to determine the eccentricities present in the cylinders, although any specimens with visible flaws were rejected. A typical specimen is shown in Fig. 10.

The physical properties of the tubing, such as Young's modulus, and the coefficient of linear thermal expansion, were obtained from the manufacturer's material specifications. These values are:

$E = 10.0 \times 10^6$ psi $\qquad \sigma_{yield} = 40.5$ ksi

$\alpha = 13.50 \times 10^{-6}$ in/in °F $\qquad \sigma_{ultimate} = 46.5$ ksi

All values were assumed to be invariant with respect to temperature and direction when used in the analysis of the tests. All of the buckling occurred at temperatures less than 392°F. The elastic analysis was not valid in the post-buckling range so the use of this constant thermal expansion coefficient was considered acceptable. The aluminum tubing used was assumed isotropic in the axial and circumferential directions. Any anisotropy in the radial direction was considered to be unimportant due to the very thin walls of the specimens.

4.3 Experimental Procedure

After measurements of the tube thickness, length, and radius were completed, electrical insulating tape was wrapped around the inside of the two ends of the specimen. This was to insure that the resistance heater would not generate an arc to the specimen during the grip assembly, and the strain indicator was nullified for the newly installed tube specimen.

The upper cross member shown in Fig. 4 was raised from the supporting collars by shims inserted while the main bolts were loosened. The upper grip assembly shown in Fig. 4 was threaded onto the tube and heater, and to the aligning plate. This aligning plate was then tightened and the upper heating terminal installed. Finally the inlet terminal for the bleed-through of gas was fitted to the top grip.

With the specimen now fastened to the testing frame, the ten thermocouples used for obtaining the temperature profile along the cylinder were attached. At each position where a thermocouple was to be installed (ref. Fig. 9) the surface was carefully cleaned, first with a degreaser, and then with a solvent. The thermocouples were then taped in position so that the tips were pressing firmly against the surface and the thermocouple cement applied. This was allowed to set overnight and then a layer of silicone was applied over the cement to provide extra strength. Curing took place for approximately 4 hours. The tape could then be removed from the thermocouple stations.

All the electronics were allowed to warm up for at least an hour before the actual test. The shim stock was then removed and the two main bolts were tightened until approximately 70 lbs. of prestress was applied to the specimen. The zeros for all the temperature outputs were checked and the fibre-optic displacement probe was calibrated and the output set to zero on the x-y recorder.

Prior to the actual test run,the power supply was turned on and the specimen heated up to about 200°F, or slightly less for thinner cylinders. The specimen was held at this temperature while the bleed-through valve was adjusted to make the temperature distribution along the tube symmetric about its half length. The temperatures were also checked with the hand-held temperature probe to insure the thermocouple readings were correct. The power supply was then shut off and the specimen allowed to cool down to nearly room temperature.

Actual tests started following the above procedure. The controller was set to yield a temperature ramp slow enough to ensure a smooth temperature rise in the tube as programmed. The temperature rise in the tube was also checked by a hand-held temperature probe at various instances during the test.

The test was continued well past the original buckling temperature to observe any secondary buckling, or load recovery, that might occur.

4.4 Results

Typical raw data output from a test areshown in Figs. 11 to 13 for test number 21. These figures show, respectively,the load cell output versus the controlling thermocouple output, the Fotonic sensor output versus the controlling thermocouple output and the recorded output for the remaining 9 thermocouples.

From this raw data plots of other results could be made for the proper information for all tests. Figs. 14 to 23 show plots of axial load versus the half-length tube-temperature rise for 5 representative tests. The point of zero temperature rise for all specimens was determined by extrapolating the curve given by the load cell output versus the controlling thermocouple output back to the point of zero load. The relevant information derived from the load-temperature plots for all of the tests is given in Table I. All temperatures refer to the temperature at the half-length of the tube. T_B and P_B refer to the temperature and axial load at the first sign of buckling,

T_M and P_M refer to the maximum temperature and axial load ever reached, and T_∇ and P_∇ refer to the largest discontinuity in the load versus temperature output.

Figs. 24 to 27 show the radial displacement at the half-length of the tube versus the temperature at the same level for several tests. The relevant information for all tests for which these data were available is given in Table II. Photographs of some typical buckling deformation patterns are shown in Figs. 28 to 31. The secondary buckling may be observed shown in Fig. 32.

The temperature profiles along the cylinder were plotted for each test. Some of these profiles are shown in Figs. 33 to 36. These curves illustrate the temperature variations along the tube length at different controlled half-length tube temperatures during the test for each case.

CHAPTER V

Discussion of Results

5.1 Buckling Phenomenon

As the tube was heated it assumed a "barrel" type of shape due to the high temperature at the central portion of the tube coupled by the fact that the ends were constrained by the end fixtures. As a result of these circumferential and axial constraints, circumferential and axial stresses could accumulate in the tube until a critical value was reached, when buckling took place. The clamping effect at the ends of the cylinder would cause the highest circumferential stresses near the ends, so it would be expected that buckling would occur near these locations. This compares to mechanical loading where only the axial stresses are present and buckling usually occurs near the middle of the cylinder.

The results from these tests indeed showed the buckling occurred near the ends of the cylinder for all but four of the tests. In all cases the buckling occurred with a violent "snap-through", accompanied by a large drop in load. In some tests (ref. Figs. 17 to 19, and 21) the load dropoff occurred in several distinct stages. This was observed to be the result of an incomplete buckling pattern at the first snap-through. The succeeding "snap-throughs" were due to the completion of the buckling pattern around the cylinder. In some of the tests where buckling occurred near the clamped ends the deformation took the form of a complete ring indentation around the specimen (ref. Fig. 28). This was usually accompanied by the more conventional diamond pattern deformation which formed adjacent to the ring. It usually occurred along with, or immediately succeeding the original ring buckling.

It was mentioned that not all the specimens buckled near the clamped ends. In fact,four tests indicated that buckling occurred nearer the center of the tube. These were test Nos. 17, 19, 21, and 22. These tests were not conducted any differently than the others, and nothing was observed to make these tests extraordinary in any other manner. The deformation pattern for these specimens exhibited a stepped-tier arrangement which was complete in some specimens and not in others.

Previous tests presented in Ref. [21] have indicated a secondary buckling occurring after the first snap-through buckling. Thielemann [32] described this phenomenon as the passing of the cylinder to succeeding equilibrium states and demonstrated that the buckling pattern of a secondary buckling deformation pattern should have one less wave than the pattern of the preceeding buckling stage. In this investigation there was no secondary buckling of this type observed. In several cases, though, a specimen which originally buckled near a clamped end subsequently buckled near the center at a higher temperature (approximately 700°F). The original buckling deformation patterns as given in Table I range from 4 to 6 waves around the cylinder, whereas this second buckling displacement pattern was typically an incomplete step-tier type of buckling with n = 6. This is, of course,not one pattern less than the previous buckling as predicted by Thielemann. This secondary buckling was sometimes tiered over a larger section of the cylinder.

Other investigators [21], [32] have reported an increasing capacity for the cylinder to support load after the initial buckling. Although the same type of secondary buckling was not observed in these tests, this load recovery was observed between the buckling stages due to the completion of the deformation patterns in tests Nos. 14 and 16, as can be seen in Figs. 12 and 14.

It is also interesting to note that in several cases the buckling process did not occur instantaneously. In tests Nos. 10, 13 and 19 a shallow buckling pattern was observed momentarily before the violent "snap-through" occurred. This is seen in the load-temperature graphs for these tests as the load levels out slightly before dropping, (ref. Figs. 16, 18 and 22).

Hoff [20] showed that the "snap-through" buckling may be delayed in some tests until after the maximum load is reached. He showed the delayed buckling to be dependent on the stiffness of the testing machine. This delayed buckling was observed in two tests. Specimen numbers 6 and 8 did not exhibit a "snap-through" buckling until after the maximum load had been reached. This is shown in Figs. 14 and 15.

5.2 Load Vs Temperature Curves

As mentioned in section 4.4,plots were made of the axial load verses the half-length tube temperature for each test, with the results summarized in Table I.

In order to compare these results with the theoretically expected behavior, the successive approximation method of Sunakawa [30], explained in section 3.3.1, was used. The equations presented in Appendix B were solved by an iteration method performed on an IBM 370/168 digital electronic computer. The six thermocouple readings on the upper half of the tube were used to represent the symmetric temperature distribution in the computations. By substituting these values into the equations

$$T(x) = \sum_i T_i \cos\left(\frac{i\pi x}{2L}\right) \qquad i = 0, 2, 4, 6, 8, 10$$

for each thermocouple position along the half length of the tube, a set of six equations with six unknowns was set up. Solving these equations the first six values of T_i were obtained. More values of T_i could also have been obtained by joining the thermocouple readings with a smooth curve and then using more temperature values from this curve. This was not done, however, as it seemed that this scheme might not be a true representation, as the temperature field thus established is known only to the accuracy of the six thermocouple points. The temperature coefficients for all the tests were strongly dominated by the first two or three terms anyway, and so six terms were considered sufficiently accurate.

The temperature distributions shown in Figs. 33 to 36 were established by the six terms used in the successive approximation method. It is seen that the six terms can represent the actual temperature in the tube quite well.

An axial load versus half-length tube temperature graph obtained using this method is given in Fig. 37. The relevant data for all the computer results and their associated test results are presented in Table III. These results are also presented in Figs. 38 and 39 which show the experimental loads and temperatures as a percentage of the theoretical values plotted against the radius-to-thickness ratio.

An immediate observation from these results is that in all but three cases the experimental temperatures were a higher percentage of the computed values than were the experimental loads. The average values for the 15 tests were:

Temperatures - 37.1 percent

Loads - 32.8 percent

In his work on very thin uniformly heated cylinders of $R/d \approx 300$ Ross et al. (Ref. [19]) found that the buckling loads were characteristically low, with an average value on 10 tests of 26 percent of the classical critical value. The buckling temperatures, however, were found to be very high, with an average value of 62 percent of the classical critical value. In his discussion Ross attributed this phenomenon to the nonlinear load-temperature effect on the pre-buckling deformations. The axial generators, which are initially straight, become curved due to thermal expansion in the middle while being clamped at the two ends. This results in a decreased stiffness in the axial direction and hence the axial load builds up slower than the expected load due to thermal expansion. Bushnell and Smith [33] discounted this explanation and attributed this effect to slippage of the end conditions. They used the BOSOR 4 computer program to show that the barrelling effect was not severe enough to cause a nonlinear load versus temperature (or end shortening) relation. The work of Hoff et al. [19] did include an evaluation of the slippage at the ends, however, and this was shown to be negligible. Additionally, it was shown that the load-end shortening curves for some cylinders, even though they remained linear, had a significantly lower slope than those for machine tested cylinders. This was again due to the barrelling effect of thermal loading. Furthermore, Frum and Baruch [16] pointed out that the use of a linear analysis may lead to buckling temperatures that are lower than those obtained from a non-linear analysis.

At first glance it would seem that the present results would tend to contradict the results of Ross et al. [19], as the critical buckling loads are higher than the critical buckling temperatures. The specimens used in these tests had threaded end portions that were much stiffer than the tube section. It was not likely to have boundary slippage at the ends, as any deformation in the circumferential direction would have forced the bulkier threaded end to become non-axisymmetric. This was unlikely as the bending stiffness of this part was far higher than the stiffness of the tube section. This was also true for angular rotation at the ends of the specimen.

The lower buckling temperatures obtained in the present investigation appear to have verified that the results of Ross et al. were due to slippage at the clamping assemblies, allowing the stresses to redistribute themselves and thus delay buckling until a higher temperature was reached. A closer look at the test specimen, however revealed that this was not necessarily the case. The length-to-radius ratio for these specimens was 11.17 while the value for the specimens of Ross et al. was 9.25. This means that the barrelling effect on these cylinders should be expected to be less severe than for cylinders of a lower length to radius ratio.

To gain a better insight into this result, a 'best fit' linear regression was used to approximate the data. The line obtained for the temperature data was:

$$\frac{T_B^E}{T_B^t} \times 100 = 2.773 + 4.798 \times (R/d)$$

with a coefficient of correlation of .620. This means that the linear fit is quite good and it is an increasing relationship. For this fit the data from test No. 12 was not included as it lies too far from the other data to have any confidence in the correlation. The prediction interval for a 90 percent confidence coefficient is also shown in Fig.39. While there is scatter, as expected, the increasing relationship seems to be proper. This result would seem to agree with the theory that the barrelling effect controls the buckling temperatures.

A linear regression analysis was also done for the buckling load data of Fig. 38. The best fit equation for these data is:

$$\frac{P_B^E}{P_B^t} \times 100 = -24.343 + .78452 \times (R/d)$$

with a coefficient of correlation of .848. The 90 percent prediction interval curves are again shown with the data. This indicates that in this range of radius to thickness ratios the data have a strong increasing linearity. This behavior was not expected, as very low load levels would have been expected due to the barrelling of the cylinder, causing the axial stiffness to decrease.

This discrepancy can be explained by the nature of cylindrical buckling. It was shown by Batdorf (Ref. [7]) that the nondimensional parameters involved in shell buckling include one which represents the shell geometry, z, and one which represents the loading conditions, K_x. For these tests these parameters are:

$$z = \frac{L^2}{Rd}\sqrt{1-\mu^2}$$

$$K_{(i)x} = \frac{12\cdot\overset{i}{\sigma x}\cdot(1-\mu^2)}{\pi^2 E}\left[\frac{L}{d}\right]^2 \text{ where } \overset{1}{\sigma x} = P_B^E/(2\pi Rd)$$

$$\overset{2}{\sigma x} = E\alpha T_B^E$$

The data pertaining to the calculation of these parameters, and the parameters, are given in Table IV. A plot of the results, as suggested by Batdorf [7] is given in Fig. 40. This figure shows that the buckling stress coefficients for these tests lie in the same region of the two theoretical curves which also enveloped the data obtained by Ross et al. [19]. It seems, then that the results cannot be observed strictly as a function of the radius to thickness ratio and axial load. The entire effect of specimen geometry must be allowed for when using the parameter z, and the entire loading effect must be allowed for using the buckling stress coefficients K_x^1 and K_x^2 . When this is done the results show that the stress coefficient for the temperature effect is consistently higher than the stress coefficient for the axial load. The results also show that, although the buckling loads in these experiments seemed to be quite high, in fact the buckling stress coefficients for the loads were quite low, as was expected.

5.3 Displacement Measurement

The numerical solution used here also gave the radial displacements along the cylinder. These are given along with the experimentally obtained displacements, in Figs. 24 to 27. In order to compare the experimental and theoretical displacements both values are given in Table II. These represent the radial displacement for a 100°F temperature rise.

Fig. 41 shows the percentage of the experimental displacement to the theoretical displacement plotted against the radius to thickness ratio. Although there is a fair amount of scatter present it can be seen that the general trend indicates that the experimental value increases as the radius-to-thickness ratio increases.

CHAPTER VI

Summary of Results

Thin cylindrical shells threaded into rigid end supports were subjected to axially symmetric heating until buckling occurred. The results of these tests were:

(1) Axial load verses half-length tube temperature increase curves were obtained for all tests and the prebuckling, buckling, and post-buckling phases were studied.

(2) The buckling for all cases occurred as a violent "snap-through" type of buckling. It usually occurred near the restrained cylinder ends.

(3) It was shown that buckling did occur, in some cases, after the maximum load had been reached.

(4) In several cases the buckling occurred in stages, as the deformation pattern completed itself around the cylinder. A secondary buckling was observed in several cases.

(5) The buckling temperatures were lower than those observed by other researchers, with an average value of 37.1 percent of the theoretical value. The buckling loads, however, were rather higher than expected, about 32.8 percent of the theoretical value.

In light of the above results the following conclusions may be drawn:

The thermal buckling of thin-walled tubes was investigated. The present results derived from tests on thin-walled tubes differed from those obtained by previous investigators for cylinders with a higher radius-to-thickness ratio, e.g. 300 in reference [21] versus 60-80 in the present investigation. These discrepancies lead one to believe that this parameter is an important one in determining the effect of thermal barrelling on buckling. The conclusion drawn by the previous researchers on cylinders with large radius-to-thickness ratios cannot be used here.

In order to determine a consistent design standard, further tests should be conducted to fill in the gaps existing in the radius-to-thickness ratios beyond the range used in the present investigation as illustrated in Figs. 38 and 39.

REFERENCES

1. LORENZ, R.: Die nichtachsensymnetrische Knickung dünnwanger Hohlzylinder, Phys. Z., Vol. 13, pp. 241-260, 1911.

2. SOUTHWELL, R.V.: On the Collapse of Tubes by External Pressure, Phil. Mag., Vol. 25, pp. 687-698, 1913.

3. VON MISES, R.: Der kritische Ausendruck zylindrischer Rohre, Z. Ver. Deutch. Ing., Vol. 58, pp. 750-755, 1914.

4. FLÜGGE, W.: Die Stabilitat der Kreiszlinderschale, Ing. - Arch., Vol. 3, pp. 463-506, 1932.

5. DONNELL, L.H.: Stability of Thin Walled Tubes Under Torsion, N.A.C.A. T.R. No. 479, 1934.

6. SINGER, J.: On the Equivalence of the Galerkin and Rayleigh-Ritz Methods, J. of the Royal Aero. Soc., Vol. 66, 1962.

7. BATDORF, S.B.: A Simplified Method of Elastic-Stability Analysis for Thin Cylindrical Shells, N.A.C.A. T.R. No. 874, 1947.

8. BATDORF, SCHILDCROUT & STEIN: Critical Stress of Thin-Walled Cylinders in Axial Compression, N.A.C.A. T.N. No. 1343, 1947.

9. BATDORF, STEIN & SCHILDCROUT: Critical Stress of Thin-Walled Cylinders in Torsion, N.A.C.A. T.N. No. 1344, 1947.

10. BATDORF, STEIN & SCHILDCROUT: Critical Combinations of Torsion and Direct Axial Stress for Thin-Walled Cylinders, N.A.C.A. T.N. No. 1345, 1947.

11. HOFF, N.J.: Buckling of Thin Cylindrical Shells Under Hoop Stresses Varying in Axial Direction, J. of Applied Mechanics, Vol. 24 #3, pp. 405-412, 1957.

12. LIBOVE, C. and TONG, K.N.: The Influence of Thickness-Wise Temperature Gradients on the Large Deflections and Stability of Thin Elastic Shells, Syracuse University Research Institute, S.U.R.I. Report No. NE 790-612T, 1961.

13. HOFF, N.J., CHAO, C.C., and MADSEN, W.A.: Buckling of a Thin-Walled Circular Cylindrical Shell Heated Along an Axial Strip, J. Appl. Mechanics, Vol. 31 #2, 1964.

14. HILL, D.W.: Buckling of a Thin Circular Cylindrical Shell Heated Along an Axial Strip, SUDAER No. 88, Dept. of Aeronautics and Astronautics, Stanford Univ., 1959.

15. ROSS, B., MAYERS, J., and JAWORSKI, A.: Buckling of Thin Circular Cylindrical Shells Heated Along an Axial Strip, Experimental Mechanics, Vol. 5 #9, pp. 247-256, 1965.

16. FRUM, Y., and BARUCH, M.: Buckling of Cylindrical Shells Heated Along Two Opposite Generators Combined With Axial Compression, T.A.E. Report No. 180, Israel Institute of Technology, 1973.

17. ANDERSON, M.S.: Combinations of Temperature and Axial Compression Required for Buckling of a Ring-Stiffened Cylinder, N.A.S.A. T.N.D - 1224.

18. ZUK, W.: Thermal Buckling of Clamped Cylindrical Shells, J. Aeronautical Sci., Vol. 24 #5, p. 359, 1957.

19. ROSS, B., HOFF, N.J., and HORTON, W.H.: The Buckling Behavior of Uniformly Heated Thin Circular Cylindrical Shells, Experimental Mechanics, Vol. 6 , pp. 529-537, 1966.

20. HOFF, N.J.: A Nonlinear Model Study of the Thermal Buckling of Thin Elastic Shells, J. of Applied Mechanics, Vol. 32 Series E No. 1, pp. 71-75, 1965.

21. ROSS, B.: The Thermal Buckling Behavior of Thin Circular Cylindrical Shells, Ph.D. Thesis, Dept. of Aeronautical Engineering, Stanford University, 1965.

22. TSEIN, H.S.: Buckling of a Column with Non-Linear Supports, J. of the Aeronautical Sciences, Vol. 9 No. 4, pp. 119-132, 1942.

23. NAVARATNA, PIAN, WITMER: Stability Analysis of Shells of Revolution by the Finite-Element Method, A.I.A.A. Journal, Vol. 6, pp. 355-361, 1968.

24. BREBBIA, C., CONNOR, J.: Geometrically Non-Linear Finite Element Analysis, A.S.C.E. J. of Eng. Mechanics, Vol. 95 #2, pp.463-483, 1969.

25. GALLAGHER, R.H., & YANG, H.T.Y.: Elastic Instability Predictions for Doubly-Curved Shells, The Air Force Second Conference on Matrix Methods in Structural Mechanics, Wright-Patterson Air-force Base, 1969, AFFDL-TR-68-150.

26. CHANG, L.K. & CARD, M.F.: Thermal Buckling Analysis for Stiffened Orthotropic Cylindrical Shells, N.A.S.A. TN-D-6332, 1971.

27. BUSHNELL, D.: Analysis of Buckling and Vibration of Ring-Stiffened, Segmented Shells of Revolution, Inter. J. of Solids and Structures, Vol. 6, pp. 157-1970.

28. BUSHNELL, D.: Finite-Difference Energy Models verses Finite-Element Models: Two Variational Approaches in One Computer Program, Numerical and Computer Methods in Structural Mechanics, Fenves, Perrone, Robinson & Schnobrich eds., Academic Press, 1973.

29. WASHIZU, K.: Variational Methods in Elasticity and Plasticity, Permagon Press, 1968.

30. SUNAKAWA, M.: Deformation and Buckling of Cylindrical Shells Subjected to Heating, Report No. 370, Aeronautical Research Institute, Univ. of Tokyo, 1962.

31. SOKOLNIKOFF, I.S.: Mathematical Theory of Elasticity, McGraw-Hill Book Co., 1965.

32. THIELEMANN, W.F.: On the Postbuckling Behavior of Thin Cylindrical Shells, Collected Papers on Instability of Shell Structures, N.A.S.A. TN-D-1510, December 1962, pp. 203-216.

33. BUSHNELL, D. & SMITH, S.: Stress and Buckling of Nonuniformly Heated Cylindrical and Conical Shells, A.I.A.A. Journal, Vol. 9, #12, pp. 2314-2322, 1971.

34. BATDORF, S.B., SCHILDCROUT, M., & STEIN, M.: Critical Stress of Thin-Walled Cylinders in Axial Compression, N.A.S.A. T.R. #887, 1947.

35. HARRIS, L., SUER, H., SKENE, W., & BENJAMIN, R.: The Stability of Thin-Walled Unstiffened Circular Cylinders under Axial Compression Including the Effects of Internal Pressure, J. of Aero. Sciences, Vol. 24, No. 8, p. 587, 1957.

APPENDIX A

Variational Methods for Equilibrium Equations

This appendix describes in detail the procedure used to derive the equilibrium equations from variational considerations. As previously stated the strain energy for a thin elastic shell with no heating is given by:

$$U = \frac{1}{2}\iint\frac{Ed}{(1-\mu^2)}\left[(\varepsilon_{xo} + \varepsilon_{yo})^2 + 2(1-\mu)(\frac{1}{4}\gamma_{xyo}^2 - \varepsilon_{xo}\,\varepsilon_{yo})\right]$$

$$+ D\left[(\frac{\partial w}{\partial x} + \frac{\partial w}{\partial y})^2 + 2(1-\mu)(\frac{\partial^2 w}{\partial x \partial y} - \frac{\partial w}{\partial x}\frac{\partial w}{\partial y})\right] dx\, dy \qquad (53)$$

The potential energy of the applied loads is:

$$v = -\iiint_v B_i\, U_i\, dv - \iint_{si} T_i^{(v)}\, u_i\, ds \qquad (A\text{-}1)$$

where $T_i^{(v)}$ = surface tractions over the boundary S_i

B_i = body force distribution

However in the problem where only thermal loading is considered, the thermal effect can be included in the strain displacement relationships equations (19), (20) and (21). The principle of stationary potential energy equation (52) then reduces to the form:

$$\delta U = 0 \qquad (A\text{-}2)$$

This strain energy is due to bending, and middle surface strain so:

$$U = U_{ms} + U_{bend} \tag{A-3}$$

where:

$$U_{ms} = \frac{1}{2}\iint \frac{Ed}{(1-\mu^2)}\left[(\varepsilon_{xo} + \varepsilon_{yo})^2 + 2(1-\mu)\left(\frac{\gamma_{x}{}^2{}_{yo}}{4} - \varepsilon_{xo}\,\varepsilon_{yo}\right)\right] dx\,dy$$

$$U_{bend} = \frac{1}{2}\iint D\left[\left(\frac{\partial w}{\partial x} + \frac{\partial w}{\partial y}\right)^2 + 2(1-\mu)\left(\frac{\partial^2 w}{\partial x \partial y} - \frac{\partial w}{\partial x}\,\frac{\partial w}{\partial y}\right)\right] dx\,dy$$

The middle surface strain energy term was derived from the form:

$$U_{ms} = \frac{1}{2}\iint [N_x\,\varepsilon_{xo} + N_y\,\varepsilon_{yo} + N_{xy}\,\varepsilon_{xyo}]\,dx\,dy \tag{A-4}$$

Introducing the thermal strains we get:

$$\varepsilon_{xo} = \frac{1}{Ed}(N_x - \mu N_y) + \alpha T$$

$$\varepsilon_{yo} = \frac{1}{Ed}(N_y - \mu N_x) + \alpha T \tag{A-5}$$

$$\gamma_{xyo} = \frac{2(1+\mu)}{Ed}\,N_{xy}$$

Solving for the forces N_x, N_y and N_{xy}

$$N_x = \frac{Ed}{1-\mu^2}[\varepsilon_{xo} + \mu\varepsilon_{yo}] - \frac{Ed\alpha T}{1-\mu}$$

$$N_y = \frac{Ed}{1-\mu^2}[\varepsilon_{yo} + \mu\varepsilon_{xo}] - \frac{Ed\alpha T}{1-\mu} \quad \text{(A-6)}$$

$$N_{xy} = \frac{Ed(1-v)}{2(1-\mu^2)} \gamma_{xyo}$$

Introducing these in equation (A-4):

$$U_{ms} = \frac{1}{2}\iint \frac{Ed}{(1-\mu^2)}[\varepsilon_{xo}^2 + 2\mu\varepsilon_{xo}\varepsilon_{yo} + \varepsilon_{yo}^2] - \frac{Ed\alpha T}{1-\mu}(\varepsilon_{xo} + \varepsilon_{yo})$$

$$+ \frac{Ed(1-\mu)}{2(1-\mu^2)} \gamma^2_{xyo} \quad dxdy$$

Rearranging ,this becomes:

$$U_{ms} = \frac{1}{2}\iint \frac{Ed}{1-\mu^2}[(\varepsilon_{xo} + \varepsilon_{yo})^2 + 2(1-\mu)(\frac{\gamma^2_{xyo}}{4} - \varepsilon_{xo}\ \varepsilon_{yo})]$$

$$- \frac{Ed\alpha T}{1-\mu}(\varepsilon_{xo} + \varepsilon_{yo})dxdy \quad \text{(A-7)}$$

The bending strain energy will not be affected by the thermal loading.

Applying the strain-displacement relationships equations (19), (20), and (21), the strain energy becomes:

$$U_{ms} = \frac{1}{2}\iint \frac{Ed}{1-\mu^2} \left\{[(\frac{\partial u}{\partial x} + \frac{\partial v}{\partial y}) + \frac{1}{2}((\frac{\partial w}{\partial x})^2 + (\frac{\partial w}{\partial y})^2)]^2 + \right.$$

$$\frac{w}{R}[\frac{w}{R} - 2(\frac{\partial u}{\partial x} + \frac{\partial v}{\partial y}) - ((\frac{\partial w}{\partial x})^2 + (\frac{\partial w}{\partial y})^2)]\Big\} \frac{2Ed}{1+\mu}\Big\{\frac{\partial u}{\partial x}\ \frac{\partial v}{\partial y} +$$

$$\frac{1}{2}\left[\frac{\partial u}{\partial x}\left(\frac{\partial w}{\partial y}\right)^2 + \frac{\partial v}{\partial y}\left(\frac{\partial w}{\partial x}\right)^2\right] + \frac{1}{4}\left(\frac{\partial w}{\partial x}\right)^2\left(\frac{\partial w}{\partial y}\right)^2 - \frac{w}{R}\left[\frac{\partial u}{\partial x} + \right. \tag{A-8}$$

$$\left.\frac{1}{2}\left(\frac{\partial w}{\partial x}\right)^2\right] - \frac{1}{4}\left[\left(\frac{\partial u}{\partial y} + \frac{\partial v}{\partial x}\right) + \frac{\partial w}{\partial x}\frac{\partial w}{\partial y}\right]^2\Big\} - \frac{Ed\alpha T}{1-\mu}\Big\{\left(\frac{\partial u}{\partial x} + \frac{\partial v}{\partial y}\right) +$$

$$\frac{1}{2}\left[\left(\frac{\partial w}{\partial x}\right)^2 + \left(\frac{\partial w}{\partial y}\right)^2\right] - \frac{w}{R}\Big\}\, dxdy$$

Applying a variation to the total strain energy equation (A-2) becomes , after much algebra

$$\frac{1}{2}\iint\Big\{I_0\ \delta u + I_1 \frac{\partial(\delta u)}{\partial x} + I_2 \frac{\partial(\delta u)}{\partial y} + I_3\ \delta v + I_4 \frac{\partial(\delta v)}{\partial x}$$

$$+ I_5 \frac{\partial(\delta v)}{\partial y} + I_6\ \delta w + I_7 \frac{\partial(\delta w)}{\partial x} + I_8 \frac{\partial(\delta w)}{\partial y} + I_9 \frac{\partial^2(\delta w)}{\partial x^2}$$

$$+ I_{10} \frac{\partial^2(\delta w)}{\partial y^2} + I_{11} \frac{\partial^2(\delta w)}{\partial x \partial y}\Big\}\, dxdy = 0 \tag{A-9}$$

where:

$$I_0 = I_3 = 0$$

$$I_1 = \frac{Ed}{1-\mu^2}\Big\{2\left[\left(\frac{\partial u}{\partial x} + \frac{\partial v}{\partial y}\right) + \frac{1}{2}\left(\left(\frac{\partial w}{\partial x}\right)^2 + \left(\frac{\partial w}{\partial y}\right)^2\right) - \frac{w}{R}\right] - 2(1-\mu)$$

$$\left[\frac{\partial v}{\partial y} + \frac{1}{2}\left(\frac{\partial w}{\partial y}\right)^2 - \frac{w}{R}\right]\Big\}$$

$$I_2 = (1-\mu) \frac{Ed}{1-\mu^2} \left\{ \left(\frac{\partial u}{\partial y} + \frac{\partial v}{\partial x}\right) + \frac{\partial w}{\partial x}\frac{\partial w}{\partial y} \right\}$$

$$I_4 = (1-u) \frac{Ed}{1-\mu^2} \left\{ \left(\frac{\partial u}{\partial y} + \frac{\partial v}{\partial x}\right) + \frac{\partial w}{\partial x}\frac{\partial w}{\partial y} \right\}$$

$$I_5 = \frac{Ed}{1-\mu^2} \left\{ 2\left[\left(\frac{\partial u}{\partial x} + \frac{\partial v}{\partial y}\right) + \frac{1}{2}\left(\left(\frac{\partial w}{\partial x}\right)^2 + \left(\frac{\partial w}{\partial y}\right)^2\right) - \frac{w}{R}\right] \right.$$

$$\left. -2(1-\mu)\left[\frac{\partial u}{\partial x} + \frac{1}{2}\left(\frac{\partial w}{\partial x}\right)^2\right] \right\}$$

$$I_6 = \frac{Ed}{1-\mu^2} \left\{ \frac{2}{R}\left[\left(\frac{\partial u}{\partial x} + \frac{\partial v}{\partial y}\right) + \frac{1}{2}\left(\left(\frac{\partial w}{\partial x}\right)^2 + \left(\frac{\partial w}{\partial y}\right)^2\right) - \frac{w}{R}\right] \right.$$

$$\left. - \frac{1}{R}\left[\frac{\partial u}{\partial x} + \frac{1}{2}\left(\frac{\partial w}{\partial x}\right)^2\right] + 2d(1+\mu)\alpha T\left[\frac{\partial^2 w}{\partial x} + \frac{\partial^2 w}{\partial y^2} + \frac{1}{R}\right] \right\}$$

$$I_7 = \frac{Ed}{1-\mu^2} \left\{ + 2\frac{\partial w}{\partial x}\left(\frac{\partial u}{\partial x} + \frac{\partial v}{\partial y}\right) + \frac{1}{2}\left(\left(\frac{\partial w}{\partial x}\right)^2 + \left(\frac{\partial w}{\partial y}\right)^2\right) - \frac{w}{R}\right]$$

$$\left. -2(1-\mu)\quad \frac{\partial v}{\partial y}\frac{\partial w}{\partial x} + \frac{1}{2}\frac{\partial w}{\partial x}\left(\frac{\partial w}{\partial y}\right)^2 - \frac{w}{R}\frac{\partial w}{\partial x} - \frac{1}{2}\frac{\partial w}{\partial y}\left[\left(\frac{\partial u}{\partial y} + \frac{\partial v}{\partial x}\right) + \frac{\partial w \partial w}{\partial x \partial y}\right] \right\}$$

$$I_8 = \frac{Ed}{1-\mu^2} \left\{ 2\frac{\partial w}{\partial y}\left[\left(\frac{\partial u}{\partial x} + \frac{\partial v}{\partial y}\right) + \frac{1}{2}\left(\left(\frac{\partial w}{\partial x}\right)^2 + \left(\frac{\partial w}{\partial y}\right)^2\right) - \frac{w}{R}\right] - \right.$$

$$\left. 2(1-\mu)\left[\frac{\partial u}{\partial x}\frac{\partial w}{\partial y} + \frac{1}{2}\frac{\partial w}{\partial y}\left(\frac{\partial w}{\partial x}\right)^2 - \frac{1}{2}\frac{\partial w}{\partial x}\left[\left(\frac{\partial u}{\partial y} + \frac{\partial v}{\partial x}\right) + \frac{\partial w}{\partial x}\frac{\partial w}{\partial y}\right]\right] \right\}$$

$$I_9 = 2D\left[\frac{\partial^2 w}{\partial x^2} + \frac{\partial^2 w}{\partial y^2} - (1-\mu)\frac{\partial^2 w}{\partial y^2}\right]$$

$$I_{10} = 2D\left[\frac{\partial^2 w}{\partial x^2} + \frac{\partial^2 w}{\partial y^2} - (1-\mu)\frac{\partial^2 w}{\partial x^2}\right]$$

$$I_{11} = 4(1-\mu)D\left[\frac{\partial^2 w}{\partial x \partial y}\right]$$

With the form of equation (A-9) it is useful to use Green's theorem to eliminate the derivatives of terms involving the delta operator. For two dimensions Green's theorem is:

$$\iint_s u \frac{w}{x_i} \, dA = \oint_r uwdl - \iint_s w \frac{u}{w_i} \, dA \qquad \text{(A-10)}$$

Thus, by using this formula,the expression of the variation of the strain energy becomes an area integral involving only terms with the delta operator, and not its derivatives, plus a series of line integrals over the boundaries. These line integrals specify the natural and kinematic boundary conditions on the shell that must be satisfied. These conditions are very important to the full understanding of the problem,but as this appendix is to deal with the development of the equilibrium equations,they shall not be included here. So after applying Green's theorem equation (A-10) becomes:

$$\frac{1}{2}\iint\left\{A_1 \, \delta u + A_2 \, \delta v + A_3 \, \delta w\right\} dxdy + \oint_r A_4 \bullet dl = 0 \qquad \text{(A-11)}$$

where:

$$A_1 = \frac{-Ed}{1-\mu^2}\left\{2\frac{\partial}{\partial x}\left\{\left[\left(\frac{\partial u}{\partial x} + \frac{\partial v}{\partial y}\right) + \frac{1}{2}\left(\left(\frac{\partial w}{\partial x}\right)^2 + \left(\frac{\partial w}{\partial y}\right)^2\right) - \frac{w}{R}\right]\right.\right.$$

$$\left.\left. -(1-\mu)\left[\frac{\partial v}{\partial y} + \frac{1}{2}\left(\frac{\partial w}{\partial y}\right)^2 - \frac{w}{R}\right]\right\} + (1-\mu)\frac{\partial}{\partial y}\left[\frac{\partial u}{\partial y} + \frac{\partial v}{\partial x} + \frac{\partial w}{\partial x}\frac{\partial w}{\partial y}\right]\right\}$$

$$A_2 = -\frac{Ed}{1-\mu^2}\Bigg\{2\frac{\partial}{\partial y}\Big\{\Big[\Big(\frac{\partial u}{\partial x}+\frac{\partial v}{\partial y}\Big)+\frac{1}{2}\Big(\Big(\frac{\partial w}{\partial x}\Big)^2+\Big(\frac{\partial w}{\partial y}\Big)^2\Big)-\frac{w}{R}\Big]$$

$$-(1-\mu)\Big[\frac{\partial u}{\partial x}+\frac{1}{2}\Big(\frac{\partial w}{\partial x}\Big)^2\Big]\Big\} + (1-\mu)\frac{\partial}{\partial x}\Big[\Big(\frac{\partial u}{\partial y}+\frac{\partial v}{\partial x}\Big)+\frac{\partial w}{\partial x}\frac{\partial w}{\partial y}\Big]\Bigg\}$$

$$A_3 = -\frac{Ed}{1-\mu^2}\Bigg\{\frac{2}{R}\Big[\Big(\frac{\partial u}{\partial x}+\frac{\partial v}{\partial y}\Big)+\frac{1}{2}\Big(\Big(\frac{\partial w}{\partial x}\Big)^2+\Big(\frac{\partial w}{\partial y}\Big)^2\Big)-\frac{w}{R}\Big]-\frac{1}{R}\Big[\frac{\partial u}{\partial x}$$

$$+\frac{1}{2}\Big(\frac{\partial w}{\partial x}\Big)^2\Big] \quad -2(1+\mu)\alpha T d\Big[\frac{\partial^2 w}{\partial x^2}+\frac{\partial^2 w}{\partial y^2}+\frac{1}{R}\Big]+\frac{\partial}{\partial x}\Big\{2\frac{\partial w}{\partial x}\Big[\Big(\frac{\partial u}{\partial x}+\frac{\partial v}{\partial y}\Big)$$

$$+\frac{1}{2}\Big(\Big(\frac{\partial w}{\partial x}\Big)^2+\Big(\frac{\partial w}{\partial y}\Big)^2\Big)-\frac{w}{R}\Big]-2(1-\mu)\Big[\frac{\partial v}{\partial y}\frac{\partial w}{\partial x}+\frac{1}{2}\frac{\partial w}{\partial x}\Big(\frac{\partial w}{\partial y}\Big)^2$$

$$-\frac{w}{R}\frac{\partial w}{\partial x}-\frac{1}{2}\frac{\partial w}{\partial y}\Big[\Big(\frac{\partial u}{\partial y}+\frac{\partial v}{\partial x}\Big)+\frac{\partial w}{\partial x}\frac{\partial w}{\partial y}\Big]\Big]\Big\}+\frac{\partial}{\partial y}\Big\{2\frac{\partial w}{\partial y}\Big[\Big(\frac{\partial u}{\partial x}+\frac{\partial v}{\partial y}\Big)$$

$$+\frac{1}{2}\Big(\Big(\frac{\partial w}{\partial x}\Big)^2+\Big(\frac{\partial w}{\partial y}\Big)^2\Big)-\frac{w}{R}\Big]-2(1-\mu)\Big[\frac{\partial u}{\partial x}\frac{\partial w}{\partial y}+\frac{1}{2}\frac{\partial w}{\partial y}\Big(\frac{\partial w}{\partial x}\Big)^2$$

$$-\frac{1}{2}\frac{\partial w}{\partial x}\Big[\Big(\frac{\partial u}{\partial y}+\frac{\partial v}{\partial x}\Big)+\frac{\partial w}{\partial x}\frac{\partial w}{\partial y}\Big]\Big]\Big\}\Bigg\} + 2D\Bigg\{\frac{\partial^2}{\partial x^2}\Big(\frac{\partial^2 w}{\partial x^2}+\frac{\partial^2 w}{\partial y^2}$$

$$-(1-\mu)\frac{\partial^2 w}{\partial y^2}\Big)+\frac{\partial^2}{\partial y^2}\Big(\frac{\partial^2 w}{\partial x^2}\ \frac{\partial^2 w}{\partial y^2}-(1-\mu)\frac{\partial^2 w}{\partial x^2}\Big)$$

$$+2(1-\mu)\frac{\partial^2}{\partial x\partial y}\Big(\frac{\partial^2 w}{\partial x\partial y}\Big)\Bigg\}$$

A_4 = a system of line integrals specifying the boundary conditions.

Providing the boundary conditions are all satisfied:

$$\oint_r A_4 \, dl = 0$$

Then, because each variation δu, δv, and δw is arbitrary, equation (A-11) yields:

$$A_1 = 0, \; A_2 = 0, \; A_3 = 0 \qquad \text{(A-12)}$$

The three equations of equilibrium for the shell then become, after some rearranging:

$$\frac{Ed}{2(1-\mu^2)} \left\{ 2 \frac{\partial}{\partial x} \left[\left(\frac{\partial u}{\partial x} + \frac{1}{2}\left(\frac{\partial w}{\partial x}\right)^2 \right) + \mu \left(\frac{\partial v}{\partial y} + \frac{1}{2}\left(\frac{\partial w}{\partial y}\right)^2 - \frac{w}{R} \right) \right] \right.$$

$$\left. + (1-\mu) \frac{\partial}{\partial y} \left[\frac{\partial u}{\partial y} + \frac{\partial v}{\partial x} + \frac{\partial w}{\partial x}\frac{\partial w}{\partial y} \right] \right\} = 0$$

$$\frac{Ed}{2(1-\mu^2)} \left\{ 2 \frac{\partial}{\partial y} \left[\left(\frac{\partial v}{\partial y} + \frac{1}{2}\left(\frac{\partial w}{\partial y}\right)^2 - \frac{w}{R} \right) + \mu \left(\frac{\partial u}{\partial x} + \frac{1}{2}\left(\frac{\partial w}{\partial x}\right)^2 \right) \right] \right. \qquad \text{(A-13)}$$

$$\left. + (1-\mu) \frac{\partial}{\partial x} \left[\frac{\partial u}{\partial y} + \frac{\partial v}{\partial x} + \frac{\partial w}{\partial x}\frac{\partial w}{\partial y} \right] \right\} = 0$$

$$\frac{Ed}{2(1-\mu^2)} \left\{ 2 \frac{\partial}{\partial x} \left(\left[\left(\frac{\partial u}{\partial x} + \frac{1}{2}\left(\frac{\partial w}{\partial x}\right)^2 \right) + \mu \left(\frac{\partial v}{\partial y} + \frac{1}{2}\left(\frac{\partial w}{\partial y}\right)^2 - \frac{w}{R} \right) \right] \frac{\partial w}{\partial y} \right) \right.$$

$$+ 2 \frac{\partial}{\partial y} \left(\left[\left(\frac{\partial v}{\partial y} + \frac{1}{2}\left(\frac{\partial w}{\partial y}\right)^2 - \frac{w}{R} \right) + \mu \left(\frac{\partial u}{\partial x} + \frac{1}{2}\left(\frac{\partial w}{\partial x}\right)^2 \right) \right] \frac{\partial w}{\partial y} \right)$$

$$+ (1-\mu) \frac{\partial}{\partial x} \left((\frac{\partial u}{\partial y} + \frac{\partial v}{\partial x} + \frac{\partial w}{\partial x} \frac{\partial w}{\partial y}) \frac{\partial w}{\partial y} \right) + (1-\mu) \frac{\partial}{\partial y} \left((\frac{\partial u}{\partial y} + \frac{\partial v}{\partial x} \right.$$

$$\left. + \frac{\partial w}{\partial x} \frac{\partial w}{\partial y}) \frac{\partial w}{\partial x} \right) \Bigg\} - D \left[\frac{\partial^4 w}{\partial x^4} + 2 \frac{\partial^4 w}{\partial x^2 \partial y^2} + \frac{\partial^4 w}{\partial y^4}\right] + \frac{Ed}{1-\mu^2} \left[(\frac{\partial v}{\partial y} + \frac{1}{2}(\frac{\partial w}{\partial y})^2 - \frac{w}{R})\right.$$

$$\left. + \mu(\frac{\partial u}{\partial x} + \frac{1}{2}(\frac{\partial w}{\partial x})^2)\right] (\frac{1}{R}) = \frac{E\alpha Td}{1-\mu} \left[\frac{\partial^2 w}{\partial x^2} + \frac{\partial^2 w}{\partial y^2} + \frac{1}{R}\right]$$

These equations can be greatly simplified if several relationships are used. For reference

$$\varepsilon_x = \left[\frac{\partial u}{\partial x} + \frac{1}{2} (\frac{\partial w}{\partial x})^2 \right]$$

$$\varepsilon_y = \left[\frac{\partial v}{\partial y} + \frac{1}{2} (\frac{\partial w}{\partial y})^2 - \frac{w}{R}\right]$$

$$\gamma_{xy} = \left[\frac{\partial u}{\partial y} + \frac{\partial v}{\partial x} + \frac{\partial w}{\partial x} \frac{\partial w}{\partial y}\right]$$

The stress functions are:

$$\frac{\partial^2 \psi}{\partial y^2} = \frac{Nx}{d} \; ; \quad \frac{\partial^2 \psi}{\partial x^2} = \frac{Ny}{d}; \quad \frac{\partial^2 \psi}{\partial x \partial y} = - \frac{Nxy}{d}$$

Using the force-strain relationships equations (A-6), the equilibrium equations become:

$$\frac{\partial Nx}{\partial x} + \frac{\partial Nxy}{\partial y} = 0 \qquad \text{x dir'n} \qquad \text{(A-14)}$$

$$\frac{\partial Ny}{\partial y} + \frac{\partial Nxy}{\partial x} = 0 \qquad \text{y dir'n} \qquad \text{(A-15)}$$

$$D\nabla^4 w = d[\frac{\partial^3\psi}{\partial x^2}\frac{\partial^2 w}{\partial y^2} - 2\frac{\partial^2\psi}{\partial y\partial x}\frac{\partial^2 w}{\partial x\partial y} + \frac{\partial^2\psi}{\partial y^2}\frac{\partial^2 w}{\partial x^2}]$$

$$+ \frac{d}{R}\frac{\partial^2\psi}{\partial x^2} \qquad \text{z dir'n} \qquad \text{(A-16)}$$

Equation (A-16) is identical to the equation (50) for radial equilibrium derived previously.

APPENDIX B

Equations of the Successive Approximation Method

The equations of equilibrium and compatability as given by Sunakawa [30] are:

$$\frac{d^4w}{dx^4}+\frac{2\nu}{R^2}\frac{d^2w}{dx^2}+\frac{w}{R^4}$$
$$=\frac{12(1-\nu^2)}{d^2}\left[\frac{\chi_{yy}}{E}w_{xx}+\frac{1}{R}\frac{\chi_{xx}}{E}-\frac{\alpha}{d(1-\nu)}\left(\frac{d}{R}\right)^2\left(\tilde{T}+R^2\frac{d^2\tilde{T}}{dx^2}\right)\right], \tag{B-1}$$
$$\nabla^4\frac{\chi}{E}=-\frac{w_{xx}}{R}-\alpha\frac{d^2\bar{T}}{dx^2}. \tag{B-2}$$

These equations differ from those of equations (50) and (51) in the following ways:

1. The loads and deformations are axisymmetric so that all terms concerning v, and $\partial/\partial y$ vanish.

2. A temperature gradient through the wall thickness is allowed, where the temperature terms are defined as:

$$\bar{T}=\frac{1}{d}\int_{-d/2}^{d/2}T(x,y,z)\,dz, \qquad \tilde{T}=\frac{1}{d^2}\int_{-d/2}^{d/2}zT(x,y,z)\,dz. \tag{B-3}$$

These temperatures are expressed as a Fourier series:

$$\bar{T}=\sum_i \bar{T}_i\cos\frac{i\pi x}{2L}, \qquad (i=0,2,4,\cdots\text{even}),$$
$$\tilde{T}=\sum_j \tilde{T}_j\cos\frac{j\pi x}{2L}, \qquad (j=0,2,4,\cdots\text{even}). \tag{B-4}$$

From the strain-deformation relationships of equations (19) to (21), and the strain equations (47) to (49) the stress function derivatives can be expressed as*:

$$\frac{\chi_{xx}}{E}=\frac{1}{(1-\nu^2)}\left[-\frac{w}{R}+\nu\left(u_x+\frac{1}{2}w_x{}^2\right)\right]-\frac{\alpha\bar{T}}{(1-\nu)},$$
$$\frac{\chi_{yy}}{E}=\frac{1}{(1-\nu^2)}\left[\left(u_x+\frac{1}{2}w_x{}^2\right)-\nu\frac{w}{R}\right]-\frac{\alpha\bar{T}}{(1-\nu)}, \qquad \text{(B-5)}$$

If the axial stress is assumed to be a constant these equations can be expressed as:

$$\frac{\chi_{yy}}{E}=\frac{1}{(1-\nu^2)}\left[\left(u_x+\frac{1}{2}w_x{}^2\right)-\nu\frac{w}{R}\right]-\frac{\alpha\bar{T}}{(1-\nu)}=-C_1.$$
$$\frac{\chi_{xx}}{E}=-\frac{w}{R}-\alpha\bar{T}-\nu C_1. \qquad \text{(B-6)}$$

Inserting these into the equilibrium equation (B-1) and neglecting higher order terms of infinitesimals it becomes:

$$\frac{d^4w}{dx^4}+4\beta^4R^2C_1\frac{d^2w}{dx^2}+4\beta^4w$$
$$=-4\beta^4R\left[\alpha\bar{T}_0+\nu C_1+\frac{\alpha\bar{T}_0}{(1-\nu)}\left(\frac{d}{R}\right)\right]$$
$$-4\beta^4R\left\{\alpha\sum_{i=2}^{\infty}\bar{T}_i\cos\frac{i\pi x}{2L}+\frac{\alpha}{(1-\nu)}\left(\frac{d}{R}\right)\sum_{j=2}^{\infty}\left[1-\frac{j^2}{4}\left(\frac{\pi R}{L}\right)^2\right]\bar{T}_j\cos\frac{j\pi x}{2L}\right\} \qquad \text{(B-7)}$$

where $$\beta^4=\frac{Ed}{4DR^2}=\frac{3(1-\nu^2)}{d^2R^2}.$$

*In this appendix subscripted variables refer to the partial differential with respect to the subscripted variable.

The general solution, after integrating equation (B-7), is:

$$-\frac{w}{R}=\left[\alpha\bar{T}_1+\nu C_1+\frac{\alpha\tilde{T}_0}{(1-\nu)}\left(\frac{d}{R}\right)\right]$$
$$+16\xi^4\left\{4\alpha\sum_{i=2}^{\infty}\frac{\bar{T}_i}{(i^4\eta^4-16i^2C_1\xi^4\eta^2+64\xi^4)}\cos\frac{i\pi x}{2L}\right.$$
$$\left.+\frac{\alpha}{(1-\nu)}\left(\frac{d}{R}\right)\sum_{j=2}^{\infty}\frac{(4-j^2\eta^2)\tilde{T}_j}{(j^4\eta^4-16j^2C_1\xi^4\eta^2+64\xi^4)}\cos\frac{j\pi x}{2L}\right\}+A(x)\,, \qquad \text{(B-8)}$$

where $\xi=R\beta\,,\qquad \eta=\frac{\pi R}{L}\,,$

The complementary solution A(x) can be shown as:

i) the case of $1-\xi^2C_1>0$,

$$A(x)=A_1e^{-\sqrt{1-\xi^2C_1}\beta x}\cos\sqrt{1+\xi^2C_1}\beta x+A_2e^{-\sqrt{1-\xi^2C_1}\beta x}\sin\sqrt{1+\xi^2C_1}\beta x$$
$$+A_3'e^{\sqrt{1-\xi^2C_1}\beta x}\cos\sqrt{1+\xi^2C_1}\beta x+A_4'e^{\sqrt{1-\xi^2C_1}\beta x}\sin\sqrt{1+\xi^2C_1}\beta x$$
$$=A_1e^{-\sqrt{1-\xi^2C_1}\beta x}\cos\sqrt{1+\xi^2C_1}\beta x+A_2e^{-\sqrt{1-\xi^2C_1}\beta x}\sin\sqrt{1+\xi^2C_1}\beta x$$
$$+A_3e^{\sqrt{1-\xi^2C_1}\beta(x-2L)}\cos\sqrt{1+\xi^2C_1}\beta(x-2L)$$
$$+A_4e^{\sqrt{1-\xi^2C_1}\beta(x-2L)}\sin\sqrt{1+\xi^2C_1}\beta(x-2L)\,, \qquad \text{(B-9)}$$

ii) the case of $1-\xi^2C_1=0$,

$$A(x)=(A_1+A_3x)\cos\sqrt{1+\xi^2C_1}\beta x+(A_2+A_4x)\sin\sqrt{1+\xi^2C_1}\beta x$$
$$=(A_1+A_3x)\cos\sqrt{2}\beta x+(A_2+A_4x)\sin\sqrt{2}\beta x\,, \qquad \text{(B-10)}$$

iii) the case of $1-\xi^2C_1<0$,

$$A(x)=A_1\cos\left[(\sqrt{\xi^2C_1+1}+\sqrt{\xi^2C_1-1})\beta x+A_3)\right]$$
$$+A_2\cos\left[(\sqrt{\xi^2C_1+1}-\sqrt{\xi^2C_1-1})\beta x+A_4\right]. \qquad \text{(B-11)}$$

The constants A_i in the complementary solution are chosen to satisfy the boundary conditions on w:

$w/_{x=0,2L} = 0 \qquad w_x/_{x=0,2L} = 0$

These constants become:

i) the case of $1-\xi^2 C_1>0$,

$$
\left.
\begin{aligned}
A_1=A_3&=-\frac{1-e^{-2\sqrt{1-\xi^2 C_1}\beta L}\left[\cos\left(2\sqrt{1+\xi^2 C_1}\beta L\right)-\bar{k}\sin\left(2\sqrt{1+\xi^2 C_1}\beta L\right)\right]}{1-e^{-4\sqrt{1-\xi^2 C_1}\beta L}+2\bar{k}e^{-2\sqrt{1-\xi^2 C_1}\beta L}\sin\left(2\sqrt{1+\xi^2 C_1}\beta L\right)}A_0\,,\\
A_2=-A_4&=-\frac{\bar{k}-e^{-2\sqrt{1-\xi^2 C_1}\beta L}\left[\bar{k}\cos\left(2\sqrt{1+\xi^2 C_1}\beta L\right)+\sin\left(2\sqrt{1+\xi^2 C_1}\beta L\right)\right]}{1-e^{-4\sqrt{1-\xi^2 C_1}\beta L}+2\bar{k}e^{-2\sqrt{1-\xi^2 C_1}\beta L}\sin\left(2\sqrt{1+\xi^2 C_1}\beta L\right)}A_0\,,
\end{aligned}
\right\}\quad \text{(B-12)}
$$

ii) the case of $1-\xi^2 C_1=0$,

$$
\left.
\begin{aligned}
&A_1=-A_0\,, &&A_2=-\frac{1-\cos 2\sqrt{2}\beta L}{2\sqrt{2}\beta L+\sin 2\sqrt{2}\beta L}A_0\,,\\
&A_3=\frac{\sqrt{2}\beta(1-\cos 2\sqrt{2}\beta L)}{2\sqrt{2}\beta L+\sin 2\sqrt{2}\beta L}A_0\,, &&A_4=-\frac{\sqrt{2}\beta\sin 2\sqrt{2}\beta L}{2\sqrt{2}\beta L+\sin 2\sqrt{2}\beta L}A_0\,,
\end{aligned}
\right\}\quad \text{(B-13)}
$$

iii) the case of $1-\xi^2 C_1<0$,

$$
\left.
\begin{aligned}
A_1&=\frac{\left(\sqrt{\xi^2 C_1+1}-\sqrt{\xi^2 C_1-1}\right)\sin\left[\left(\sqrt{\xi^2 C_1+1}-\sqrt{\xi^2 C_1-1}\right)\beta L\right]}{\sqrt{\xi^2 C_1-1}\sin\left(2\sqrt{\xi^2 C_1+1}\beta L\right)+\sqrt{\xi^2 C_1+1}\sin\left(2\sqrt{\xi^2 C_1-1}\beta L\right)}A_0\,,\\
A_2&=-\frac{\left(\sqrt{\xi^2 C_1+1}+\sqrt{\xi^2 C_1-1}\right)\sin\left[\left(\sqrt{\xi^2 C_1+1}+\sqrt{\xi^2 C_1-1}\right)\beta L\right]}{\sqrt{\xi^2 C_1-1}\sin\left(2\sqrt{\xi^2 C_1+1}\beta L\right)+\sqrt{\xi^2 C_1+1}\sin\left(2\sqrt{\xi^2 C_1-1}\beta L\right)}A_0\,,\\
A_3&=-\left(\sqrt{\xi^2 C_1+1}+\sqrt{\xi^2 C_1-1}\right)\beta L\,,\\
A_4&=-\left(\sqrt{\xi^2 C_1+1}-\sqrt{\xi^2 C_1-1}\right)\beta L\,,
\end{aligned}
\right\}\quad \text{(B-14)}
$$

where

$$
\begin{aligned}
A_0=&\left[\alpha\bar{T}_0+\nu C_1+\frac{\alpha\bar{T}_0}{(1-\nu)}\left(\frac{d}{R}\right)\right]+16\xi^4\left\{4\alpha\sum_{i=2}^{\infty}\frac{\bar{T}_i}{(i^4\eta^4-16i^2C_1\xi^4\eta^2+64\xi^4)}\right.\\
&\left.+\frac{\alpha}{(1-\nu)}\left(\frac{d}{R}\right)\sum_{j=2}^{\infty}\frac{(4-j^2\eta^2)\bar{T}_j}{(j^4\eta^4-16j^2C_1\xi^4\eta^2+64\xi^4)}\right\}.
\end{aligned}\qquad \text{(B-15)}
$$

where $\quad \bar{k}=\left(\dfrac{1-\xi^2 C_1}{1+\xi^2 C_1}\right)^{\frac{1}{2}}$.

The deformation mode is thus expressed in terms of the eigenvalue C_1 using equations (B-8) to (B-15).

In order to determine C_1 the compatibility equation (B-2) is expressed, using equations (B-4) and (B-8) as:

$$
\begin{aligned}
\frac{\chi}{E}=&-\frac{C_1}{2}y^2-\frac{C_2}{2}x^2+16\xi^4\iint\left\{4\alpha\sum_{i=2}^{\infty}\frac{\bar{T}_i}{(i^4\eta^4-16i^2C_1\xi^4\eta^2+64\xi^4)}\cos\frac{i\pi x}{2L}\right.\\
&\left.+\frac{\alpha}{(1-\nu)}\left(\frac{d}{R}\right)\sum_{j=2}^{\infty}\frac{(4-j^2\eta^2)\bar{T}_j}{(j^4\eta^4-16j^2C_1\xi^4\eta^2+64\xi^4)}\cos\frac{j\pi x}{2L}\right\}dx\,dx\\
&+\iint A(x)\,dx\,dx-\alpha\iint\sum_{i=2}^{\infty}\bar{T}_i\cos\frac{i\pi x}{2L}dx\,dx\,.
\end{aligned}\qquad \text{(B-16)}
$$

The axial and circumferential stresses become:

$$
\left.
\begin{aligned}
&\frac{\bar{\sigma}_{11}}{E}=\frac{\chi_{yy}}{E}=-C_1\,,\\
&\frac{\bar{\sigma}_{22}}{E}=\frac{\chi_{xx}}{E}=-C_2+16\xi^4\Bigg\{4\alpha\sum_{i=2}^{\infty}\frac{\bar{T}_i}{(i^4\gamma^4-16i^2C_1\xi^4\gamma^2+64\xi^4)}\cos\frac{i\pi x}{2L}\\
&\qquad+\frac{\alpha}{(1-\nu)}\left(\frac{d}{R}\right)\sum_{j=2}^{\infty}\frac{(4-j^2\gamma^2)\tilde{T}_j}{(j^4\gamma^4-16j^2C_1\xi^4\gamma^2+64\xi^4)}\cos\frac{j\pi x}{2L}\Bigg\}\\
&\qquad+A(x)-\alpha\sum_{i=2}^{\infty}\bar{T}_i\cos\frac{i\pi x}{2L}\\
&\quad=-\frac{w}{R}-\alpha\bar{T}-\left[\nu C_1+C_2+\frac{\alpha\tilde{T}_0}{(1-\nu)}\left(\frac{d}{R}\right)\right],\\
&\frac{\bar{\sigma}_{12}}{E}=-\frac{\chi_{xy}}{E}=0\,.
\end{aligned}
\right\}
\qquad \text{(B-17)}
$$

The constants C_1 and C_2 are determined by applying the boundary conditions:

$$\int_0^{2L} u_x\, d_x = 0 \qquad\qquad v_y = 0$$

This yields:

$$-C_1=-\alpha\bar{T}_0+\frac{\nu\alpha\tilde{T}_0}{(1-\nu)}\left(\frac{d}{R}\right)+\frac{\nu}{2L}\int_0^{2L}A(x)\,dx+\frac{1}{4L}\int_0^{2L}w_x^2dx\,, \qquad \text{(B-18)}$$

$$-C_2=\frac{\alpha\tilde{T}_0}{(1-\nu)}\left(\frac{d}{R}\right), \qquad \text{(B-19)}$$

where the integrals on the right hand side of equation (B-18) are given by:

$$\frac{1}{2L}\int_0^{2L} A(x)\,dx = F_1(A):$$

i) the case of $1-\xi^2 C_1>0$,

$$F_1(A)=\frac{\sqrt{1+\xi^2 C_1}}{2\beta L}\left[A_1\{\bar{k}+e^{-2\sqrt{1-\xi^2 C_1}\beta L}[-\bar{k}\cos(2\sqrt{1+\xi^2 C_1}\beta L)+\sin(2\sqrt{1+\xi^2 C_1}\beta L)]\}\right. \tag{B-20}$$
$$\left.+A_2\{1-e^{-2\sqrt{1-\xi^2 C_1}\beta L}[\cos(2\sqrt{1+\xi^2 C_1}\beta L)+\bar{k}\sin(2\sqrt{1+\xi^2 C_1}\beta L)]\}\right],$$

ii) the case of $1-\xi^2 C_1=0$,

$$F_1(A)=-\frac{2\sqrt{2}(1-\cos 2\sqrt{2}\beta L)}{2\beta L(2\sqrt{2}\beta L+\sin 2\sqrt{2}\beta L)}A_0, \tag{B-21}$$

iii) the case of $1-\xi^2 C_1<0$,

$$F_1(A)=\frac{1}{\beta L}\left\{\frac{\sin[(\sqrt{\xi^2 C_1+1}+\sqrt{\xi^2 C_1-1})\beta L]}{\sqrt{\xi^2 C_1+1}+\sqrt{\xi^2 C_1-1}}A_1+\frac{\sin[(\sqrt{\xi^2 C_1+1}-\sqrt{\xi^2 C_1-1})\beta L]}{\sqrt{\xi^2 C_1+1}-\sqrt{\xi^2 C_1-1}}A_2\right\} \tag{B-22}$$

$$\frac{1}{4L}\int_0^{2L} w_x{}^2\,dx = F_2\left(\frac{1}{2}w_x{}^2\right):$$

i) the case of $1-\xi^2 C_1>0$,

$$F_2\left(\frac{1}{2}w_x{}^2\right)=\frac{1}{2}(1+\xi^2 C_1)\xi^2\left\{(1-e^{-4\sqrt{1-\xi^2 C_1}\beta L})\frac{(B_1{}^2+B_2{}^2)}{4\sqrt{1-\xi^2 C_1}\beta L}\right.$$
$$+(1-e^{-4\sqrt{1-\xi^2 C_1}\beta L}\cos[4\sqrt{1+\xi^2 C_1}\beta L])$$
$$\times\frac{2\sqrt{1+\xi^2 C_1}\beta L}{16(\beta L)^2}[\bar{k}(B_1{}^2-B_2{}^2)+2B_1B_2]$$
$$+e^{-4\sqrt{1-\xi^2 C_1}\beta L}\sin[4\sqrt{1+\xi^2 C_1}\beta L]$$
$$\times\left[\frac{2\sqrt{1+\xi^2 C_1}\beta L}{16(\beta L)^2}[(B_1{}^2-B_2{}^2)-2\bar{k}B_1B_2]\right]$$
$$-e^{-2\sqrt{1-\xi^2 C_1}\beta L}\left[(B_1{}^2-B_2{}^2)\cos(2\sqrt{1+\xi^2 C_1}\beta L)\right.$$
$$\left.\left.+\left(\frac{B_1{}^2+B_2{}^2}{2\sqrt{1+\xi^2 C_1}\beta L}+2B_1B_2\right)\sin(2\sqrt{1+\xi^2 C_1}\beta L)\right]\right\}$$
$$+8\sqrt{1+\xi^2 C_1}\xi^5\gamma_i\left[4\alpha\sum_{i=2}^{\infty}\frac{i\,T_i}{(i^4\gamma_i{}^4-16i^2C_1\xi^4\gamma_i{}^2+64\xi^4)}f_1(i)\right.$$
$$\left.+\frac{\alpha}{(1-\nu)}\left(\frac{d}{R}\right)\sum_{j=2}^{\infty}\frac{j(4-j^2\gamma_j{}^2)\bar{T}_j}{(j^4\gamma_j{}^4-16j^2C_1\xi^4\gamma_j{}^2+64\xi^4)}f_1(j)\right]+g(i,j), \tag{B-23}$$

ii) the case of $1-\xi^2C_1=0$,

$$F_2\left(\frac{1}{2}w_x^2\right)=\frac{R^2}{4}\Big[[(A_3^2+A_4^2)+(A_2A_3-A_1A_4)2\sqrt{2}\beta+2(A_1^2+A_2^2)\beta^2]$$

$$-[A_3(A_4-A_1\sqrt{2}\beta)-A_4(A_3+A_2\sqrt{2}\beta)]2\sqrt{2}\beta L+\frac{8}{3}(A_3^2+A_4^2)(\beta L)^2$$

$$+\frac{1}{4\sqrt{2}\beta L}\Big\{[A_3A_4-(A_1A_3-A_2A_4)\sqrt{2}\beta-4A_1A_2\beta^2]$$

$$+[(A_1A_3-A_2A_4)\sqrt{2}\beta+([A_3^2-A_4^2]+[A_2A_3+A_1A_4]2\sqrt{2}\beta)2\sqrt{2}\beta L$$

$$+4A_1A_2\beta^2+A_3A_4(16[\beta L]^2-1)]\cos 4\sqrt{2}\beta L$$

$$+\Big[(A_2A_3+A_1A_4)\sqrt{2}\beta+(2A_3A_4-[A_1A_3-A_2A_4]2\sqrt{2}\beta)2\sqrt{2}\beta L$$

$$+2(A_2^2-A_1^2)\beta^2-\frac{1}{2}(A_3^2-A_4^2)(16[\beta L]^2-1)\Big]\sin 4\sqrt{2}\beta L\Big\}\Big]$$

$$+8\xi^4\eta R\Big[4\alpha\sum_{i=2}^{\infty}\frac{\pi i^2\widetilde{T}_i}{(i^4\eta^4-16i^2C_1\xi^4\eta^2+64\xi^4)[(\pi i)^2-8(\beta L)^2]}f_2(i)$$

$$+\frac{\alpha}{(1-\nu)}\left(\frac{d}{R}\right)\sum_{j=2}^{\infty}\frac{\pi j^2(4-j^2\eta^2)\widetilde{T}_j}{(j^4\eta^4-16j^2C_1\xi^4\eta^2+64\xi^4)[(\pi j)^2-8(\beta L)^2]}f_2(j)\Big]$$

$$+g(i,j)\,, \tag{B-24}$$

iii) the case of $1-\xi^2C_1<0$,

$$F_2\left(\frac{1}{2}w_x^2\right)=\frac{1}{2}\xi^3\Big[[(\xi^2C_1+\sqrt{\xi^4C_1^2-1})A_1^2+(\xi^2C_1-\sqrt{\xi^4C_1^2-1})A_2^2]$$

$$-\frac{A_1A_2}{\beta L}\left[\frac{1}{\sqrt{\xi^2C_1+1}}\sin(2\sqrt{\xi^2C_1+1}\beta L)-\frac{1}{\sqrt{\xi^2C_1-1}}\sin(2\sqrt{\xi^2C_1-1}\beta L)\right]$$

$$-\frac{1}{2\beta L}\Big[\frac{(\xi^2C_1+\sqrt{\xi^4C_1^2-1})A_1^2}{(\sqrt{\xi^2C_1+1}+\sqrt{\xi^2C_1-1})}\sin[2(\sqrt{\xi^2C_1+1}+\sqrt{\xi^2C_1-1})\beta L]$$

$$+\frac{(\xi^2C_1-\sqrt{\xi^4C_1^2-1})A_2^2}{(\sqrt{\xi^2C_1+1}-\sqrt{\xi^2C_1-1})}\sin[2(\sqrt{\xi^2C_1+1}-\sqrt{\xi^2C_1-1})\beta L]\Big]\Big]$$

$$-8\xi^5\eta\Big[4\alpha\sum_{i=2}^{\infty}\frac{2\pi i^2\widetilde{T}_i}{(i^4\eta^4-16i^2C_1\xi^4\eta^2+64\xi^4)}f_3(i)$$

$$+\frac{\alpha}{(1-\nu)}\left(\frac{d}{R}\right)\sum_{j=2}^{\infty}\frac{2\pi j^2(4-j^2\eta^2)\widetilde{T}_j}{(j^4\eta^4-16j^2C_1\xi^4\eta^2+64\xi^4)}f_3(j)\Big]+g(i,j)\,, \tag{B-25}$$

where

$$\left.\begin{array}{l}B_1=\bar{k}A_1-A_2\,,\\ B_2=A_1+\bar{k}A_2\,,\end{array}\right\} \tag{B-26}$$

$$f_1(k)=(1-e^{-2\sqrt{1-\xi^2C_1}\beta L}\cos[2\sqrt{1+\xi^2C_1}\beta L])\Big[\frac{(\pi k+2\sqrt{1+\xi^2C_1}\beta L)B_1-2\sqrt{1-\xi^2C_1}\beta LB_2}{(\pi k)^2+8(\beta L)^2+4\pi k\sqrt{1+\xi^2C_1}\beta L}$$

$$+\frac{(\pi k-2\sqrt{1+\xi^2C_1}\beta L)B_1+2\sqrt{1-\xi^2C_1}\beta LB_2}{(\pi k)^2+8(\beta L)^2-4\pi k\sqrt{1+\xi^2C_1}\beta L}\Big]$$

$$-e^{-2\sqrt{1-\xi^2C_1}\beta L}\sin[2\sqrt{1+\xi^2C_1}\beta L]\Big[\frac{2\sqrt{1-\xi^2C_1}\beta LB_1+(\pi k+2\sqrt{1+\xi^2C_1}\beta L)B_2}{(\pi k)^2+8(\beta L)^2+4\pi k\sqrt{1+\xi^2C_1}\beta L}$$

$$+\frac{-2\sqrt{1-\xi^2C_1}\beta LB_1+(\pi k-2\sqrt{1+\xi^2C_1}\beta L)B_2}{(\pi k)^2+8(\beta L)^2-4\pi k\sqrt{1+\xi^2C_1}\beta L}\Big], \tag{B-27}$$

$$
\begin{aligned}
f_2(k) = &-\left[A_2\sqrt{2}\,\beta + A_3\frac{(\pi k)^2-24(\beta L)^2}{(\pi k)^2-8(\beta L)^2}\right] \\
&+\left[(A_2+2A_4L)\sqrt{2}\,\beta + A_3\frac{(\pi k)^2-24(\beta L)^2}{(\pi k)^2-8(\beta L)^2}\right]\cos 2\sqrt{2}\,\beta L \\
&+\left[(-A_1+2A_3L)\sqrt{2}\,\beta + A_4\frac{(\pi k)^2+8(\beta L)^2}{(\pi k)^2-8(\beta L)^2}\right]\sin 2\sqrt{2}\,\beta L\,,
\end{aligned}
\tag{B-28}
$$

$$
\begin{aligned}
f_3(k) = &\frac{(\sqrt{\xi^2C_1+1}+\sqrt{\xi^2C_1-1})A_1}{(\pi k)^2-8(\xi^2C_1+\sqrt{\xi^4C_1^2-1})(\beta L)^2}\sin\left[(\sqrt{\xi^2C_1+1}+\sqrt{\xi^2C_1-1})\beta L\right] \\
&+\frac{(\sqrt{\xi^2C_1+1}-\sqrt{\xi^2C_1-1})A_2}{(\pi k)^2-8(\xi^2C_1-\sqrt{\xi^4C_1^2-1})(\beta L)^2}\sin\left[(\sqrt{\xi^2C_1+1}-\sqrt{\xi^2C_1-1})\beta L\right],
\end{aligned}
\tag{B-29}
$$

$$
\begin{aligned}
g(i,j) = 16\xi^8\eta^2\Bigg[&4\alpha\sum_{i=2}^{\infty}\frac{iT_i}{(i^4\eta^4-16i^2C_1\xi^4\eta^2+64\xi^4)} \\
&+\frac{\alpha}{(1-\nu)}\left(\frac{d}{R}\right)\sum_{j=2}^{\infty}\frac{j(4-j^2\eta^2)\tilde{T}_j}{(j^4\eta^4-16j^2C_1\xi^4\eta^2+64\xi^4)}\Bigg]^2.
\end{aligned}
\tag{B-30}
$$

By using equations (B-20) to (B-30) and assuming a temperature distribution equation (B-18) becomes a transcendental equation for C_1. This can be solved by a standard iterative technique. Equations (B-17) can then be solved for the corresponding stresses for that temperature distribution and equation (B-8) can be solved for the displacements.

```
C
C
C                                        APPENDIX C
C
C
C      PROGRAM LISTING FOR SUCCESSIVE APPROXIMATION SOLUTION
C
C
C      MAIN PROGRAM
C
C
      REAL L,T(10),X(10)
      COMMON /AREA1/ R,D,L,E,ALP,ADT,SQ,V,SNQ,T
      COMMON /AREA3/ NT
      READ(5,700) ZXC,NT
  700 FORMAT(F10.5,I5)
      READ(5,100)R,L,D,E,ALP
  100 FORMAT(3F10.5,F10.0,F10.7)
      READ(5,300)(T(I),I=1,NT)
      READ(5,300)(X(I),I=1,NT)
  300 FORMAT(7F10.5)
      WRITE(6,400)
  400 FORMAT('1',T20,'THE THERMAL BUCKLING OF A CLAMPED CYLINDER'//)
      WRITE(6,500)
  500 FORMAT('0',T10,'RADIUS',T25,'HALF LENGTH',T40,'THICKNESS',T55,
     &'MODULUS',T70,'ALPHA'/)
      WRITE(6,600)R,L,D,E,ALP
  600 FORMAT('0',T10,F10.5,T25,F10.5,T40,F10.5,T55,F10.0,T70,F10.7)
      V=.3
      XST=ZXC
      ADT=0.
      EPS=.00002
      CALL TEMP(X)
      WRITE(6,402)
  402 FORMAT('0',T10,'THE TEMPERATURE COEFFICENTS ARE')
      WRITE(6,401)(T(K),K=1,NT)
  401 FORMAT('0',7F10.5)
      DO 10 KKK=1,100
      ADT=ADT+ZXC/ALP
      DO 12 MI=1,NT
   12 T(MI)=T(MI)*ADT
C
C
C      PREPARE ITERATION
C
C
      IER=0
      XMO=0.
      XR=XST+ZXC/2.
      XL=XST-ZXC/2.
C
C
C      START ITERATION LOOP
C
C
      DO 6 I=1,300
  140 XM=.5*(XL+XR)
      FXR=FCT(XR)
      IF(I-1)120,130,120
  130 FXL=FCT(XL)
      TAST=FXL*FXR
      IF(TAST.LE.0.)GO TO 120
      XR=XR+2.*ZXC
```

```
      XL=XL-2.*ZXC
      IF(XL.LE.0.)XL=ZXC
      GO TO 140
  120 FXM=FCT(XM)
      TEST=FXR*FXM
      IF(TEST)20,30,40
   40 XR=XM
      GO TO 21
   20 XL=XM
      GO TO 21
   30 IF(FXR.EQ.0.)XM=XL
   21 C1=XM
C
C
C     TEST ON SATISFACTORY RESULTS
C
C
      TOL=C1
      VAL=FCT(TOL)
      TOL=EPS
      Y=XM-XMO
      Z=ABS(C1)
      IF(Z-1.)4,4,3
    3 TOL=TOL*Z
    4 IF(ABS(Y)-TOL)5,5,6
    5 IF(ABS(VAL)-10.*TOL)7,7,6
    6 XMO=XM
C
C     END OF ITERATION LOOP
C
C     NO CONVERGENCE
C
      IER=1
    7 GO TO 9
C
C
C     ERROR FOR ZERO DIVISION
C
C
    8 IER=2
    9 CONTINUE
      PD=C1*E*3.14159*D*R*2.
      WRITE(6,200)ADT,PD,IER
      WRITE(6,220)
  200 FORMAT('0',T5,'LOAD AT MTEMP=',F8.3,'IS EQUAL TO ',F10.2,'IER='
     &,I2)
  220 FORMAT('0',T10,'X(FROM END)',T30,'W-DISPL',T45,'HOOP STESS')
      CALL DISPL(C1)
      XST=C1
      DO 42 KIM=1,NT
   42 T(KIM)=T(KIM)/ADT
   10 CONTINUE
      STOP
      END
```

```
      FUNCTION FCT(C1)
C
C
C     TRANSCENDENTAL FUNCTION SUBROUTINE
C
C
      REAL L,T(10)
      COMMON /AREA1/ R,D,L,E,ALP,ADT,SQ,V,SNQ,T
      COMMON /AREA2/ A1,A2,A3,A4,A0,B,XX,XY,BB1,BB2
      COMMON /AREA3/ NT
      B=(3.*(1.-V*V)/(D*D*R*R))**(.25)
      SQ=R*B
      SNQ=3.14159*R/L
      TEST=1.-SQ*SQ*C1
      IF(TEST)30,20,11
   11 C=SQRT((1.-SQ*SQ*C1)/(1.+SQ*SQ*C1))
      XX=SQRT(TEST)*B*L
      XY=SQRT(1.+SQ*SQ*C1)*B*L
      CALL SUM(C1,SU1)
      A0=T(1)*ALP+V*C1+64.*ALP*SQ**4*SU1
      IF(XX.GT.30.)XX=30.
      A1=-(1.-EXP(-2.*XX)*(COS(2.*XY)-C*SIN(2.*XY)))/(1.-EXP(-4.*
     &XX)+2.*C*EXP(-2.*XX)*SIN(2.*XY))*A0
      A3=A1
      A2=-(C-EXP(-2.*XX)*(C*COS(2.*XY)+SIN(2.*XY)))/(1.-EXP(-4.*XX
     &)+2.*C*EXP(-2.*XX)*SIN(2.*XY))*A0
      A4=-A2
      F1A=SQRT(1.+SQ*SQ*C1)/(2.*B*L)*(A1*(C+EXP(-2.*XX)*(-C*COS(2
     &.*XY)+SIN(2.*XY)))+A2*(1.-EXP(-2.*XX)*(COS(2.*XY)+C*SIN(2.*
     &XY))))
      BB1=C*A1-A2
      BB2=A1+C*A2
      CALL SUM1(C1,SU2,SU3)
      F2W=.5*(1.+SQ*SQ*C1)*SQ*SQ*((1.-EXP(-4.*XX))*(BB1*BB1+BB2*B
     &B2)/(4.*XX)+(1.-EXP(-4.*XX)*COS(4.*XY))*(2.*XY)/(16.*B*B*L*
     &L)*(C*(BB1*BB1-BB2*BB2)+2.*BB1*BB2)+EXP(-4.*XX)*SIN(4.*XY)*(2
     &.*XY/(16.*B*B*L*L)*((BB1*BB1-BB2*BB2)-2.*C*BB1*BB2))-EXP(-2.
     &*XX)*((BB1*BB1-BB2*BB2)*COS(2.*XY)+((BB1*BB1+BB2*BB2)/(2.*
     &XY)+2.*BB1*BB2)*SIN(2.*XY)))
     & +32.*ALP*SNQ*SQ**5*SQRT(1.+SQ*SQ*C1)*SU2+(SU3*16.*ALP
     & *SNQ*SQ**4)**2
      FCT=T(1)*ALP-V*F1A-F2W-C1
      GO TO 23
   20 CONTINUE
      XX=B*SQRT(2.)
      SINA=SIN(2.*XX*L)
      COSA=COS(2.*XX*L)
      A0=ADT+V*C1
      A1=-A0
      A2=(1.-COSA)/(2.*XX*L+SINA)*A0
      A3=XX*(1.-COSA)/(2.*XX*L+SINA)*A0
      A4=-(XX*SINA)/(XX*L*2.+SINA)*A0
      F1A=-XX*(1.-COSA)/(2.*B*L*(2.*XX*L+SINA))*A0
      F2W=R*R/4.*(((A3*A3+A4*A4)+(A2*A3-A1*A4)*2.*XX+2.*B*B*
     &(A1*A1+A2*A2))-(A3*(A4-A1*XX)-A4*(A3+A2*XX))*2.*XX*L+8./3.*
     &(A3*A3+A4*A4)*B*B*L*L+1./(4.*XX*L)*((A3*A4-(A1*A3-A2*A4)*XX
     &-4.*A1*A2*B*B)+((A1*A3-A2*A4)*XX+((A3*A3-A4*A4)+(A2*A3+A1*A4)
     &*2.*XX)*2.*XX*L+4.*A1*A2*B*B+A3*A4*(16.*B*B*L*L-1.))*COS
     &(4.*XX*L)+((A2*A3+A1*A4)*XX+(2.*A3*A4-(A1*A3-A2*A4)*2.*XX)*
     &2.*XX*L+2.*(A2*A2-A1*A1)*B*B-.5*(A3*A3-A4*A4)*(16.*B*B*L*L-
     &1.))*SIN(4.*XX*L)))
      FCT=ADT-V*F1A-F2W-C1
      GO TO 23
```

```
   30 CONTINUE
      XX=SQRT(SQ*SQ*C1-1.)
      XY=SQRT(SQ*SQ*C1+1.)
      YX=XX+XY
      ZX=XY-XX
      A0=ADT+V*C1
      A1=ZX*SIN(ZX*B*L)/(XX*SIN(XY*2.*B*L)+XY*SIN(2.*XX*B*L))*AC
      A2=-YX*SIN(YX*B*L)/(XX*SIN(2.*XY*B*L)+XY*SIN(2.*XX*B*L))*AC
      A3=-YX*B*L
      A4=-ZX*B*L
      F1A=1./(B*L)*(SIN(YX*B*L)/YX*A1+SIN(ZX*B*L)/ZX*A2)
      F2W=.5*SQ*SQ*(((SQ*SQ*C1+SQRT(SQ*SQ*SQ*SQ*C1*C1-1.))*A1*A1+
     &(SQ*SQ*C1-SQRT(SQ*SQ*SQ*SQ*C1*C1-1.))*A2*A2)-A1*A2/B/L*(SIN
     &(2.*XY*B*L)/XY-SIN(2.*XX*B*L)/XX)-1./(2.*B*L)*((SQ*SQ*C1+
     &SQRT(SQ*SQ*SQ*SQ*C1*C1-1.)) *A1*A1*SIN(2.*YX*B*L)/YX+(SQ*SQ
     &*C1-SQRT(SQ*SQ*SQ*SQ*C1*C1-1.))*A2*A2*SIN(2.*ZX*B*L)/ZX))
      FCT=ADT-V*F1A-F2W-C1
   23 RETURN
      END
```

```
      SUBROUTINE DISPL(C1)
C
C
C     SUBROUTINE FOR SOLVING FOR DISPLACEMENTS AND STRESSES
C
C
      REAL L,T(10)
      COMMON /AREA1/ R,D,L,E,ALP,ADT,SQ,V,SNQ,T
      COMMON /AREA2/ A1,A2,A3,A4,AC,B,XX,XY,BB1,BB2
      COMMON /AREA3/ NT
      X=0.
      TEST=1.-SQ*SQ*C1
      DO 70 JJJ=1,41
      IF(TEST)1,2,3
    3 CONTINUE
      XXX=SQRT(TEST)*B*X
      XXY=SQRT(1.+SQ*SQ*C1)*B*X
      XXL=SQRT(1.-SQ*SQ*C1)*B*(X-2.*L)
      XYL=SQRT(1.+SQ*SQ*C1)*B*(X-2.*L)
      IF(XXL.LT.-30.)XXL=-30.
      IF(XXX.GT.30.)XXX=30.
      AX=A1*EXP(-XXX)*COS(XXY)+A2*EXP(-XXX)*SIN(XXY)+A3*EXP(XXL)*
     &COS(XYL)+A4*EXP(XXL)*SIN(XYL)
      CALL SUM2(C1,X,SU4,SU5)
      GO TO 60
    2 CONTINUE
      XX=B*SQRT(2.)*X
      AX=(A1+A3*X)*COS(XX)+(A2+A4*X)*SIN(XX)
      GO TO 60
    1 CONTINUE
      XX=SQRT(SQ*SQ*C1-1.)
      XY=SQRT(SQ*SQ*C1+1.)
      YX=XX+XY
      ZX=XY-XX
      AX=A1*COS(YX*B*X+A3)+A2*COS(ZX*B*X+A4)
   60 WDR=-(T(1)*ALP+V*C1)-AX-64.*ALP*SQ**4*SU4
      S22DE=-WDR-(T(1)+SU5)*ALP-V*C1
      W=WDR*R
      S22=S22DE*E
      WRITE(6,300)X,W,S22
  300 FORMAT(' ',T10,F6.3,T30,F9.6,T45,F8.0)
      X=X+L/40.
   70 CONTINUE
      RETURN
      END
```

```
      SUBROUTINE SUM(C1,SU1)
C
C
C     SUMMATION SUBROUTINE
C
C
      COMMON /AREA1/ R,D,L,E,ALP,ADT,SQ,V,SNQ,T
      COMMON /AREA2/ A1,A2,A3,A4,AC,B,XX,XY,BB1,BB2
      COMMON /AREA3/ NT
      REAL L,T(10)
      SU1=0.
      PI=3.14159
      DO 10 II=2,NT
      I=(II-1*1)*2
      SD=T(II)/((I*SNQ)**4-16.*I*I*C1*SNQ*SNQ
     & *SQ**4+64.*SQ**4)
      SU1=SU1+SD
   10 CONTINUE
      RETURN
      END
```

```
      SUBROUTINE SUM1(C1,SU2,SU3)
C
C
C     SUMMATION SUBROUTINE
C
C
      COMMON /AREA1/ F,D,L,E,ALP,ADT,SQ,V,SNQ,T
      COMMON /AREA2/ A1,A2,A3,A4,A5,B,XX,XY,BB1,BB2
      COMMON /AREA3/ NT
      REAL L,T(10)
      SU2=0.
      SU3=0.
      PI=3.14159
      DO 10 II=2,NT
      I=(II-1*1)*2
      SD=T(II)/(((I*SNQ)**4-16.*I*I*C1*SNQ*SNQ
     & *SQ**4+64.*SQ**4)
      F1IA=1.-EXP(-2.*XX)*COS(2.*XY)
      F1IB=((PI*I+2.*XY)*BB1-2.*XX*BB2)/(PI*PI*I*I+8.*B*B*L*L
     & +4.*PI*I*XY)+((PI*I-2.*XY)*BB1+2.*XX*BB2)/(PI*PI*I*I
     & +8.*B*B*L*L-4.*PI*I*XY)
      F1IC=EXP(-2.*XX)*SIN(2.*XY)
      F1ID=(2.*XX*BB1+(PI*I+2.*XY)*BB2)/(PI*PI*I*I+8.*B*B*L*L
     & +4.*PI*I*XY)+(-2.*XX*BB1+(PI*I-2.*XY)*BB2)/(PI*PI*I*I
     & +8.*B*B*L*L-4.*PI*I*XY)
      F1I=F1IA*F1IB-F1IC*F1ID
      SU2=SU2+SD*I*F1I
      SU3=SU3+SD*I
   10 CONTINUE
      RETURN
      END
```

```
      SUBROUTINE SUM2(C1,X,SU4,SU5)
C
C
C     SUMMATION SUBROUTINE
C
C
      COMMON /AREA1/ R,D,L,E,ALP,ADT,SQ,V,SNQ,T
      COMMON /AREA2/ A1,A2,A3,A4,A0,B,XX,XY,BB1,BB2
      COMMON /AREA3/ NT
      REAL L,T(10)
      SU4=0.
      SU5=0.
      PI=3.14159
      DO 10 II=2,NT
      I=(II-1)*2
      SD=T(II)/(((I*SNQ)**4-16.*I*I*C1*SNQ*SNQ*SQ**4+64.*SQ**4
     S )*COS(I*PI*X/2./L)
      SU4=SU4+SD
      SU5=SU5+T(II)*COS(I*PI*X/2./L)
   10 CONTINUE
      RETURN
      END
```

```
      SUBROUTINE TEMP(X)
C
C
C     SUBROUTINE FOR SOLVING FOR THE TEMPERATURE COEFFICIENTS
C
C
      COMMON /AREA1/ P,D,L,E,ALP,ACT,SQ,V,SNO,T
      COMMON /AREA3/ NT
      REAL L,T(10),X(10),A(10,10),WKAREA(15)
      DO 13 I=1,NT
      DO 13 J=1,NT
   13 A(I,J)=COS(2.*(J-1)*X(I)/2./L*3.14159)
      CALL LEQT1F(A,1,NT,10,T,3,WKAREA,IER)
      RETURN
      END
```

THE THERMAL BUCKLING OF A CLAMPED CYLINDER

RADIUS	HALF LENGTH	THICKNESS	MODULUS	ALPHA
0.89100	5.05000	0.01060	10000000.	0.0000135

THE TEMPERATURE COEFFICENTS ARE

0.88890 -0.15252 -0.06873 -0.01191 -0.03639 -0.05179

LOAD AT MTEMP= 14.815IS EQUAL TO 111.27IER= 0

X(FROM END)	W-DISPL	HOOP STESS
0.0	0.0	-1698.
0.126	-0.000128	-277.
0.252	-0.000163	76.
0.379	-0.000163	7.
0.505	-0.000169	-3.
0.631	-0.000177	-0.
0.757	-0.000185	0.
0.884	-0.000192	0.
1.010	-0.000198	0.
1.136	-0.000202	0.
1.262	-0.000204	0.
1.389	-0.000204	0.
1.515	-0.000204	0.
1.641	-0.000202	0.
1.767	-0.000201	-0.
1.894	-0.000200	-0.
2.020	-0.000201	-0.
2.146	-0.000202	-0.
2.272	-0.000205	-0.
2.399	-0.000209	-0.
2.525	-0.000214	-0.
2.651	-0.000220	0.
2.777	-0.000225	0.
2.904	-0.000229	0.
3.030	-0.000232	0.
3.156	-0.000234	0.
3.282	-0.000234	0.
3.409	-0.000234	0.
3.535	-0.000232	0.
3.661	-0.000229	0.
3.787	-0.000226	-0.
3.914	-0.000224	-0.
4.040	-0.000222	-0.
4.166	-0.000221	-0.
4.292	-0.000221	-0.
4.419	-0.000222	-0.
4.545	-0.000224	-0.
4.671	-0.000225	-0.
4.797	-0.000227	0.
4.924	-0.000228	0.
5.050	-0.000228	0.

LOAD AT MTEMP= 29.630IS EQUAL TO 218.13IER= 0

X(FROM END)	W-DISPL	HOOP STESS
0.0	-0.000000	-3373.
0.126	-0.000256	-531.
0.252	-0.000325	159.
0.379	-0.000323	11.
0.505	-0.000336	-7.

0.631	-0.000353	-0.
0.757	-0.000369	0.
0.884	-0.000383	0.
1.010	-0.000394	1.
1.136	-0.000402	1.
1.262	-0.000406	1.
1.389	-0.000407	0.
1.515	-0.000405	0.
1.641	-0.000403	0.
1.767	-0.000400	-0.
1.894	-0.000398	-0.
2.020	-0.000399	-0.
2.146	-0.000402	-0.
2.272	-0.000408	-0.
2.399	-0.000417	-0.
2.525	-0.000427	-0.
2.651	-0.000437	0.
2.777	-0.000448	0.
2.904	-0.000456	0.
3.030	-0.000463	0.
3.156	-0.000466	0.
3.282	-0.000467	0.
3.409	-0.000465	0.
3.535	-0.000461	0.
3.661	-0.000456	0.
3.787	-0.000450	-0.
3.914	-0.000446	-0.
4.040	-0.000442	-0.
4.166	-0.000440	-0.
4.292	-0.000441	-0.
4.419	-0.000443	-0.
4.545	-0.000445	-0.
4.671	-0.000449	0.
4.797	-0.000452	0.
4.924	-0.000454	0.
5.050	-0.000455	0.

LOAD AT MTEMP= 44.444IS EQUAL TO 322.95IER= 0

X(FROM END)	W-DISPL	HOOP STESS
0.0	-0.000000	-5038.
0.126	-0.000385	-765.
0.252	-0.000487	250.
0.379	-0.000483	13.
0.505	-0.000503	-12.
0.631	-0.000528	0.
0.757	-0.000551	1.
0.884	-0.000572	1.
1.010	-0.000589	1.
1.136	-0.000600	1.
1.262	-0.000607	1.
1.389	-0.000608	1.
1.515	-0.000606	1.
1.641	-0.000602	0.
1.767	-0.000598	-0.
1.894	-0.000596	-1.
2.020	-0.000597	-1.
2.146	-0.000601	-1.
2.272	-0.000610	-1.
2.399	-0.000623	-1.
2.525	-0.000638	-0.
2.651	-0.000654	0.
2.777	-0.000669	1.
2.904	-0.000683	1.
3.030	-0.000692	1.
3.156	-0.000698	1.

3.282	-0.000699	1.
3.409	-0.000696	1.
3.535	-0.000690	0.
3.661	-0.000682	0.
3.787	-0.000674	-0.
3.914	-0.000666	-0.
4.040	-0.000661	-1.
4.166	-0.000659	-1.
4.292	-0.000659	-1.
4.419	-0.000662	-0.
4.545	-0.000666	-0.
4.671	-0.000671	0.
4.797	-0.000676	0.
4.924	-0.000679	0.
5.050	-0.000680	1.

LOAD AT MTEMP= 59.259IS EQUAL TO 424.94IER= 0

X(FROM END)	W-DISPL	HOOP STESS
0.0	0.0	-6639.
0.126	-0.000514	-978.
0.252	-0.000648	350.
0.379	-0.000641	13.
0.505	-0.000667	-17.
0.631	-0.000701	1.
0.757	-0.000732	2.
0.884	-0.000760	2.
1.010	-0.000783	2.
1.136	-0.000796	3.
1.262	-0.000806	2.
1.389	-0.000808	2.
1.515	-0.000805	1.
1.641	-0.000800	0.
1.767	-0.000795	-1.
1.894	-0.000792	-1.
2.020	-0.000793	-2.
2.146	-0.000799	-2.
2.272	-0.000811	-2.
2.399	-0.000828	-1.
2.525	-0.000848	-0.
2.651	-0.000869	0.
2.777	-0.000890	1.
2.904	-0.000908	2.
3.030	-0.000920	2.
3.156	-0.000928	2.
3.282	-0.000929	2.
3.409	-0.000925	1.
3.535	-0.000917	1.
3.661	-0.000907	0.
3.787	-0.000896	-0.
3.914	-0.000886	-1.
4.040	-0.000879	-1.
4.166	-0.000876	-1.
4.292	-0.000876	-1.
4.419	-0.000880	-1.
4.545	-0.000886	-0.
4.671	-0.000892	0.
4.797	-0.000899	1.
4.924	-0.000903	1.
5.050	-0.000904	1.

LOAD AT MTEMP= 74.074IS EQUAL TO 526.94IER= 0

X(FROM END)	W-DISPL	HOOP STESS
0.0	0.0	-8340.
0.126	-0.000645	-1172.

0.252	-0.000809	457.
0.379	-0.000799	10.
0.505	-0.000832	-23.
0.631	-0.000874	1.
0.757	-0.000914	3.
0.834	-0.000948	3.
1.010	-0.000976	4.
1.136	-0.000996	4.
1.262	-0.001006	4.
1.389	-0.001008	3.
1.515	-0.001005	1.
1.641	-0.000993	0.
1.767	-0.000991	-1.
1.894	-0.000988	-2.
2.020	-0.000989	-3.
2.146	-0.000997	-3.
2.272	-0.001012	-3.
2.399	-0.001033	-2.
2.525	-0.001058	-1.
2.651	-0.001085	0.
2.777	-0.001111	2.
2.904	-0.001133	3.
3.030	-0.001149	3.
3.156	-0.001158	3.
3.282	-0.001159	3.
3.409	-0.001155	2.
3.535	-0.001144	1.
3.661	-0.001131	0.
3.787	-0.001118	-1.
3.914	-0.001106	-1.
4.040	-0.001097	-2.
4.166	-0.001093	-2.
4.292	-0.001093	-2.
4.419	-0.001098	-1.
4.545	-0.001105	-0.
4.671	-0.001114	0.
4.797	-0.001121	1.
4.924	-0.001127	1.
5.050	-0.001128	2.

LOAD AT MTEMP= 88.889IS EQUAL TO 628.93IER= 0

X(FROM END)	W-DISPL	HOOP STESS
0.0	0.0	-9990.
0.126	-0.000778	-1345.
0.252	-0.000972	573.
0.379	-0.000956	3.
0.505	-0.000997	-30.
0.631	-0.001048	2.
0.757	-0.001095	4.
0.884	-0.001137	4.
1.010	-0.001170	6.
1.136	-0.001194	6.
1.262	-0.001206	5.
1.389	-0.001209	4.
1.515	-0.001204	2.
1.641	-0.001196	0.
1.767	-0.001188	-2.
1.894	-0.001184	-3.
2.020	-0.001185	-4.
2.146	-0.001195	-4.
2.272	-0.001213	-4.
2.399	-0.001238	-3.
2.525	-0.001268	-1.
2.651	-0.001300	1.
2.777	-0.001331	2.

2.904	-0.001358	4.
3.030	-0.001377	5.
3.156	-0.001388	5.
3.282	-0.001390	4.
3.409	-0.001384	3.
3.535	-0.001372	2.
3.661	-0.001356	0.
3.787	-0.001340	-1.
3.914	-0.001325	-2.
4.040	-0.001315	-3.
4.166	-0.001310	-3.
4.292	-0.001310	-3.
4.419	-0.001316	-2.
4.545	-0.001325	-1.
4.671	-0.001335	0.
4.797	-0.001344	1.
4.924	-0.001350	2.
5.050	-0.001353	2.

LOAD AT MTEMP= 103.704IS EQUAL TO 730.93IER= 0

X(FROM END)	W-DISPL	HOOP STESS
0.0	0.0	-11641.
0.126	-0.000913	-1496.
0.252	-0.001135	698.
0.379	-0.001113	-8.
0.505	-0.001162	-37.
0.631	-0.001221	4.
0.757	-0.001276	5.
0.884	-0.001325	6.
1.010	-0.001364	8.
1.136	-0.001391	8.
1.262	-0.001406	7.
1.389	-0.001409	5.
1.515	-0.001404	3.
1.641	-0.001394	0.
1.767	-0.001385	-3.
1.894	-0.001379	-5.
2.020	-0.001381	-6.
2.146	-0.001393	-6.
2.272	-0.001414	-5.
2.399	-0.001443	-4.
2.525	-0.001478	-2.
2.651	-0.001516	1.
2.777	-0.001552	3.
2.904	-0.001583	5.
3.030	-0.001605	6.
3.156	-0.001618	7.
3.282	-0.001620	6.
3.409	-0.001613	5.
3.535	-0.001599	3.
3.661	-0.001581	1.
3.787	-0.001562	-1.
3.914	-0.001545	-3.
4.040	-0.001533	-4.
4.166	-0.001527	-4.
4.292	-0.001526	-4.
4.419	-0.001534	-2.
4.545	-0.001544	-1.
4.671	-0.001556	1.
4.797	-0.001567	2.
4.924	-0.001574	3.
5.050	-0.001577	3.

LOAD AT MTEMP= 118.519IS EQUAL TO 851.46IER= 0

X(FROM END)	W-DISPL	HOOP STESS
0.0	0.0	-13386.
0.126	-0.001059	-1621.
0.252	-0.001309	844.
0.379	-0.001276	-26.
0.505	-0.001335	-45.
0.631	-0.001403	6.
0.757	-0.001466	7.
0.884	-0.001522	8.
1.010	-0.001567	11.
1.136	-0.001597	11.
1.262	-0.001614	10.
1.389	-0.001618	7.
1.515	-0.001612	4.
1.641	-0.001601	0.
1.767	-0.001590	-3.
1.894	-0.001584	-6.
2.020	-0.001586	-8.
2.146	-0.001599	-8.
2.272	-0.001623	-7.
2.399	-0.001656	-5.
2.525	-0.001697	-2.
2.651	-0.001740	1.
2.777	-0.001781	5.
2.904	-0.001816	7.
3.030	-0.001842	9.
3.156	-0.001857	9.
3.282	-0.001859	8.
3.409	-0.001851	6.
3.535	-0.001835	4.
3.661	-0.001814	1.
3.787	-0.001792	-2.
3.914	-0.001773	-4.
4.040	-0.001759	-5.
4.166	-0.001752	-6.
4.292	-0.001753	-5.
4.419	-0.001760	-3.
4.545	-0.001772	-1.
4.671	-0.001786	1.
4.797	-0.001798	3.
4.924	-0.001806	4.
5.050	-0.001810	5.

LOAD AT MTEMP= 133.333IS EQUAL TO 953.46IER= 0

X(FROM END)	W-DISPL	HOOP STESS
0.0	0.0	-15036.
0.126	-0.001198	-1723.
0.252	-0.001474	938.
0.379	-0.001434	-47.
0.505	-0.001499	-54.
0.631	-0.001576	9.
0.757	-0.001647	8.
0.884	-0.001710	10.
1.010	-0.001760	13.
1.136	-0.001795	14.
1.262	-0.001814	12.
1.389	-0.001818	9.
1.515	-0.001811	5.
1.641	-0.001799	0.
1.767	-0.001787	-4.
1.894	-0.001780	-8.
2.020	-0.001782	-10.
2.146	-0.001797	-11.
2.272	-0.001824	-9.
2.399	-0.001861	-6.

2.525	-0.001907	-3.
2.651	-0.001955	2.
2.777	-0.002002	6.
2.904	-0.002041	9.
3.030	-0.002070	11.
3.156	-0.002087	11.
3.282	-0.002090	10.
3.409	-0.002081	8.
3.535	-0.002062	5.
3.661	-0.002039	1.
3.787	-0.002014	-2.
3.914	-0.001992	-5.
4.040	-0.001977	-7.
4.166	-0.001969	-7.
4.292	-0.001970	-6.
4.419	-0.001978	-4.
4.545	-0.001992	-2.
4.671	-0.002007	1.
4.797	-0.002021	4.
4.924	-0.002030	5.
5.050	-0.002034	6.

LOAD AT MTEMP= 148.148IS ECUAL TO 1055.45IER= 0

X(FROM END)	W-DISPL	HOOP STESS
0.0	0.0	-16687.
0.126	-0.001340	-1800.
0.252	-0.001639	1140.
0.379	-0.001590	-74.
0.505	-0.001664	-62.
0.631	-0.001750	12.
0.757	-0.001828	10.
0.884	-0.001898	13.
1.010	-0.001954	17.
1.136	-0.001993	17.
1.262	-0.002014	15.
1.389	-0.002018	11.
1.515	-0.002011	6.
1.641	-0.001997	0.
1.767	-0.001983	-6.
1.894	-0.001975	-10.
2.020	-0.001978	-15.
2.146	-0.001994	-13.
2.272	-0.002024	-11.
2.399	-0.002066	-8.
2.525	-0.002117	-3.
2.651	-0.002171	2.
2.777	-0.002222	7.
2.904	-0.002266	11.
3.030	-0.002299	14.
3.156	-0.002317	14.
3.282	-0.002320	13.
3.409	-0.002310	10.
3.535	-0.002290	6.
3.661	-0.002263	1.
3.787	-0.002236	-3.
3.914	-0.002212	-6.
4.040	-0.002194	-8.
4.166	-0.002186	-9.
4.292	-0.002187	-8.
4.419	-0.002196	-5.
4.545	-0.002211	-2.
4.671	-0.002228	1.
4.797	-0.002243	4.
4.924	-0.002254	6.
5.050	-0.002258	7.

TABLE I TEST RESULTS †

TEST No	Buckling Temp. T_B(°F)	Buckling Load P_B(lbs)	Maximum Load Temp. T_M(°F)	Maximum Load P_M(lbs)	Largest Temp. Change T_∇(°F)	Largest Load Change ∇P_∇(lbs)	n**	Secondary Buckling
6	307	1600	293	1675	307	830	4+ ring	yes
7	250	2040	250	2040	280	48	ring	no
8	310	1340	307	1360	310	485	5+ ring	no
9*								
10	225	1180	240	1190	240	730	4+ ring	no
11	280	1790	280	1790	280	930	6+ ring	yes
12	155	875	155	875	200	235	4	no
13	260	1910	275	1950	285	630	6	yes
14	205	1760	205	1760	228	600	6	yes
15	290	2120	290	2120	290	1450	6	yes
16	245	1790	245	1790	255	850	6+ ring	yes
17*								
18	295	1900	295	1900	295	1140	6	yes
19	350	2470	360	2480	360	1460	9 tiered	no
20	270	2060	270	2060	270	1340	6	no
21	315	1930	315	1930	315	1345	10 tiered	no
22	301	1795	301	1795	301	1205	9 tiered	no

† Tests number 1 to 5 were used for testing the systems.
* Data not available for tests 9 and 17.
** Number of circumferential half waves in buckling pattern. All but step-tiered patterns were complete.

TABLE II DISPLACEMENT RESULTS

Test No.	$R/_d$	Experimental Displ. W_E^*(in)	Theoretical Displ. W_T^* (in)	$\frac{WE}{W_T} \times 100$
12	98.9	.0020	.0015	133.
13	81.1	.0009	.0015	60.
14	81.1	.0013	.0015	86.7
15	64.0	.0007	.0015	46.7
16	63.8	.0004	.0015	26.7
18	78.7	.0011	.0015	73.3
19	61.5	.0012	.0015	80.0
20	66.7	.0006	.0015	40.0
21	84.1	.0004	.0015	26.7

*Displacements correspond to centerline radial displacement for ΔT equal to 100°F.

TABLE III COMPARISON OF EXPERIMENTAL AND THEORETICAL RESULTS

	$\frac{\text{Radius}}{\text{Thickness}}$	Length (in)	Exp. Buckling Temp. T_B^E (°F)	Theor. Buckling* Temp. T_B^E (°F)	$\frac{T_B^t}{T_B^E} \times 100$	Exp. Buckling Load P_B^E (lbs)	Theor. Buckling* Load P_B^t (lbs)	$\frac{P_B^E}{P_B^t} \times 100$
6	59.5	9.875	307	829	37.0	1600	7400	21.6
7	64.0	9.875	250	1000	25.0	2040	7500	27.4
8	74.4	9.875	310	775	40.0	1340	5500	24.4
9								
10	66.2	9.87	225	770	29.2	1180	6600	17.9
11	81.1	9.87	280	700	40.0	1790	4590	39.0
12	98.9	9.87	155	480	32.3	875	2750	31.8
13	81.1	10.16	260	651	39.9	1910	4548	42.0
14	81.1	10.12	205	650	31.5	1760	4601	38.3
15	64.0	10.15	290	835	34.7	2120	7440	28.5
16	63.8	10.15	245	811	30.2	1790	7000	25.6
17								
18	78.7	10.16	295	655	45.0	1900	4852	39.2
19	61.5	10.16	350	865	40.5	2470	8100	30.5
20	66.7	10.17	270	800	33.8	2060	6800	30.3
21	84.1	10.10	315	620	50.8	1930	4300	44.9
22	84.1	10.17	301	655	46.0	1795	4250	42.2

*Theoretical results based on successive approximation method of Sunakawa [30].

TABLE IV DIMENSIONLESS COEFFICIENTS

Test No.	Radius (in)	Thickness (in)	Length (in)	T_B^E (°F)	P_B^E lbs	Coefficient $z \times 10^{-3}$	Coefficient $K_x^1 \times 10^{-3}$	Coefficient $K_x^2 \times 10^{-3}$
6	.893	.015	9.875	307	1600	6.95	1.00	2.45
7	.891	.014	9.875	250	2040	7.42	1.49	2.18
8	.893	.012	9.875	310	1340	9.19	1.68	3.82
9								
10	.894	.0135	9.875	225	1180	8.159	1.03	2.41
11	.893	.011	9.875	280	1790	10.03	2.89	3.61
12	.890	.009	9.875	155	875	12.29	2.57	3.09
13	.893	.011	10.16	260	1910	10.03	3.13	3.73
14	.892	.011	10.13	205	1760	9.97	2.81	2.72
15	.894	.014	10.15	290	2120	7.88	1.67	2.41
16	.894	.014	10.15	245	1790	7.86	1.39	2.01
17								
18	.892	.011	10.16	295	1900	9.74	2.79	3.71
19	.890	.0145	10.16	350	2470	7.54	1.71	2.74
20	.894	.0135	10.17	270	2060	8.24	1.71	2.42
21	.891	.011	10.10	315	1930	10.30	3.43	4.43
22	.891	.011	10.17	301	1775	10.45	3.24	4.35

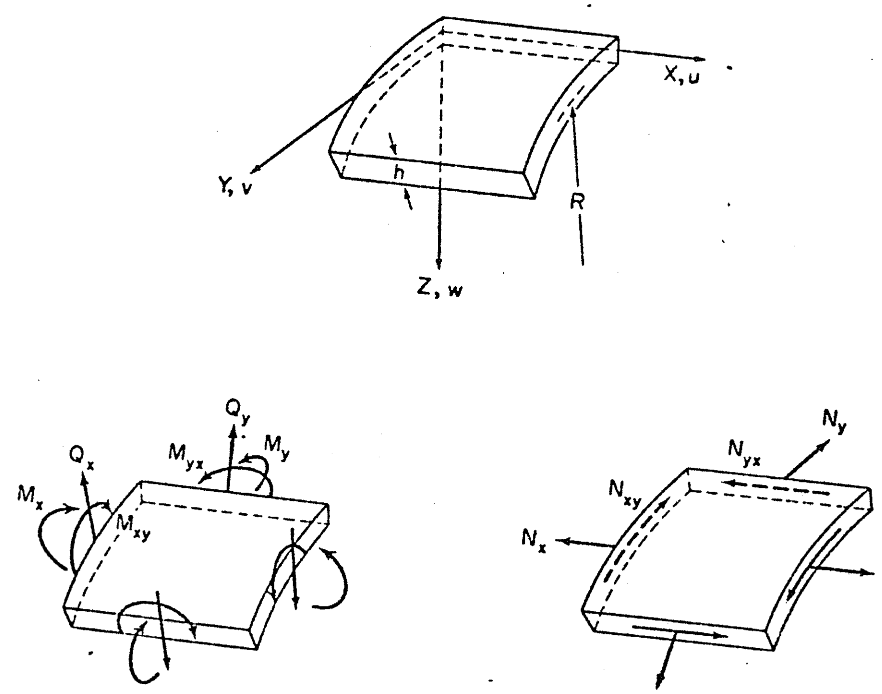

A) CYLINDRICAL COORDINATES & FORCES

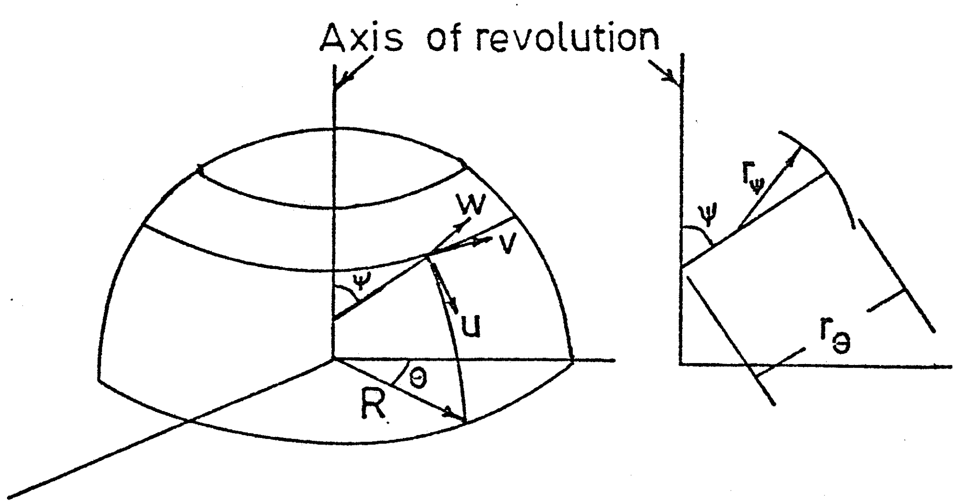

B) ANGULAR COORDINATES

Figure 1. Coordinate Systems.

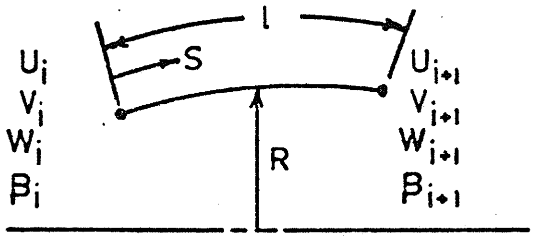

$$U = \gamma_1 + \gamma_6 \cdot S$$
$$V = \gamma_3 + \gamma_4 \cdot S$$
$$W = \gamma_5 + \gamma_6 \cdot S + \gamma_7 \cdot S^2 + \gamma_8 \cdot S^3$$

A) FINITE ELEMENT MODEL

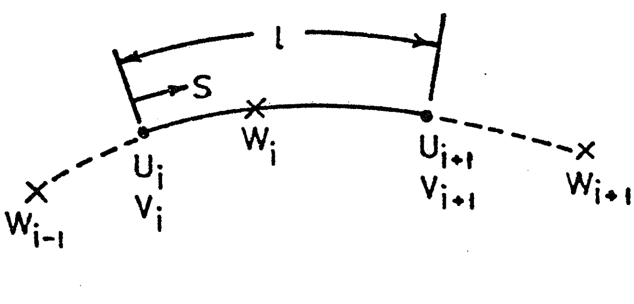

$$U = \gamma_1 + \gamma_2 \cdot S$$
$$V = \gamma_3 + \gamma_4 \cdot S$$
$$W = \gamma_5 + \gamma_6 \cdot S + \gamma_7 \cdot S^2$$

B) FINITE DIFFERENCE MODEL

Figure 2. Finite Element - Finite Difference Models.

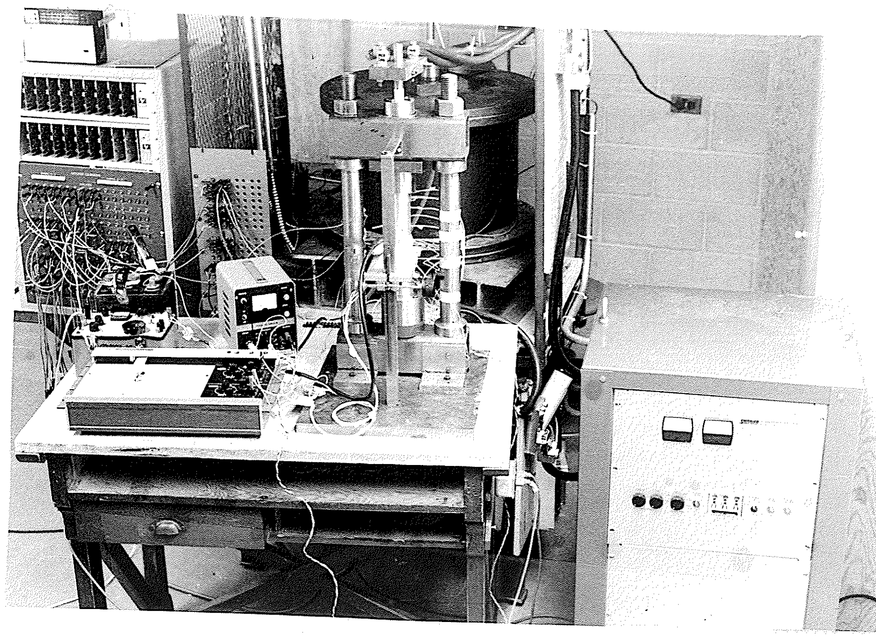

Figure 3. Overall Test Set-up.

1. Lower Crossmember
2. Support Column.
3. Upper Cross-member.
4. Main Compression Bolt.
5. Upper Heater Grip.
6. Bleed-Through Valve.
7. Heater Assembly.
8. Fibre-Optic Probe.
9. Test Specimen.
10. Lower Grip Assembly.
11. Lower Heater Grip.
12. Load Cell.
13. Aligning Plate.
14. Upper Grip Assembly.
15. Micrometer Adjustment.

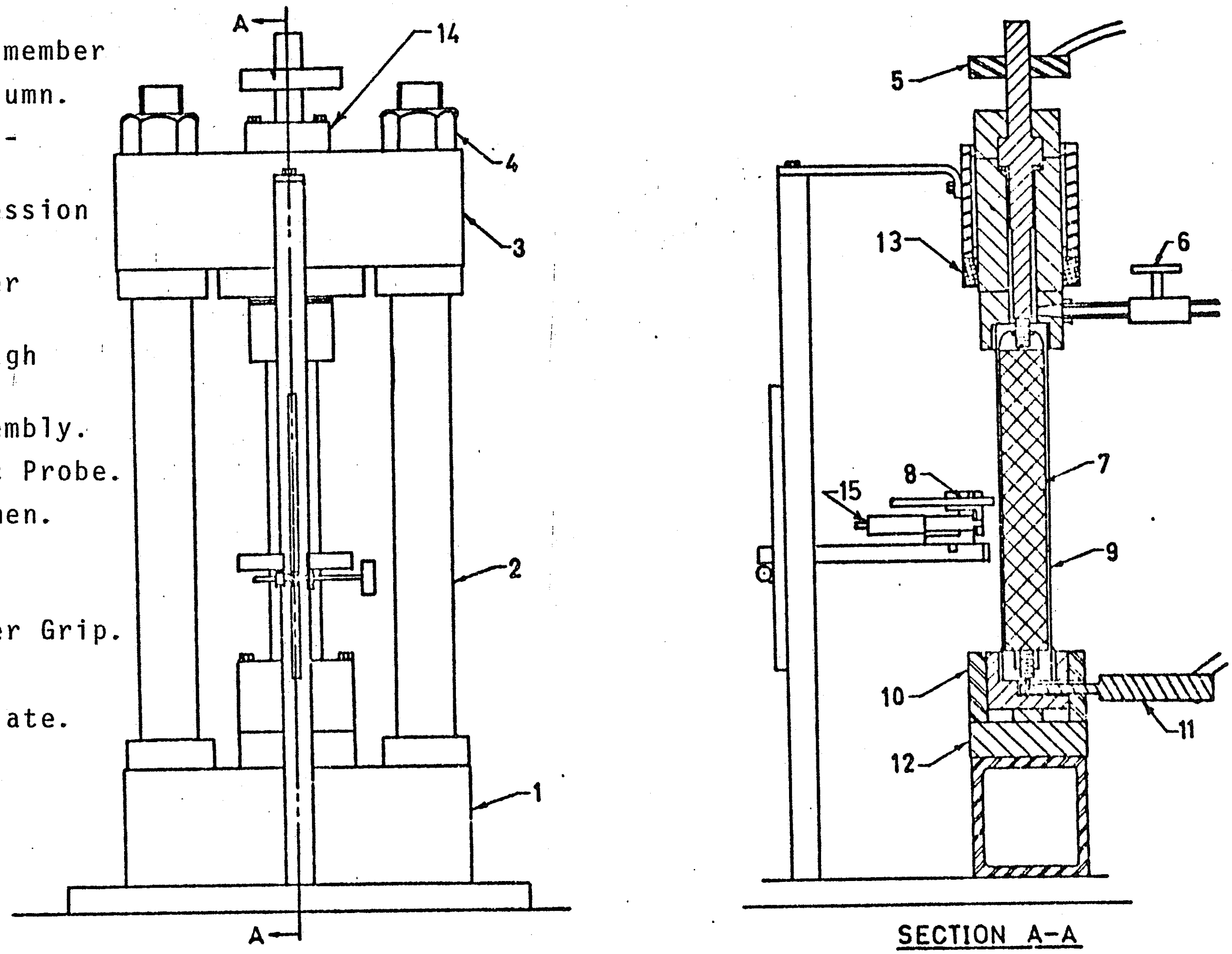

Figure 4. Test Set-up Details.

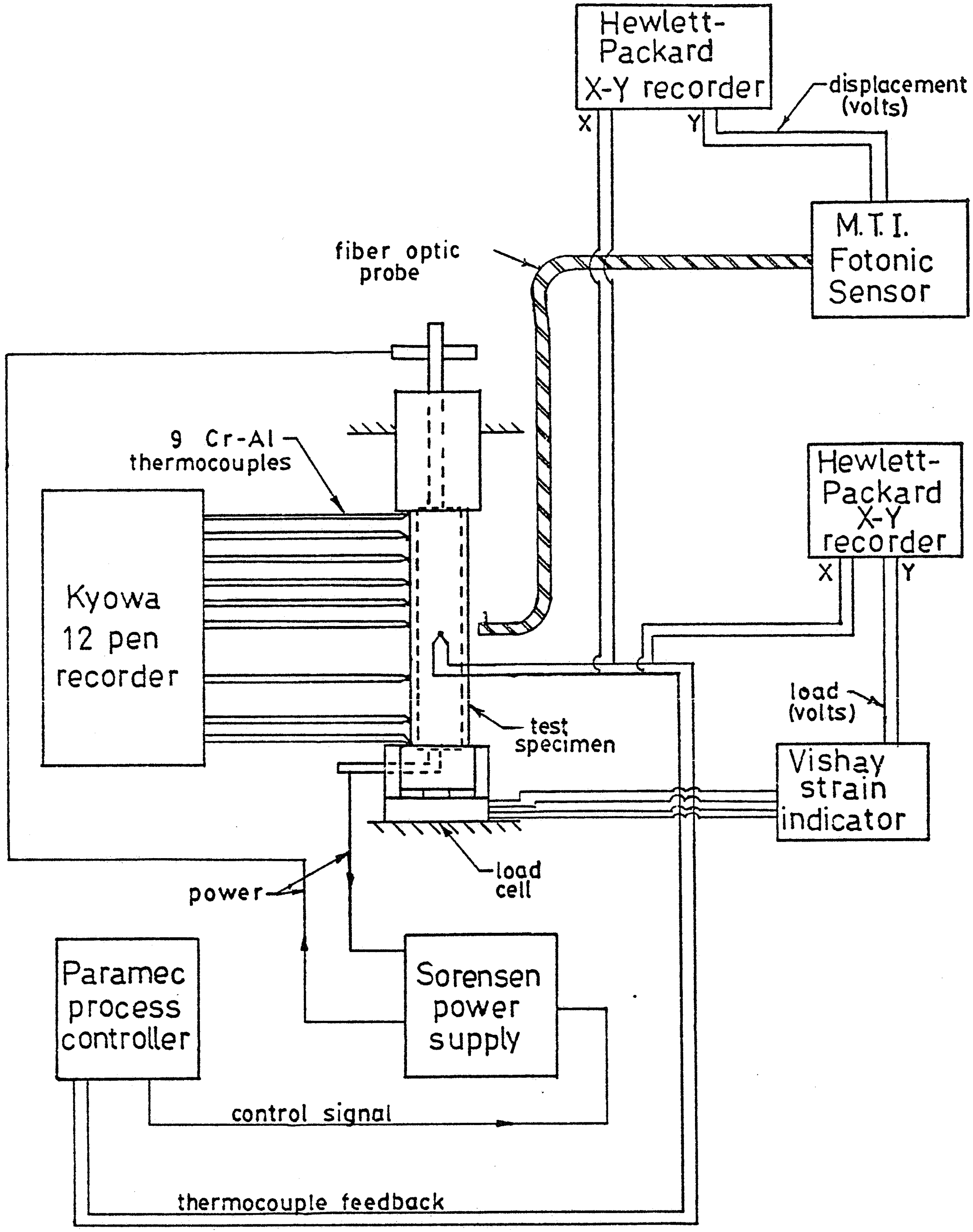

Figure 5. Test Set-up Schematic.

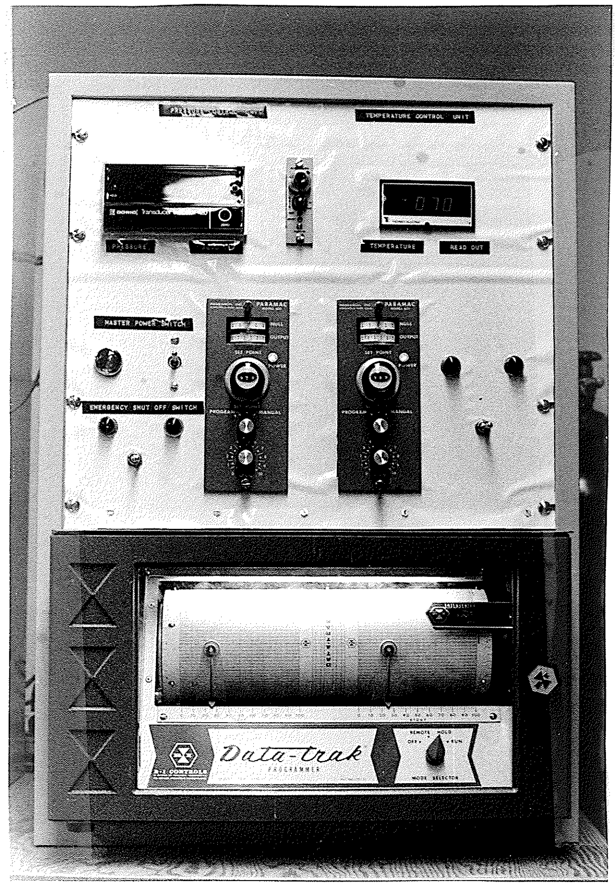

Figure 6. Temperature Control Unit.

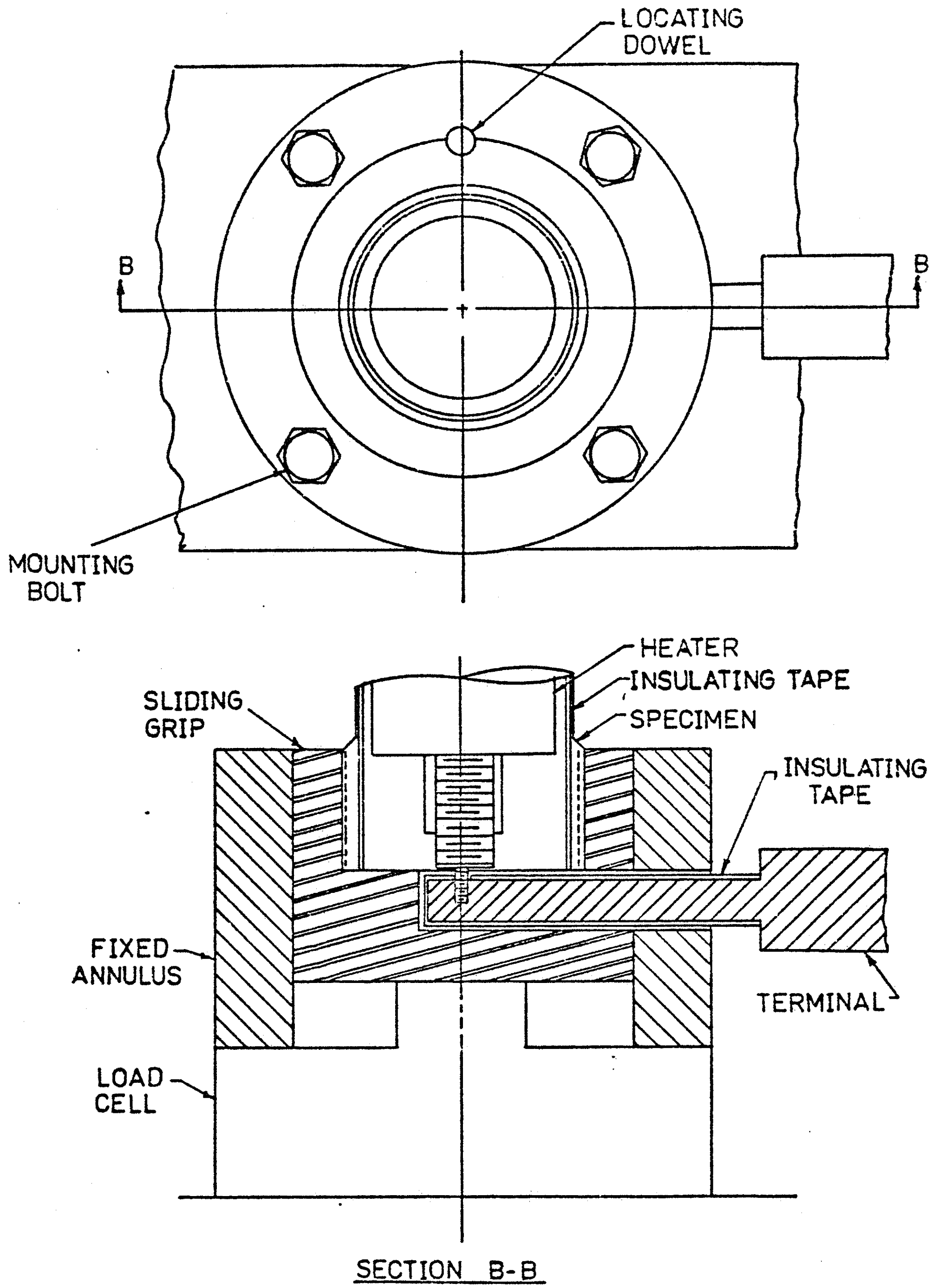

Figure 7. Details of Load Measurement Apparatus.

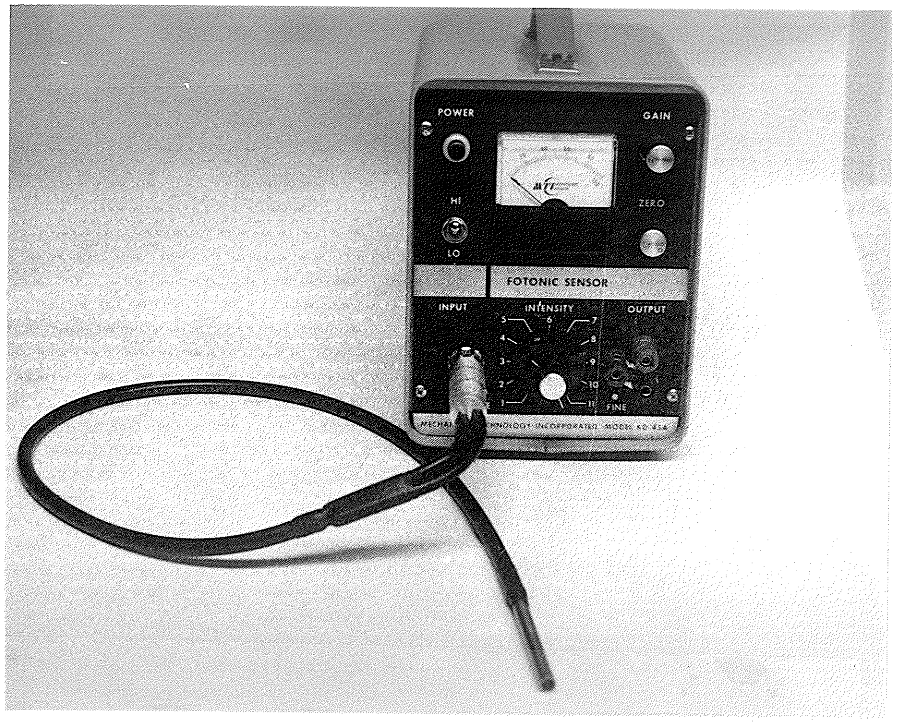

Figure 8. Fotonic Sensor.

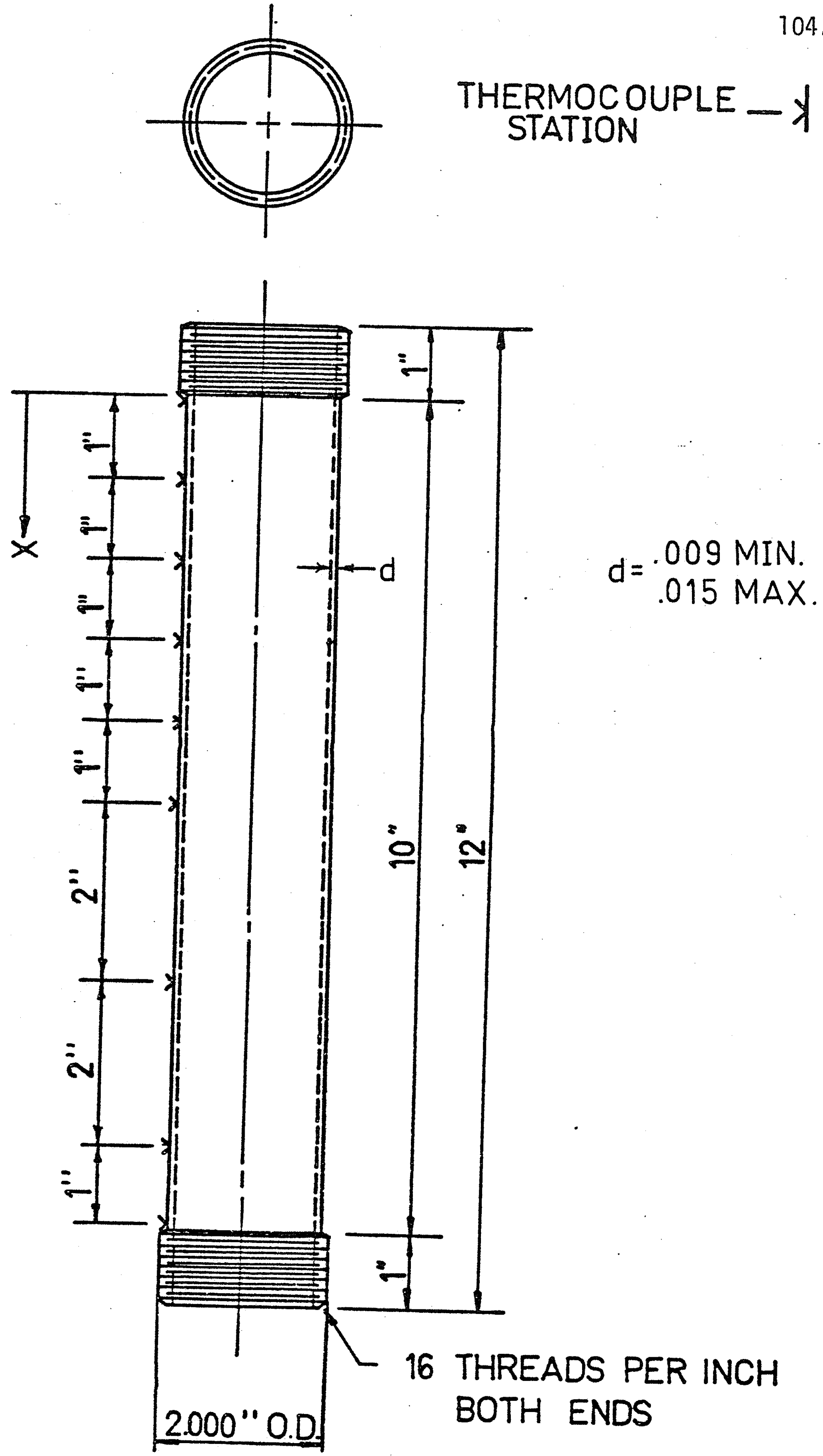

Figure 9. Dimensions of Test Specimen.

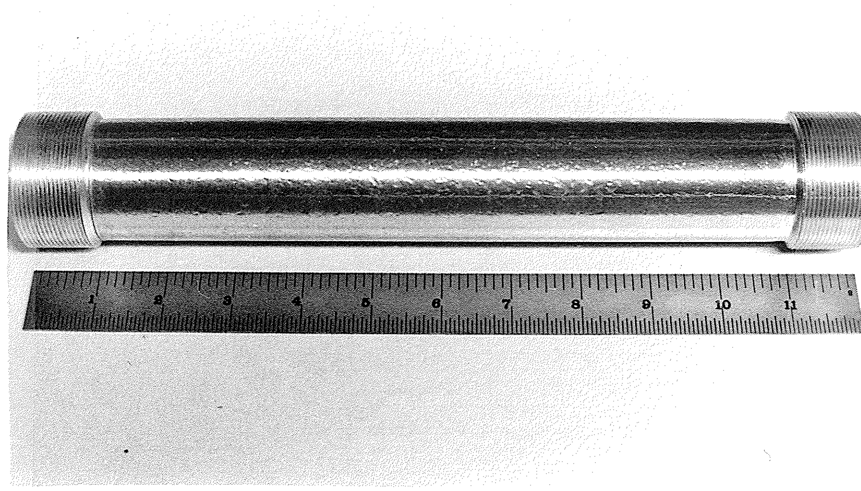

Figure 10. Photograph of Test Specimen.

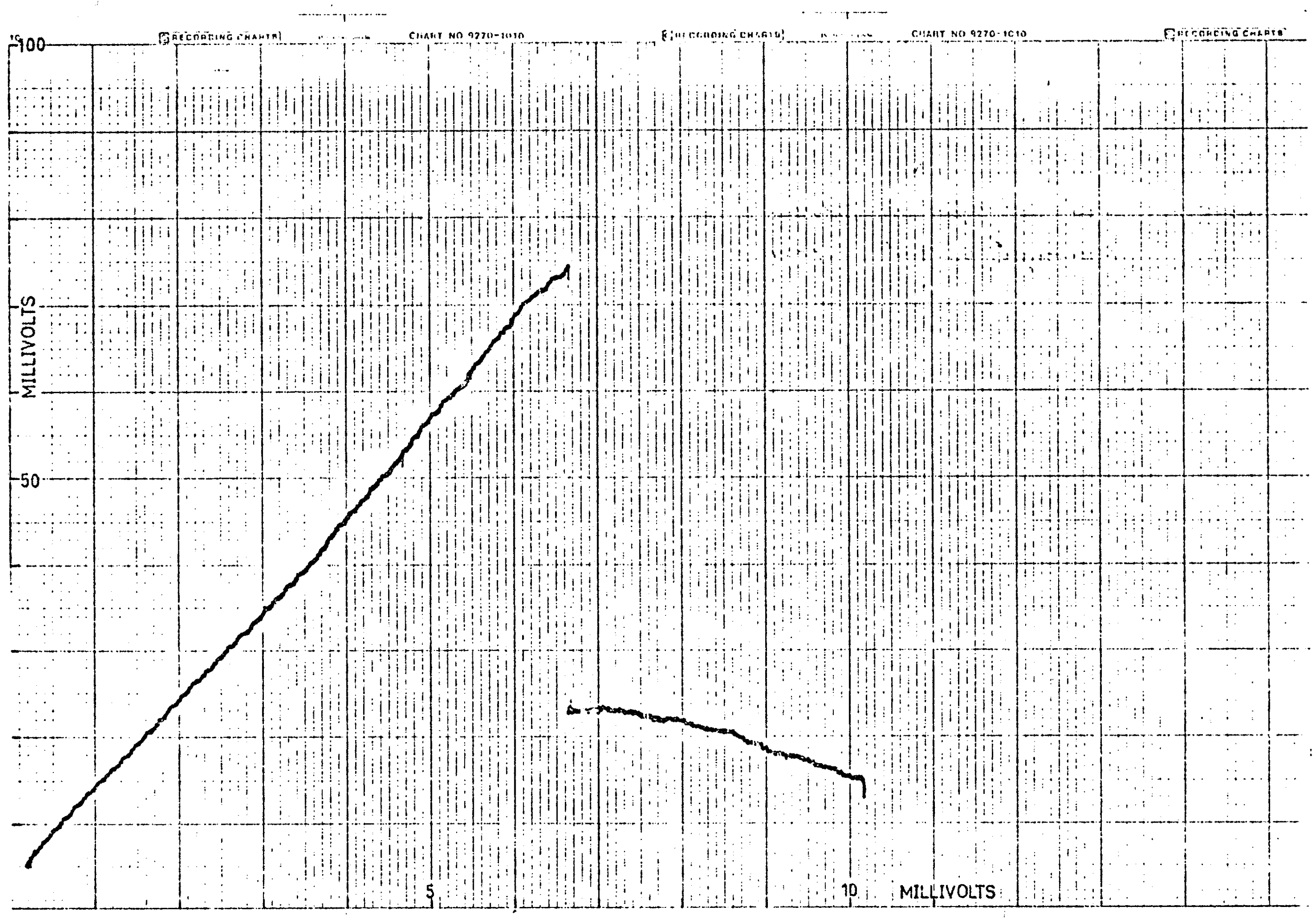

Figure 11. Load Cell Output Vs. Central Thermocouple Output.

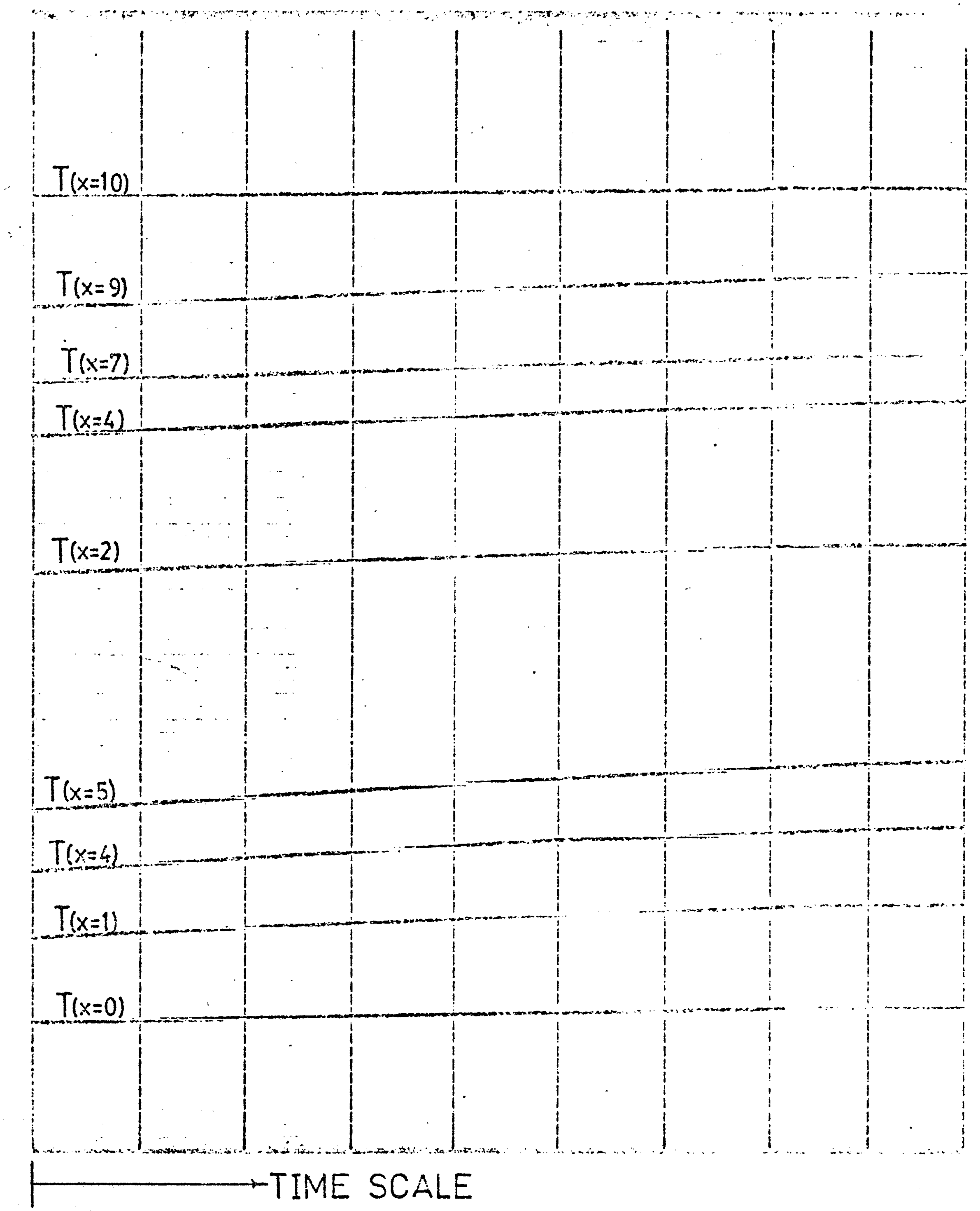

Figure 12. Typical Thermocouple Output.

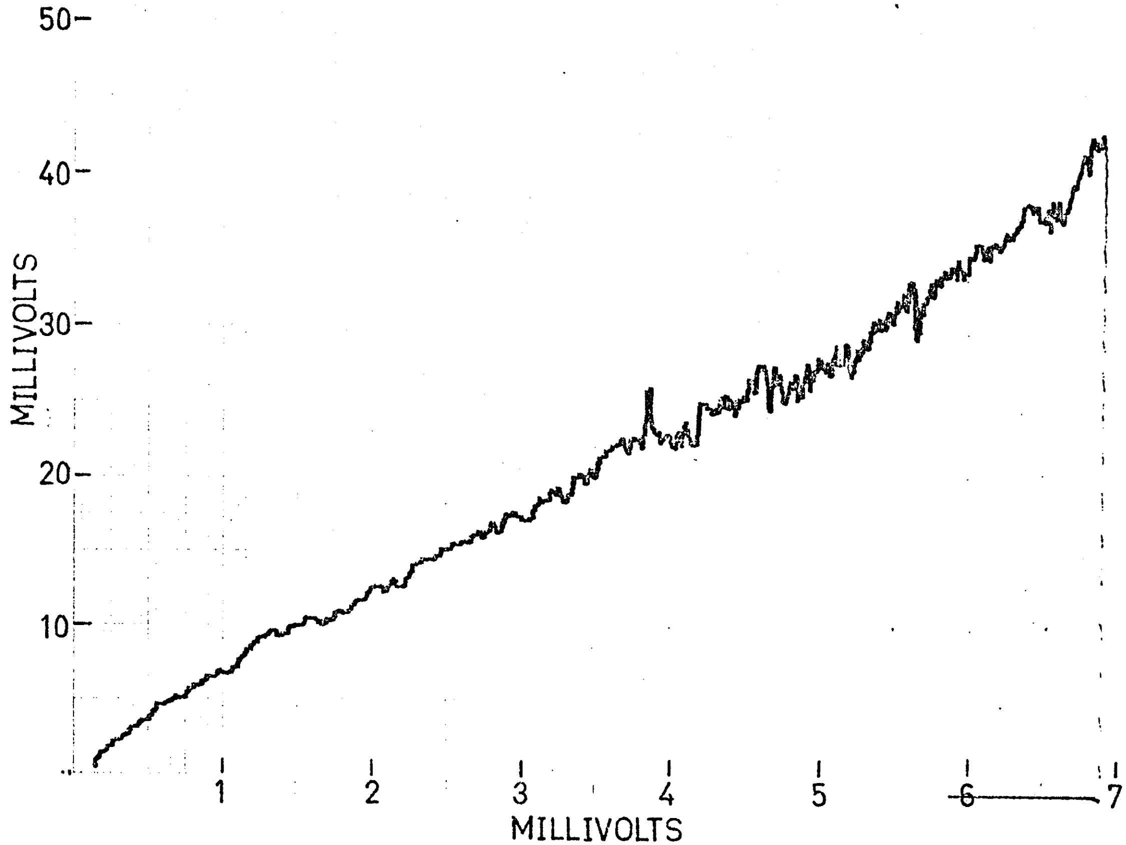

Figure 13. Fotonic Sensor Output Vs. Central Thermocouple Output.

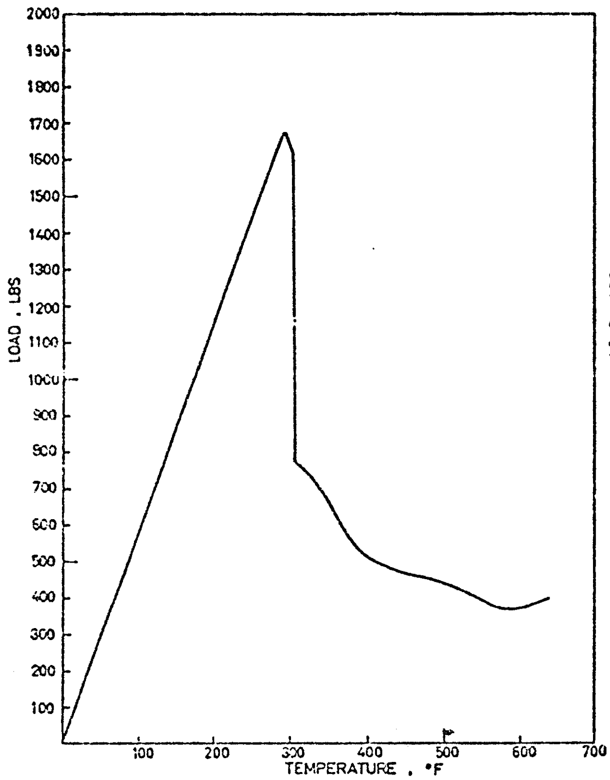

Figure 14. Axial Load Vs. Mid-Span Temperature
Test No. 6

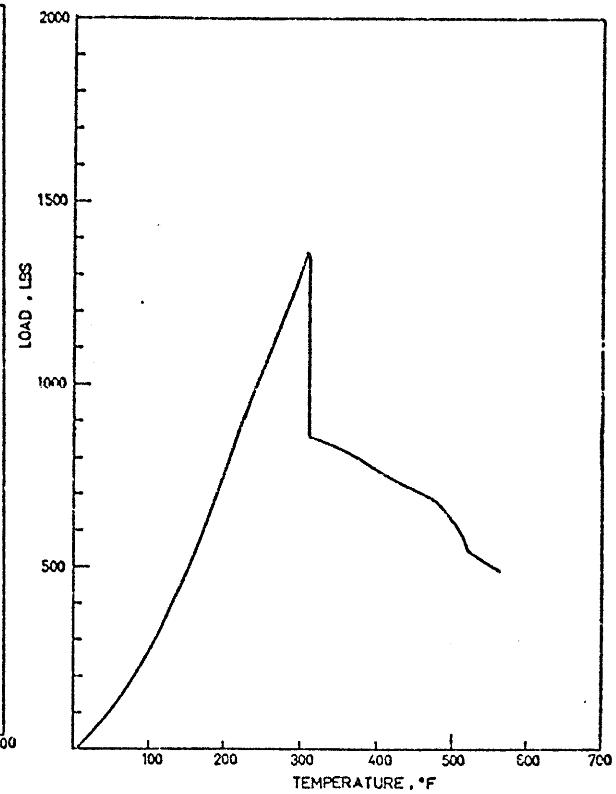

Figure 15. Axial Load Vs. Mid-Span Temperature
Test No. 8

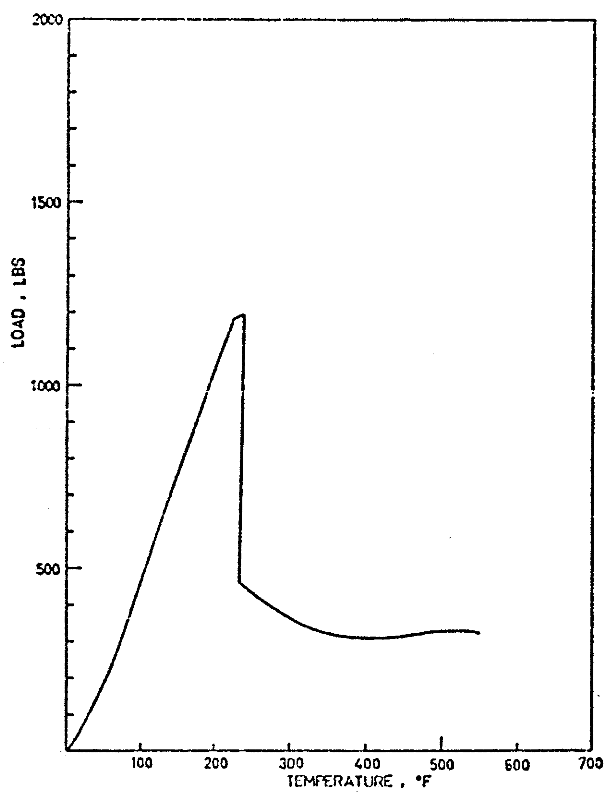

Figure 16. Axial Load Vs. Mid-Span Temperature
Test No. 10

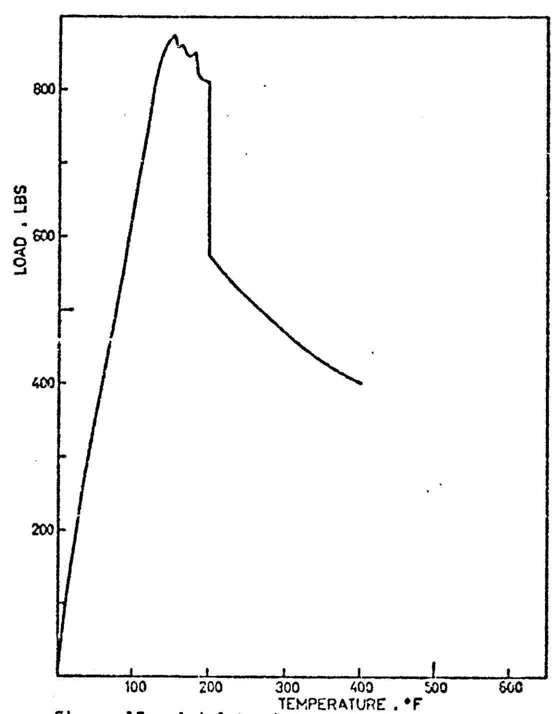

Figure 17. Axial Load Vs. Mid-Span Temperature
Test No. 12

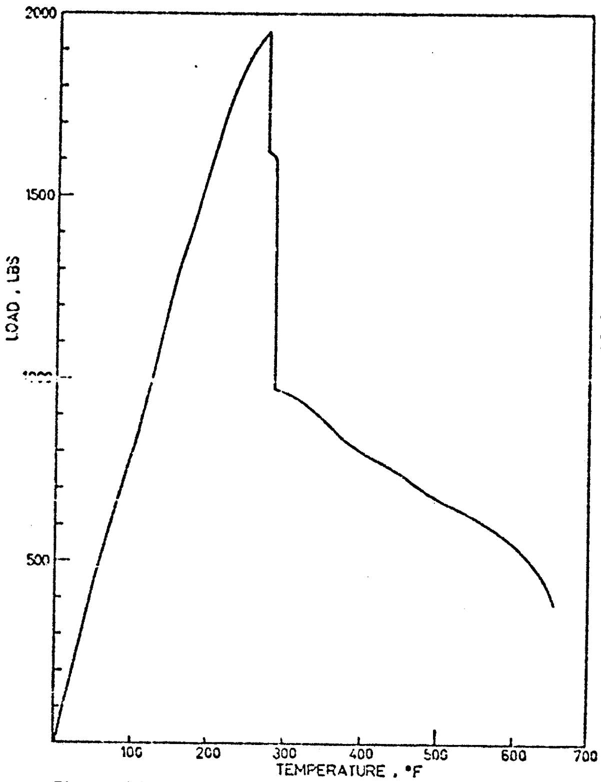

Figure 18. Axial Load Vs. Mid-Span Temperature
Test No. 13

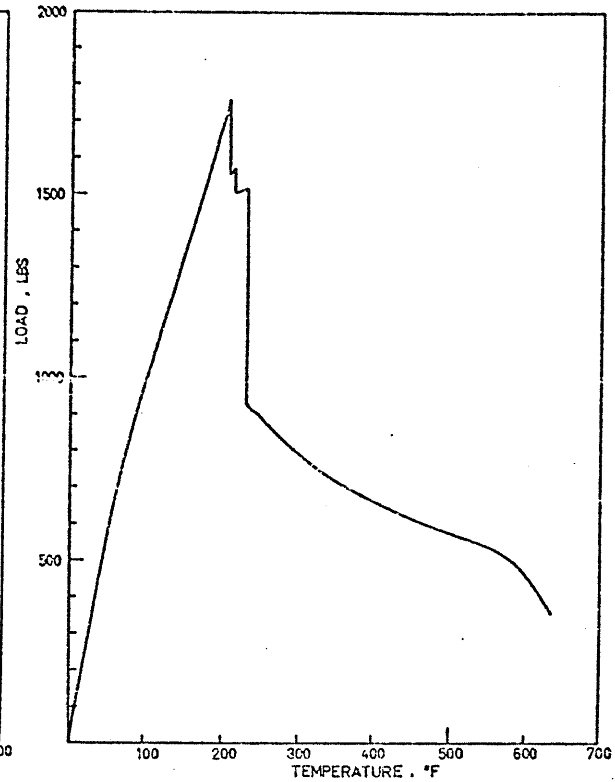

Figure 19. Axial Load Vs. Mid-Span Temperature
Test No. 14

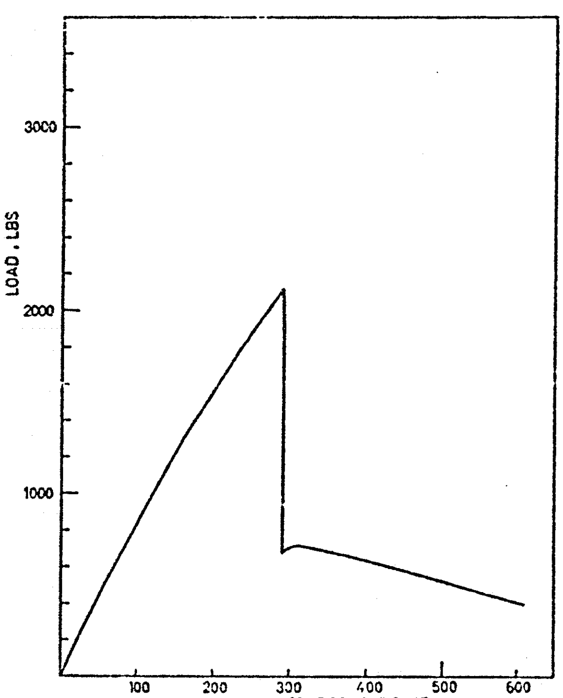

Figure 20. Axial Load Vs. Mid-Span Temperature
Test No. 15

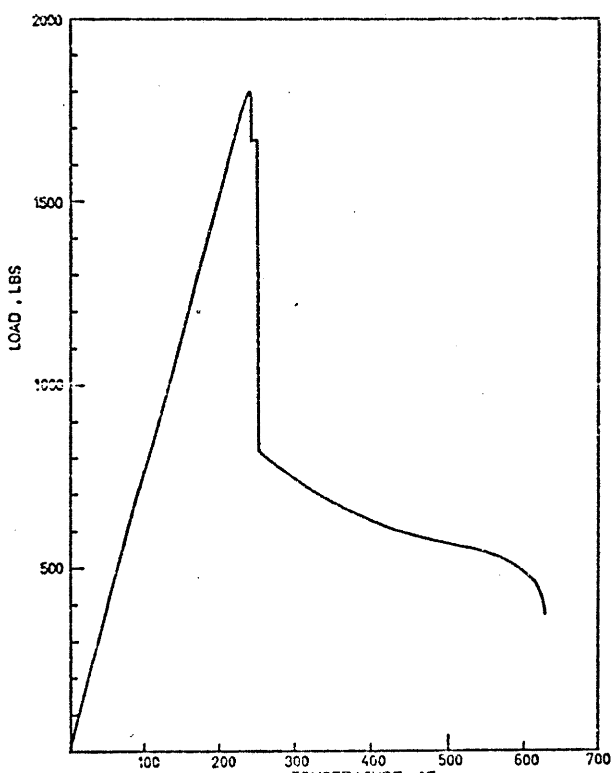

Figure 21. Axial Load Vs. Mid-Span Temperature
Test No. 16

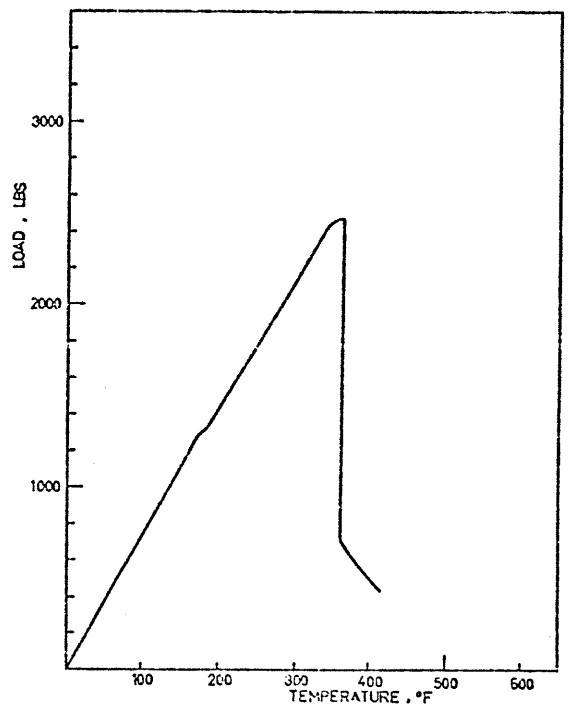

Figure 22. Axial Load Vs. Mid-Span Temperature
Test No. 19

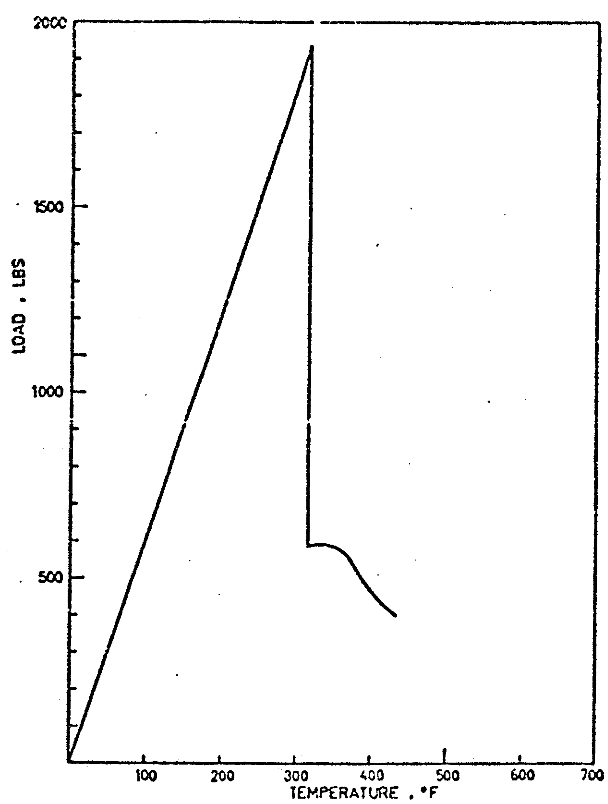

Figure 23. Axial Load Vs. Mid-Span Temperature
Test No. 21

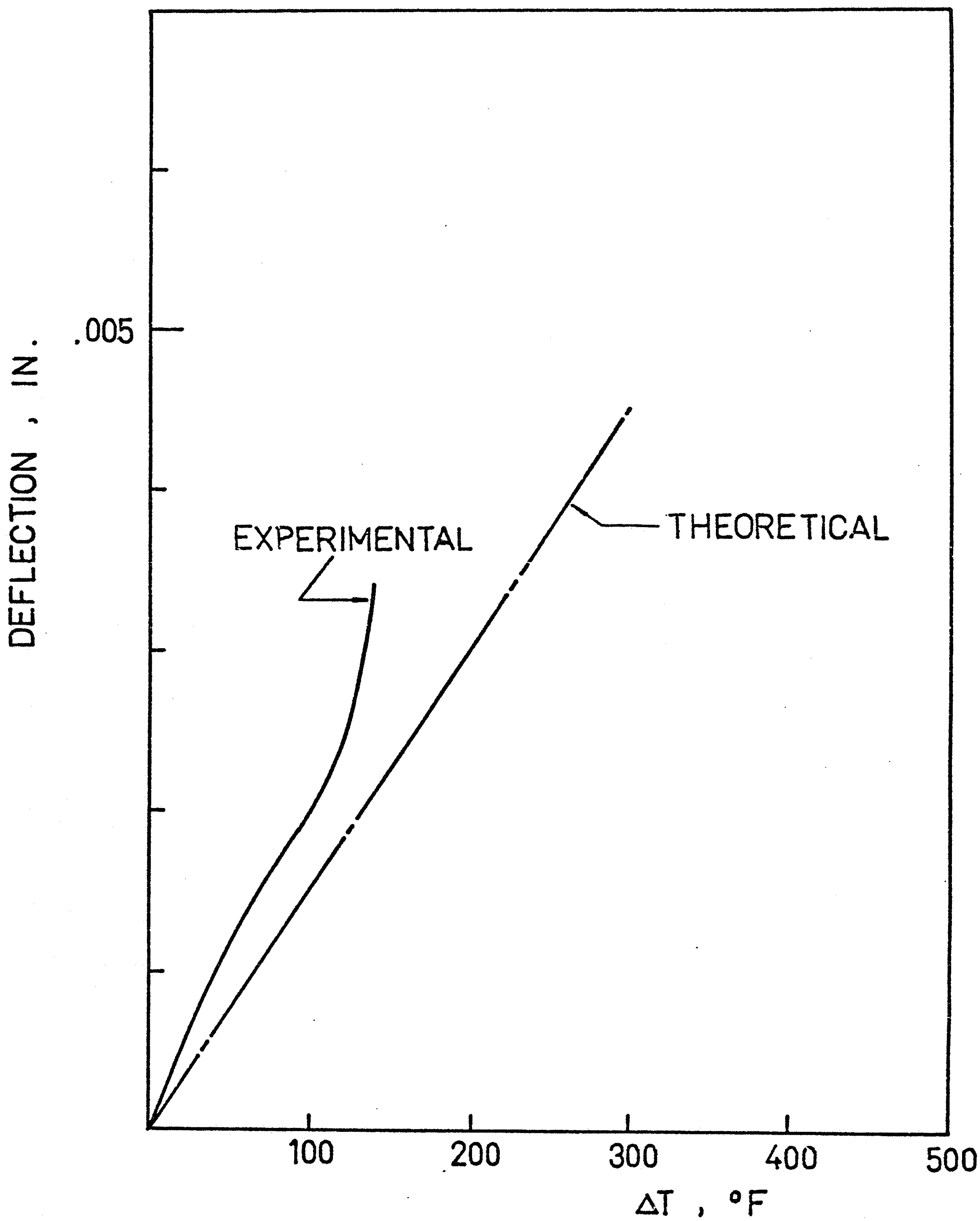

Figure 24. Mid-Span Radial Deflection. Test No. 12.

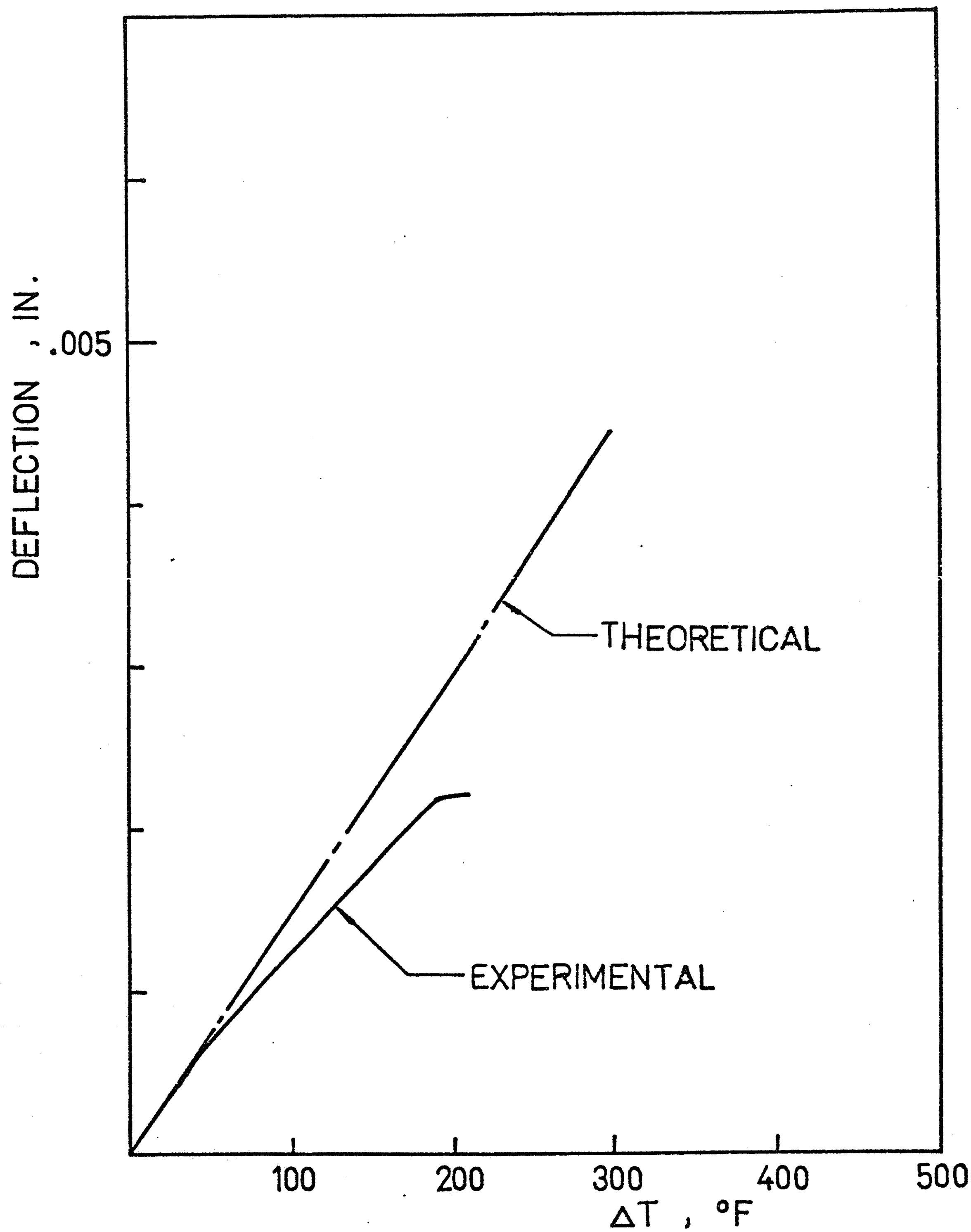

Figure 25. Mid-Span Radial Deflection. Test No. 14.

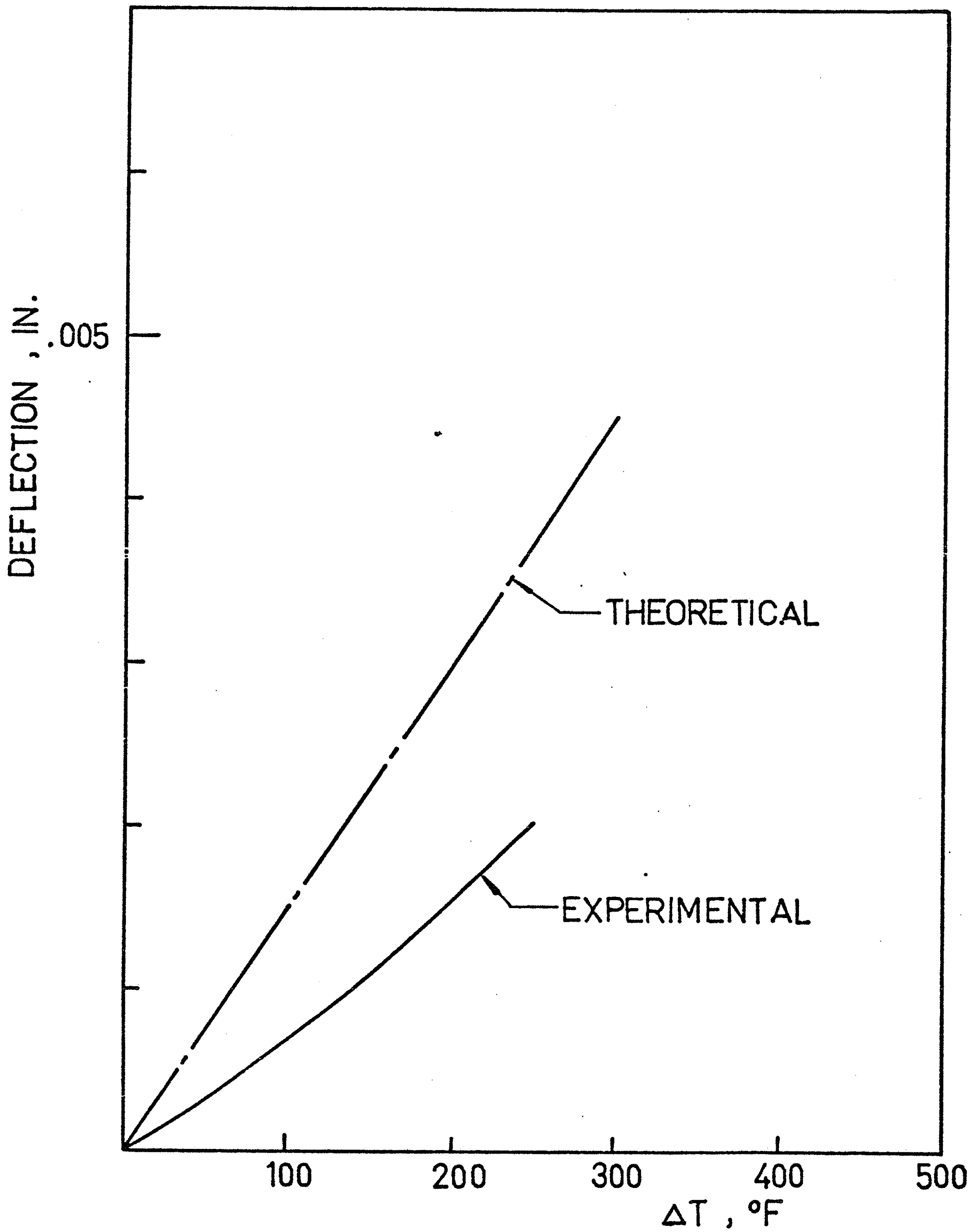

Figure 26. Mid-Span Radial Deflection. Test No. 15.

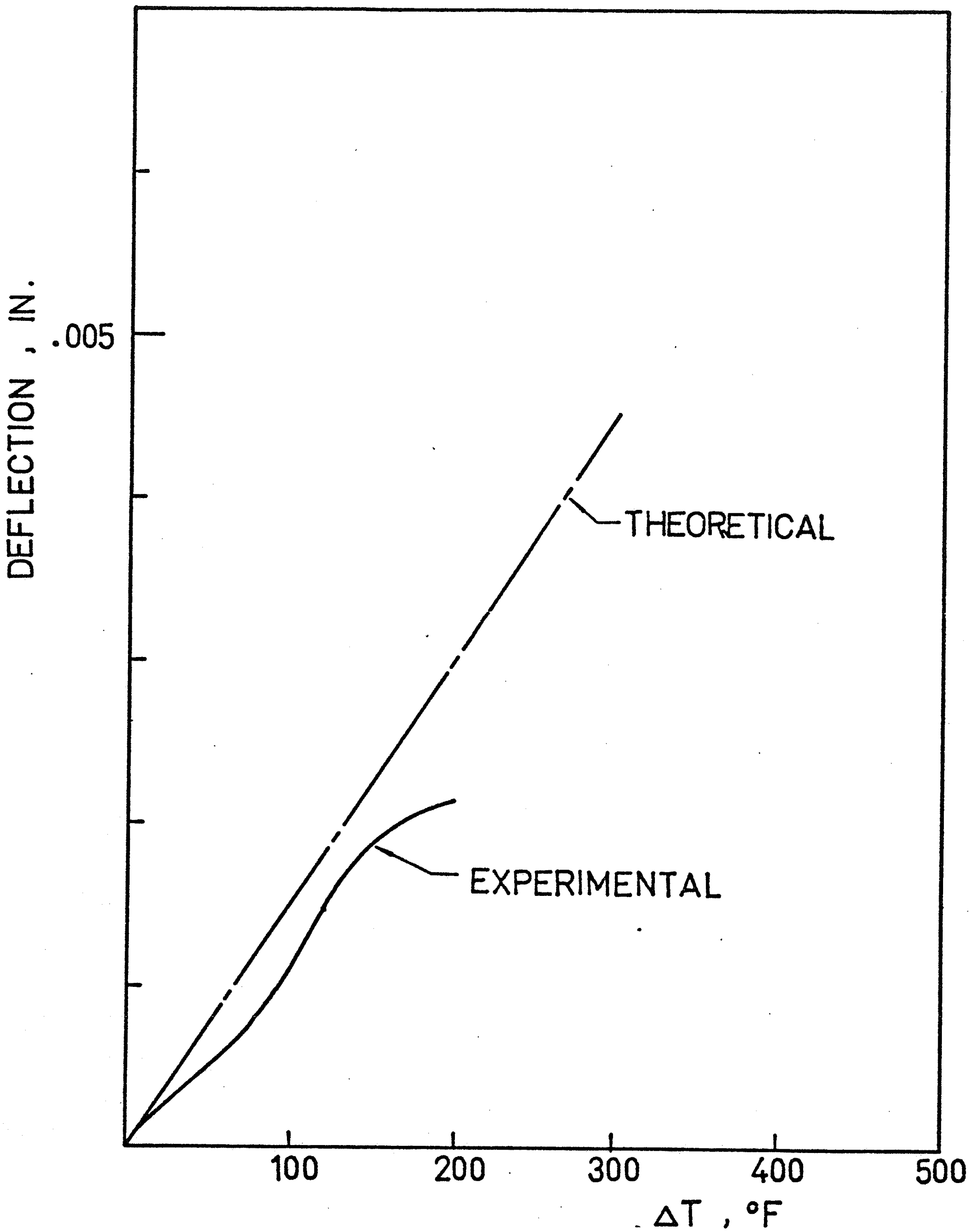

Figure 27. Mid-Span Radial Deflection. Test No. 19.

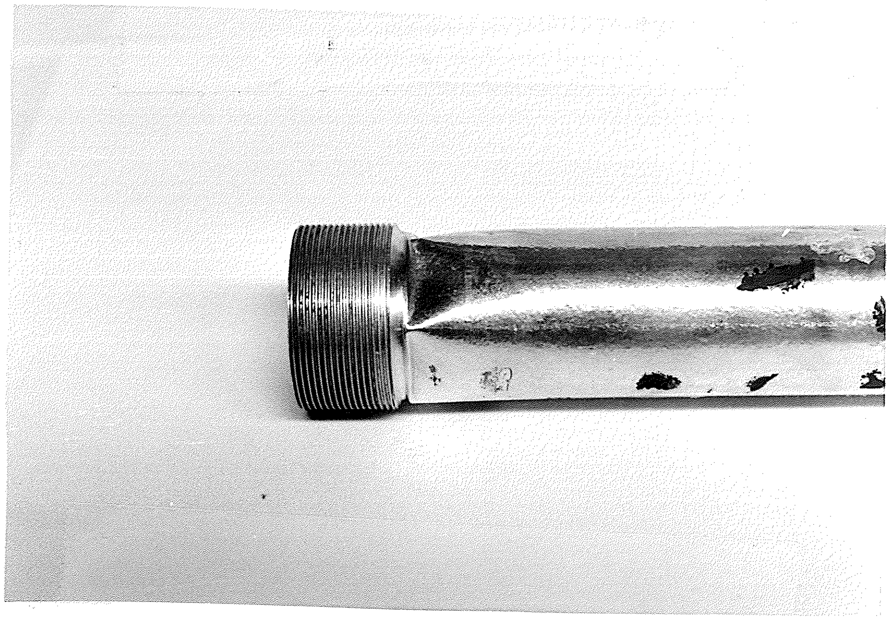

Figure 28. Buckling Pattern. Test No. 8.

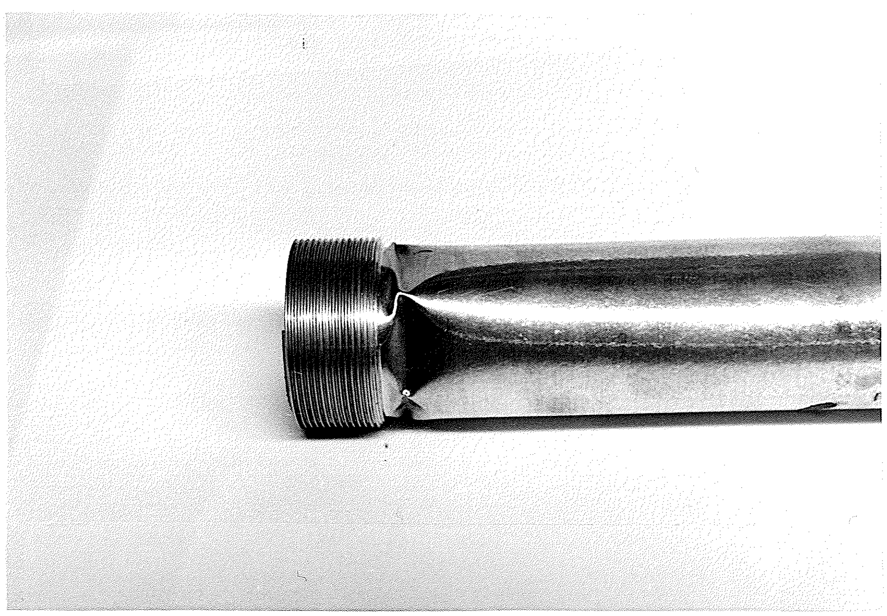

Figure 29. Buckling Pattern. Test No. 14.

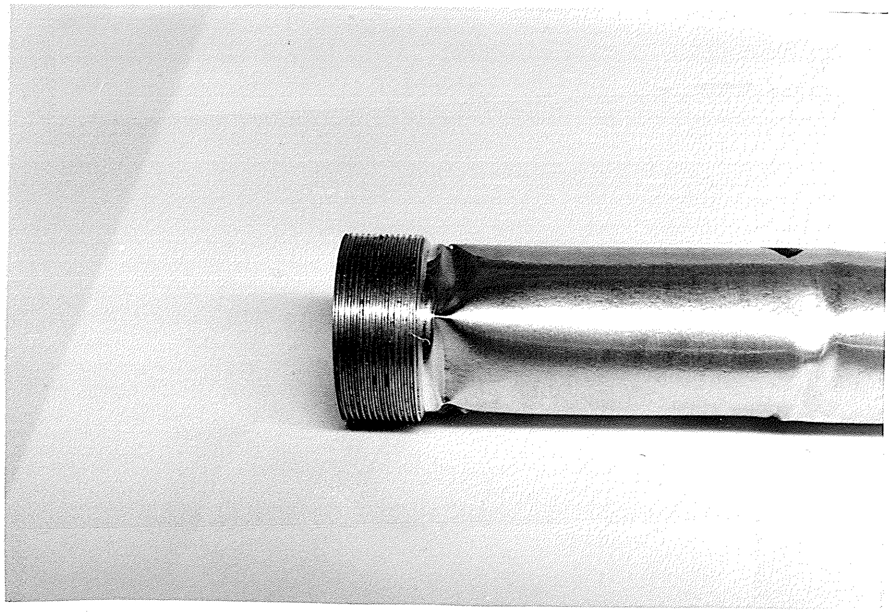

Figure 30. Buckling Pattern. Test No. 18.

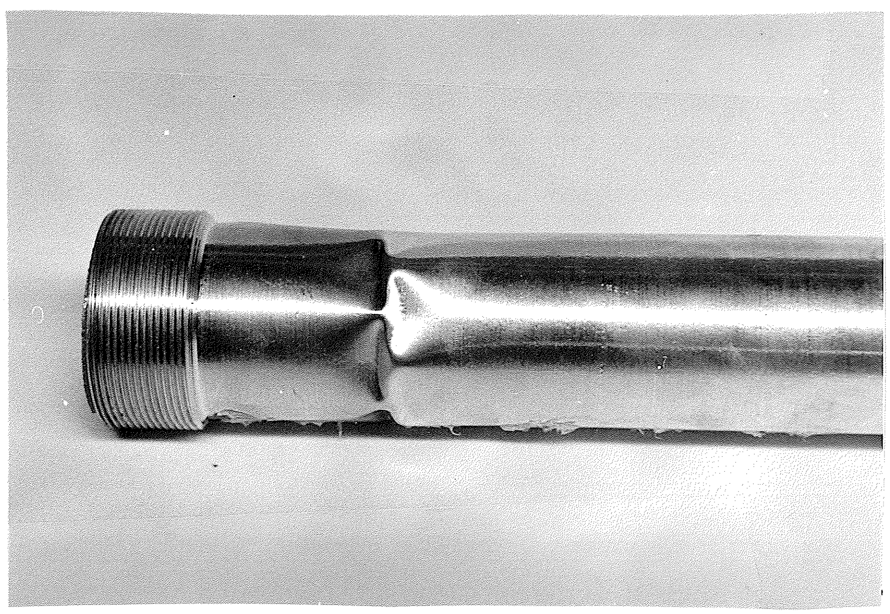

Figure 31. Buckling Pattern. Test No. 21.

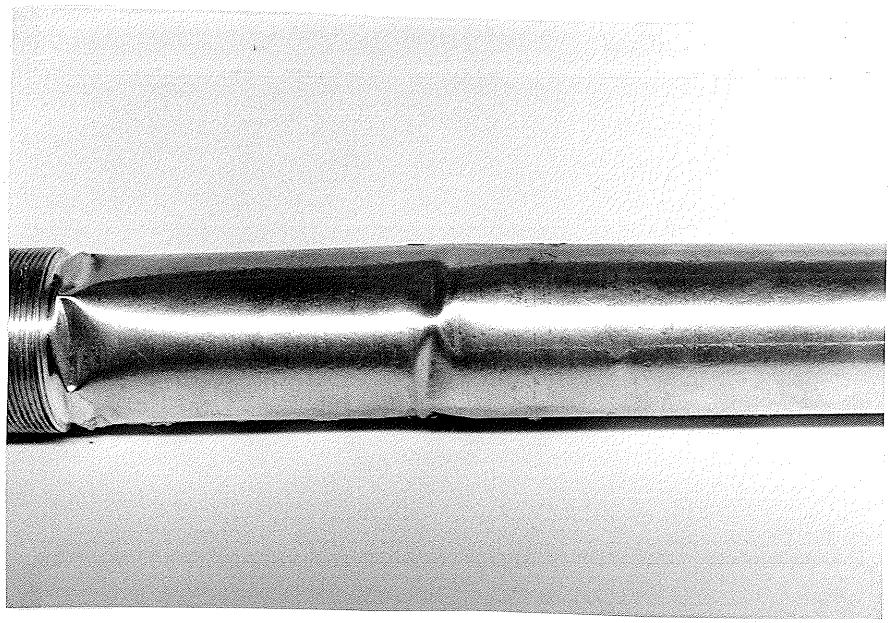

Figure 32. Secondary Buckling. Test No. 18.

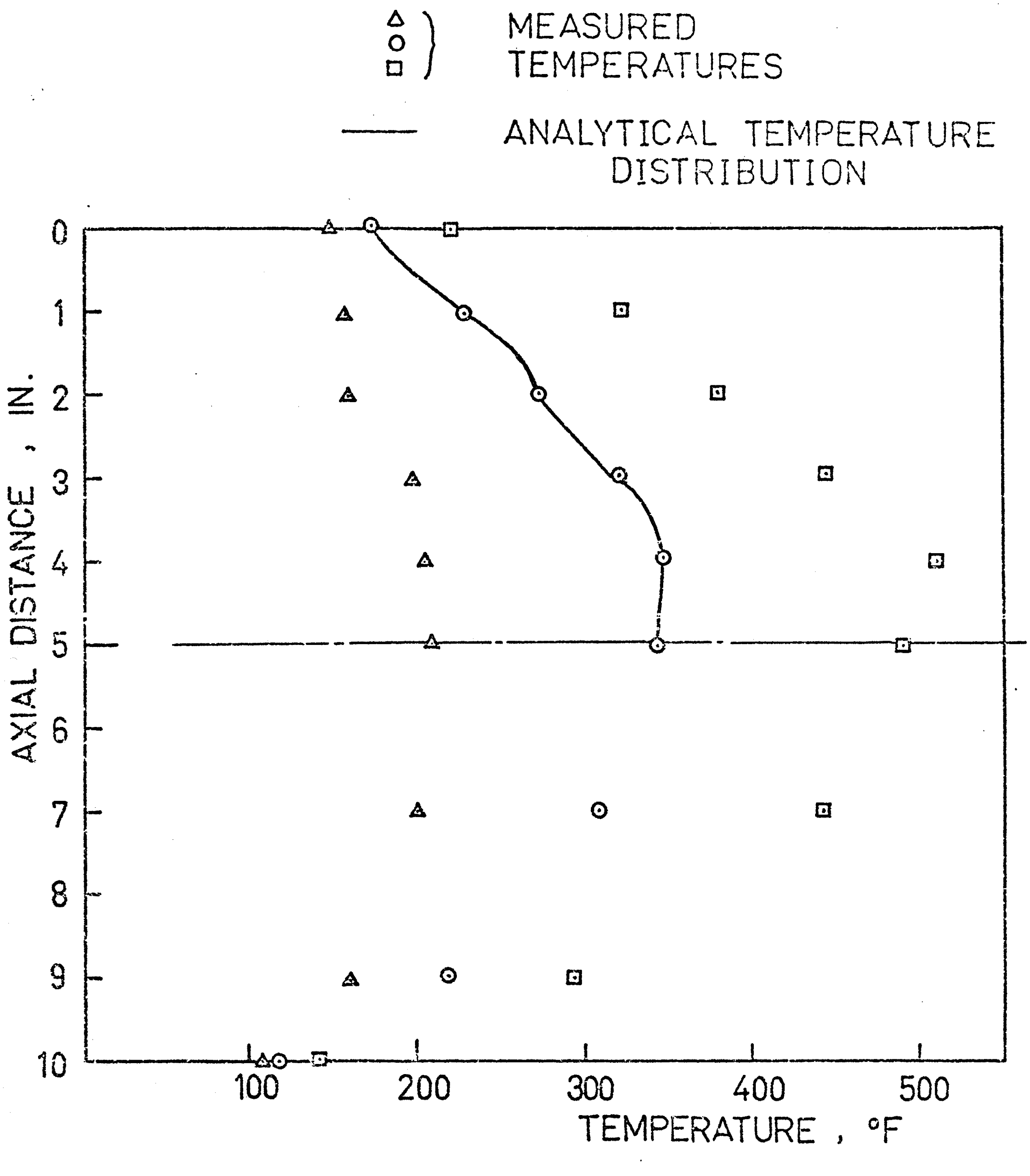

Figure 33. Temperature Distribution. Test No. 11.

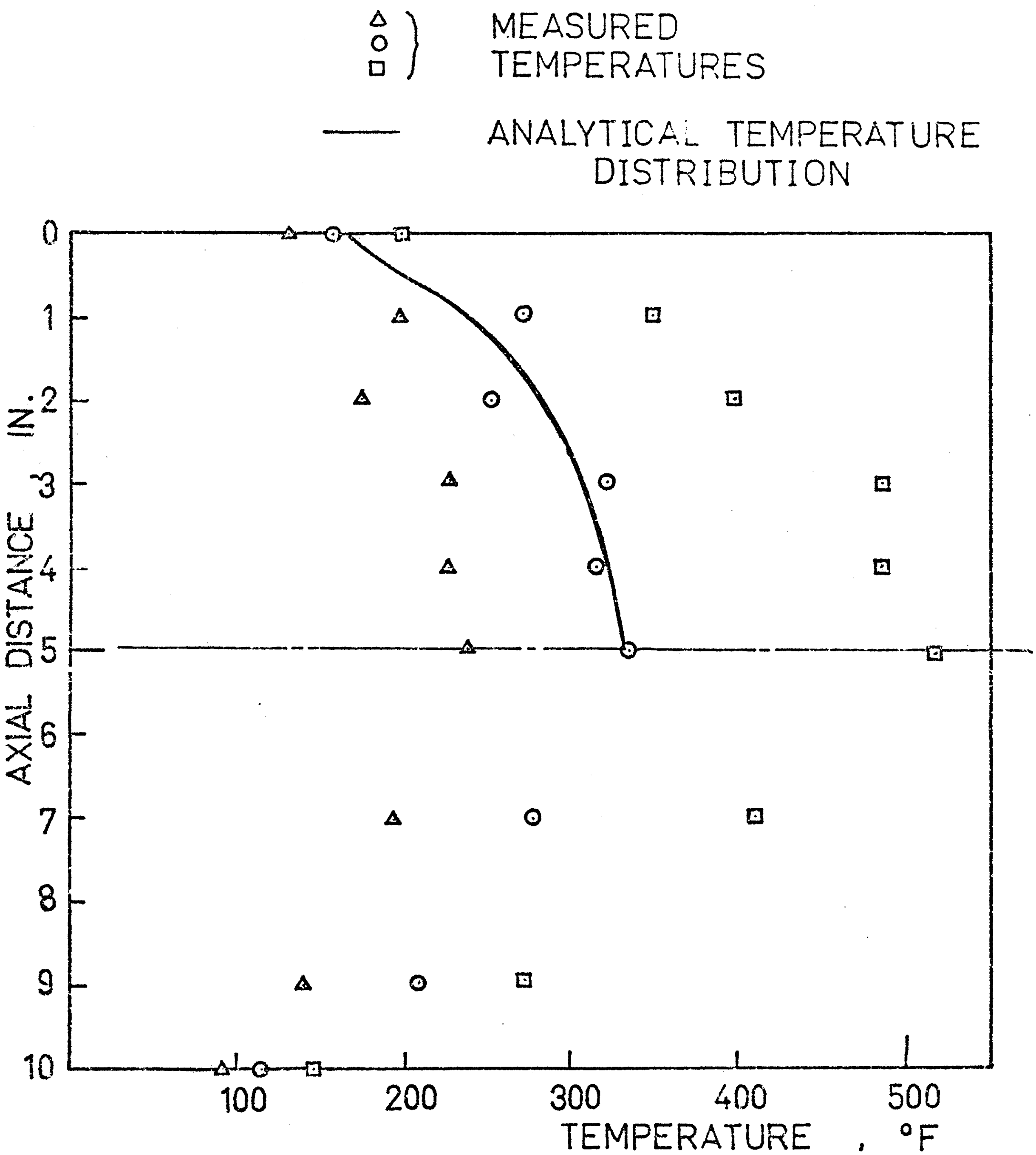

Figure 34. Temperature Distribution. Test No. 16.

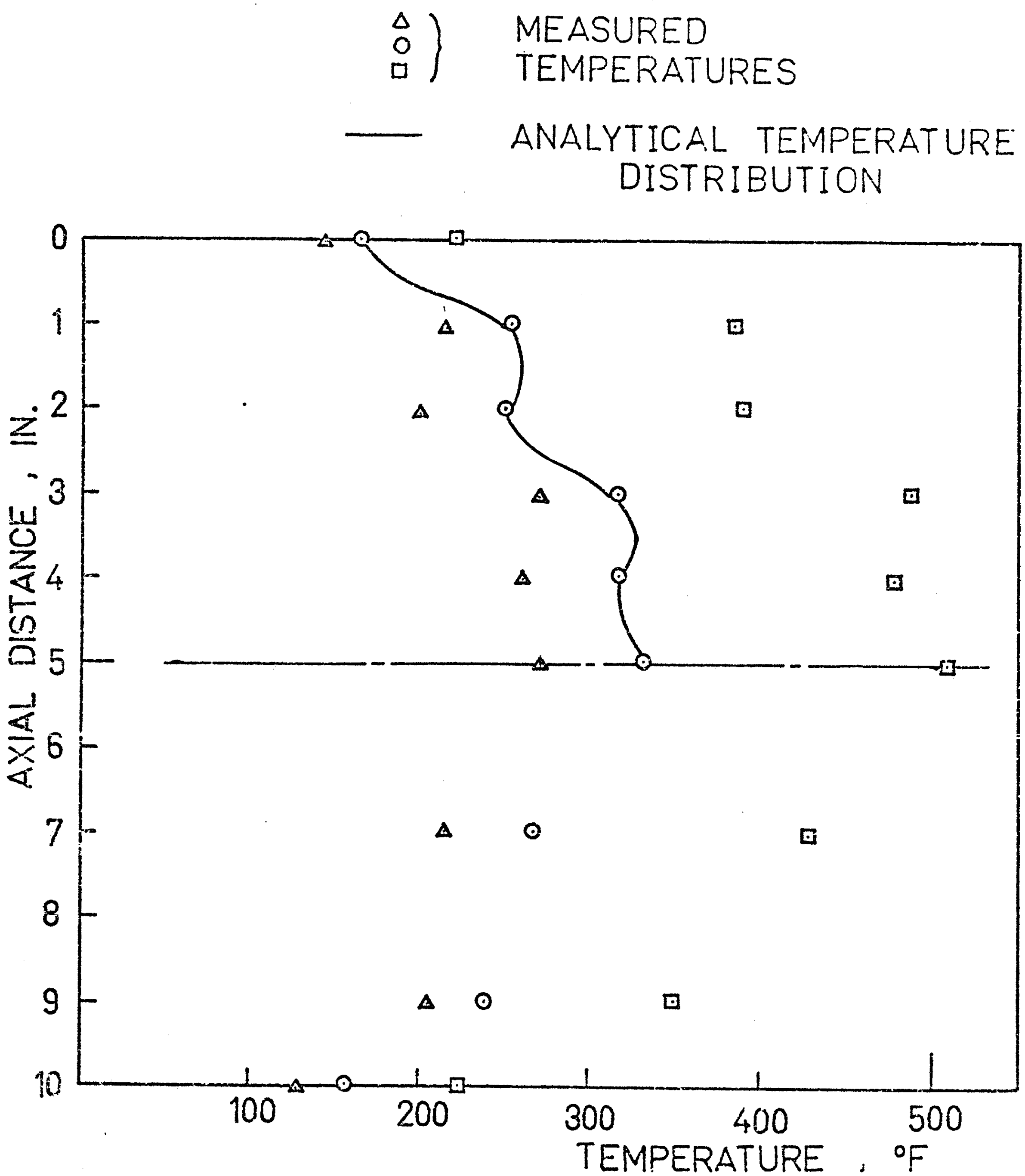

Figure 35. Temperature Distribution. Test No. 20.

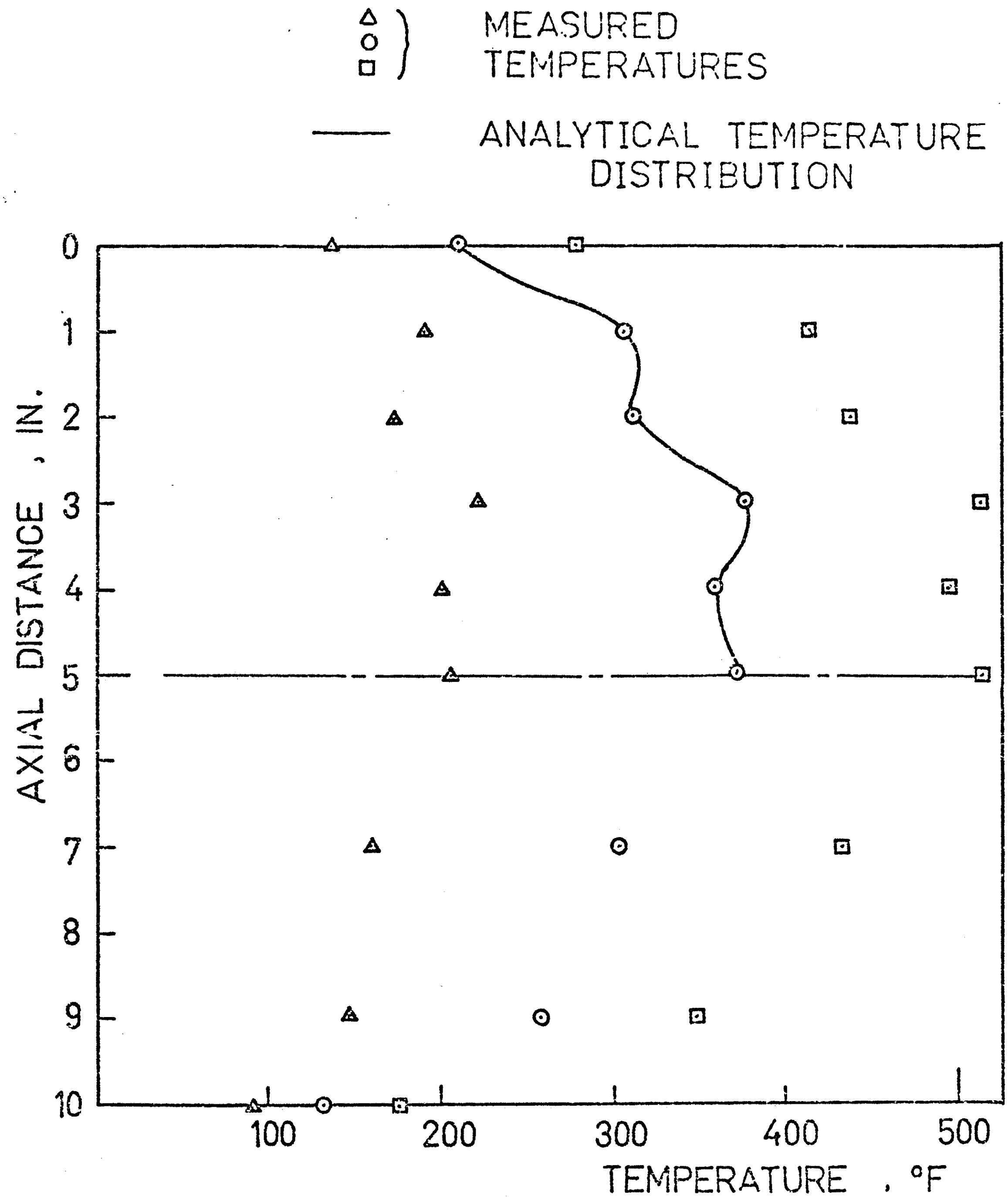

Figure 36. Temperature Distribution. Test No. 21.

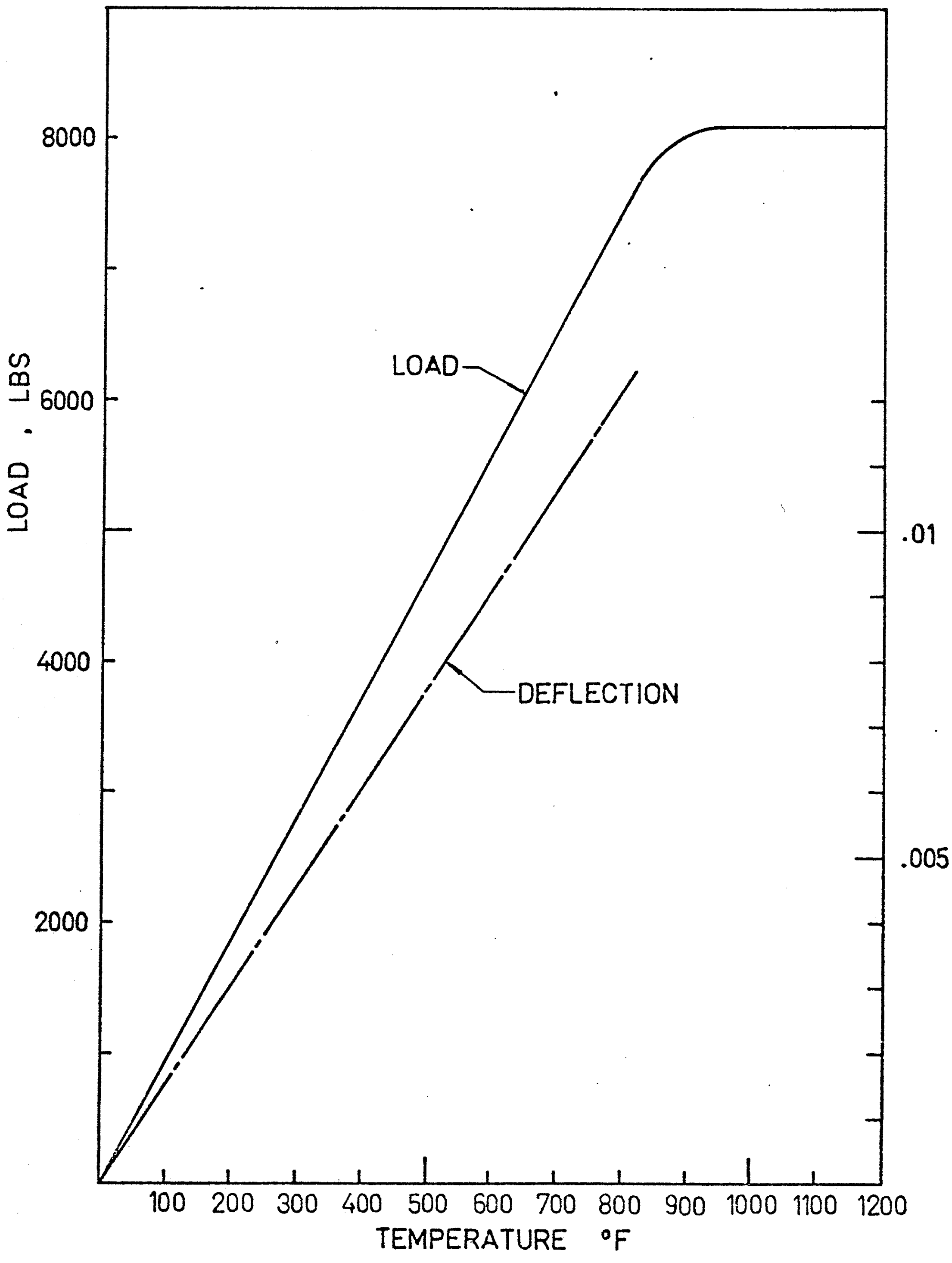

Figure 37. Theoretical Load Vs. Mid-Span Temperature Plot for Test No. 19.

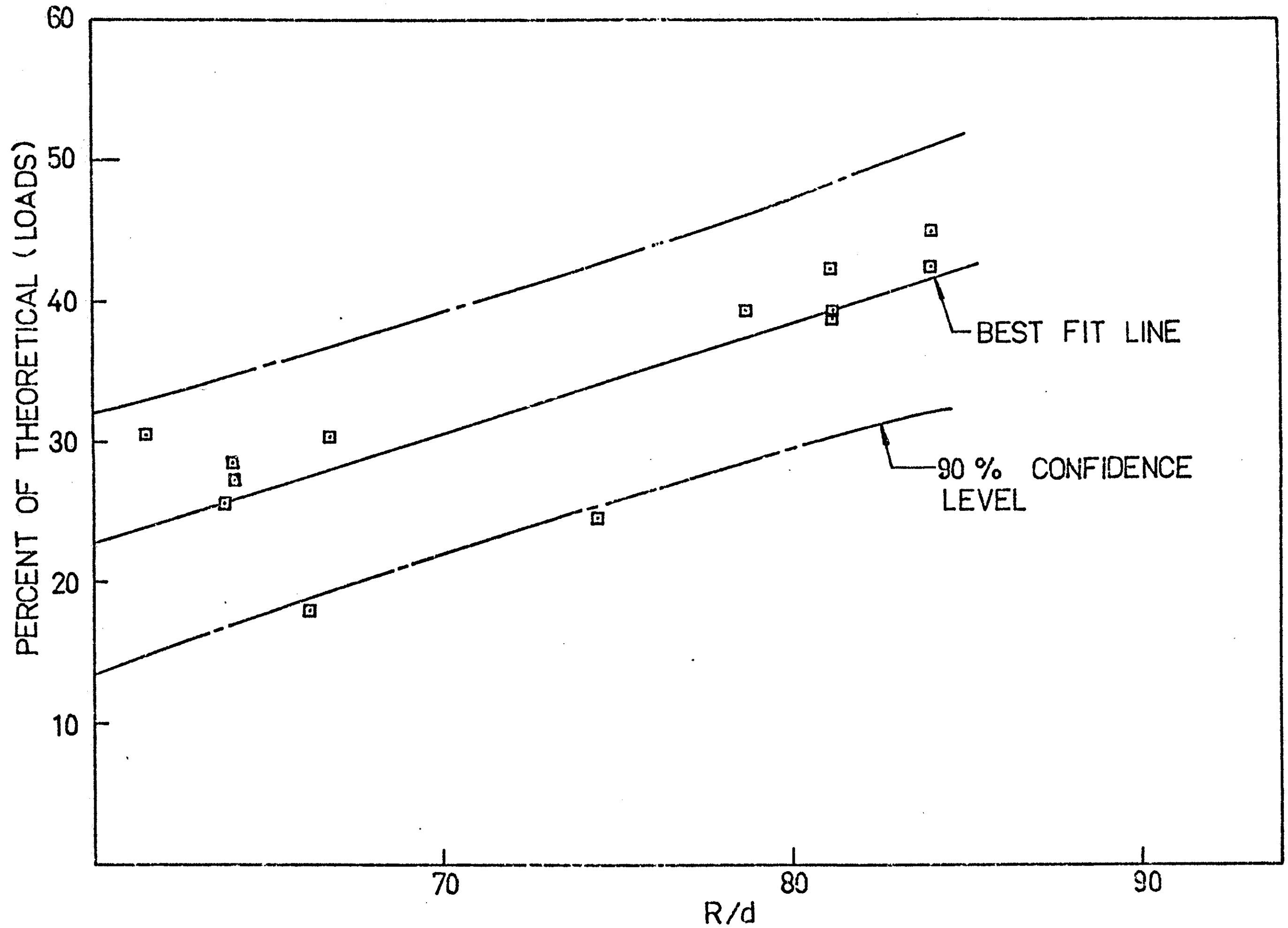

Figure 38. Percentage Theoretical Loads Vs. Radius to Thickness Ratio.

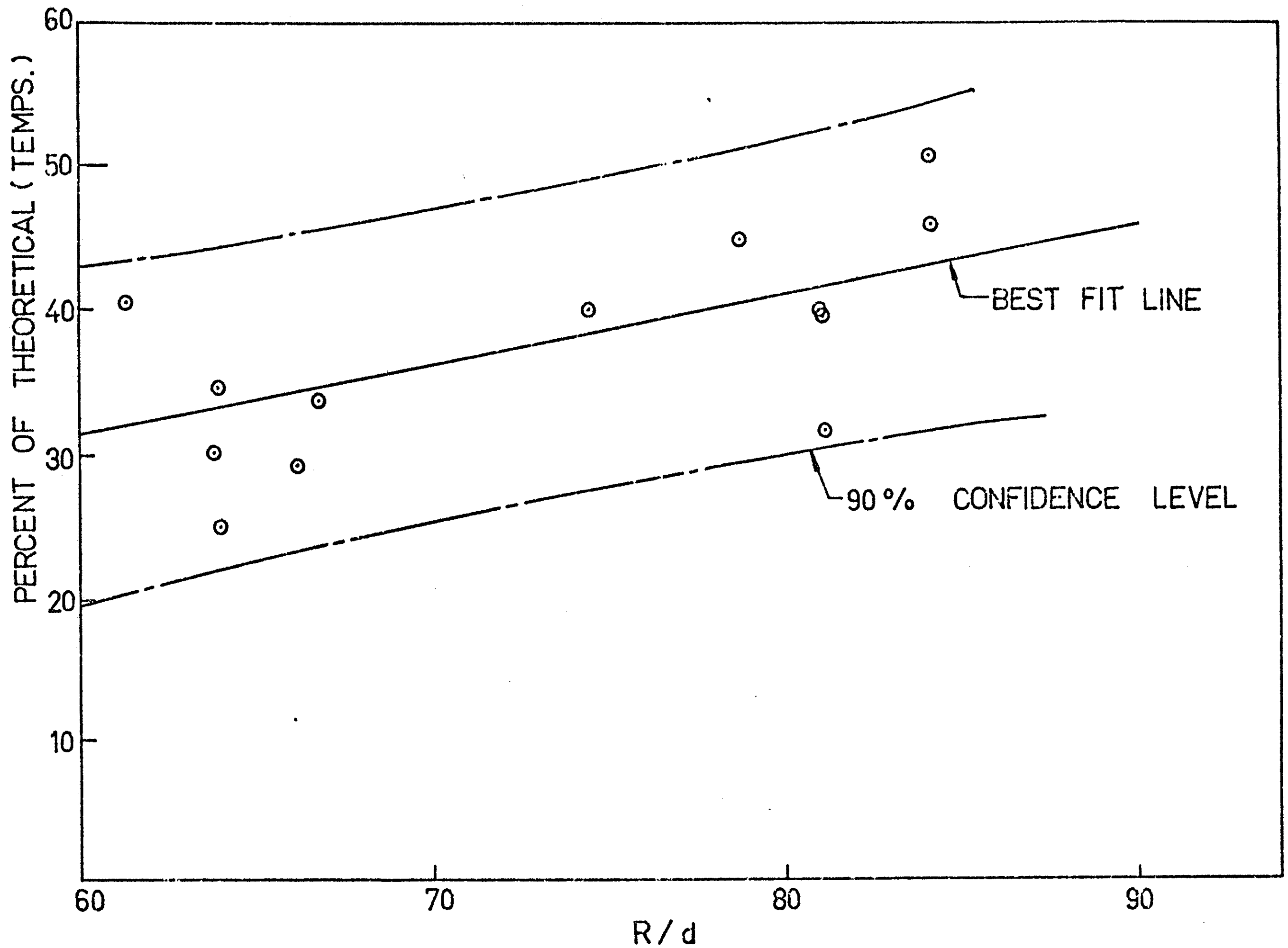

Figure 39. Percentage Theoretical Temperatures Vs. Radius to Thickness Ratio.

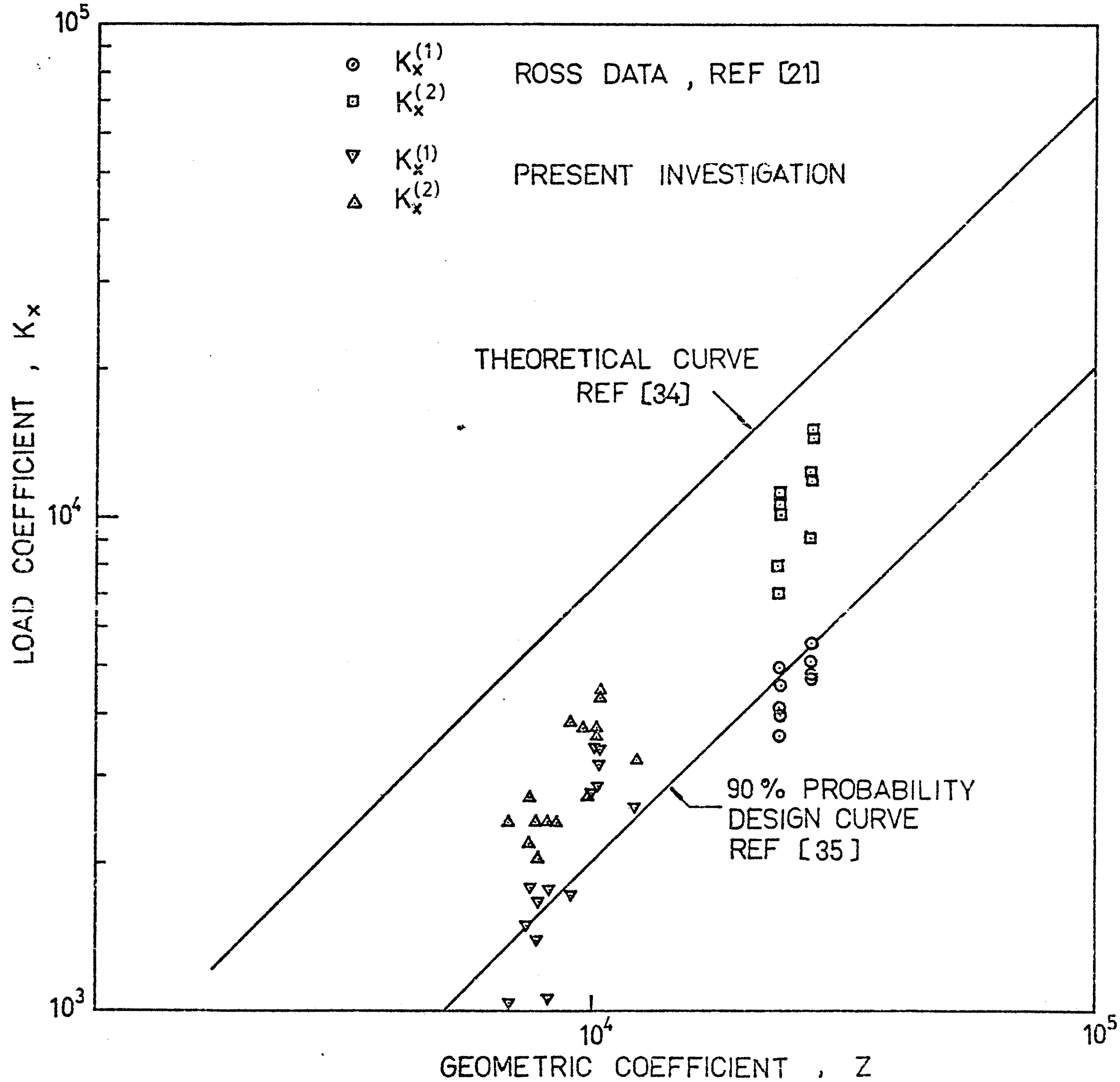

Figure 40. Dimensionless Test Results.

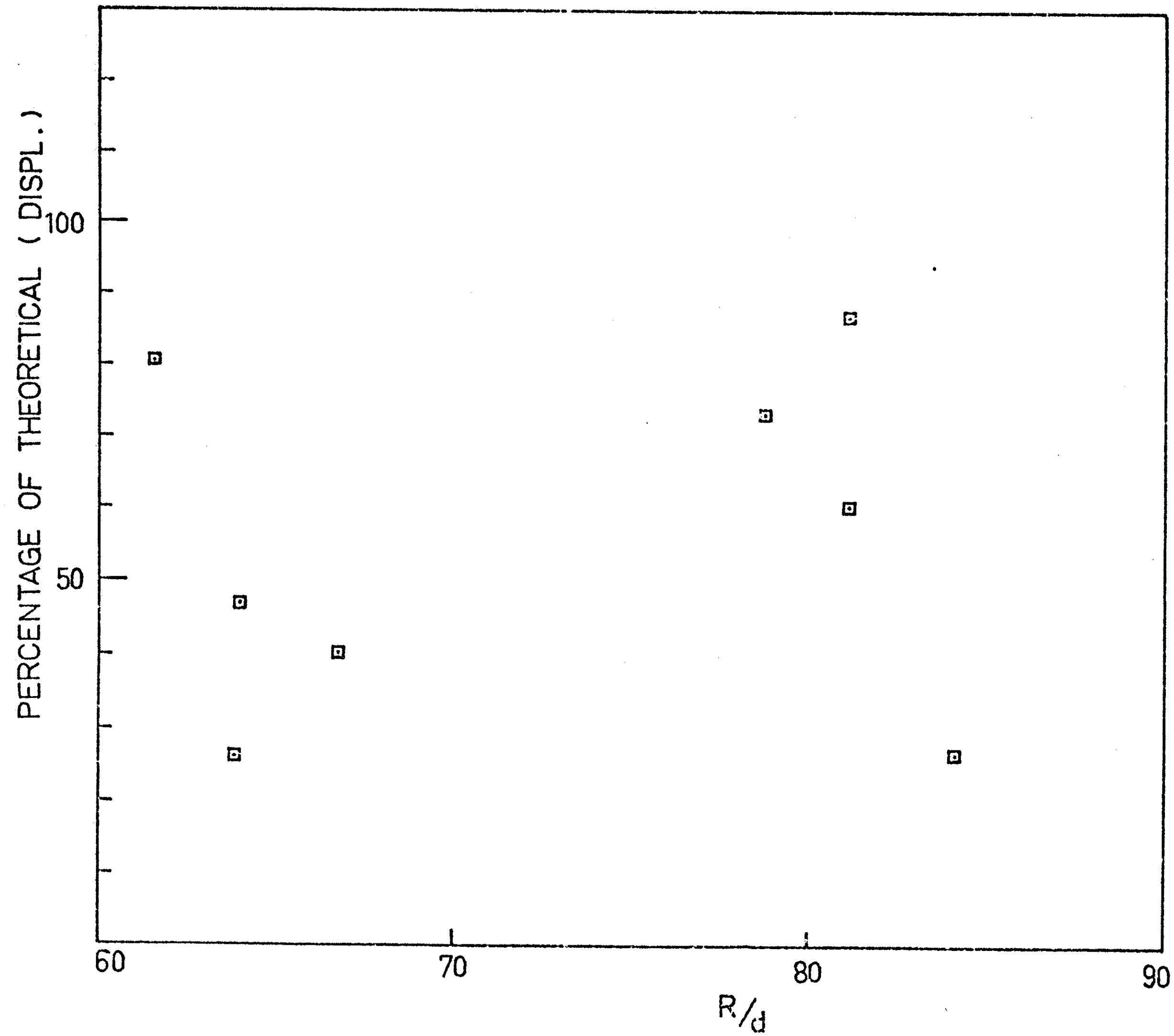

Figure 41. Percentage Theoretical Deflections Vs. Radius to Thickness Ratio.